การเกิดของไทเทเนียบนแผ่นไทเทเนียมโดยวิธีไฮโดรเทอร์มอลเพื่อการประยุกต์ใช้ในการแยกน้ำ

นางสาวนิสา เดชรัตน์

ศูนย์วิทยทรัพยากร
จุฬาลงกรณ์มหาวิทยาลัย

วิทยานิพนธ์นี้เป็นส่วนหนึ่งของการศึกษาตามหลักสูตรปริญญาวิศวกรรมศาสตรมหาบัณฑิต

สาขาวิชาวิศวกรรมเคมี ภาควิชาวิศวกรรมเคมี
คณะวิศวกรรมศาสตร์ จุฬาลงกรณ์มหาวิทยาลัย

ปีการศึกษา 2553

ลิขสิทธิ์ของจุฬาลงกรณ์มหาวิทยาลัย

GROWTH OF TITANIA ON TITANIUM PLATE VIA HYDROTHERMAL METHOD FOR THE APPLICATION IN WATER SPLITTING

Miss Nisa Dechrat

ศูนย์วิทยทรัพยากร
จุฬาลงกรณ์มหาวิทยาลัย

A Thesis Submitted in Partial Fulfillment of the Requirements
for the Degree of Master of Engineering Program in Chemical Engineering
Department of Chemical Engineering
Faculty of Engineering
Chulalongkorn University
Academic Year 2010
Copyright of Chulalongkorn University

Thesis Title	GROWTH OF TITANIA ON TITANIUM PLATE VIA HYDROTHERMAL METHOD FOR THE APPLICATION IN WATER SPLITTING
By	Miss Nisa Dechrat
Field of Study	Chemical Engineering
Thesis Advisor	Assistant Professor Varong Pavarajarn, Ph.D.
Thesis Co-advisor	Nawin Viriya-empikul, D.Eng

Accepted by the Faculty of Engineering, Chulalongkorn University in Partial Fulfillment of the Requirements for the Master's Degree

.....Dean of the Faculty of Engineering
(Associate Professor Boonsom Lerdhirunwong, Dr.Ing.)

THESIS COMMITTEE

.....Chairman
(Apinan Soottitantawat, D.Eng.)

.....Thesis Advisor
(Assistant Professor Varong Pavarajarn, Ph.D.)

.....Thesis Co-advisor
(Nawin Viriya-empikul, D.Eng.)

.....Examiner
(Akawat Sirisuk, Ph.D.)

.....External Examiner
(Kajornsak Faungnawakij, D.Eng.)

นิสา เดชรัตน์: การเกิดของไทเทเนียบนแผ่นไทเทเนียมโดยวิธีไฮโดรเทอร์มอลเพื่อการประยุกต์ใช้ในการแยกน้ำ (GROWTH OF TITANIA ON TITANIUM PLATE VIA HYDROTHERMAL METHOD FOR THE APPLICATION IN WATER SPLITTING) อ.ที่ปรึกษาวิทยานิพนธ์หลัก: ผศ.ดร.วรงค์ ปวราจารย์, อ.ที่ปรึกษาวิทยานิพนธ์ร่วม: ดร.นาวิน วิริยะเอี่ยมพิกุล, 81 หน้า.

งานวิจัยนี้ศึกษาสภาวะในการสังเคราะห์ไทเทเนียแบบฟิล์มบางบนแผ่นไทเทเนียมด้วยวิธีไฮโดรเทอร์มอล โดยศึกษาประสิทธิภาพในการเร่งปฏิกิริยาการย่อยสลายสีย้อมเมธิลลีนบลูภายใต้รังสีเหนือม่วงในเครื่องปฏิกรณ์ขนาดไมโคร จากนั้นนำไทเทเนียแบบฟิล์มบางที่มีประสิทธิภาพในการเร่งปฏิกิริยาการย่อยสลายที่ดีที่สุดไปเป็นขั้วแอโนดสำหรับปฏิกิริยาเคมีไฟฟ้าโดยใช้แสงในการแยกน้ำ จากงานวิจัยนี้พบว่าสามารถสังเคราะห์ไทเทเนียแบบฟิล์มบางบนแผ่นไทเทเนียมด้วยวิธีไฮโดรเทอร์มอลได้โดยผลิตภัณฑ์หลักจากการสังเคราะห์มีรูปร่างเป็นเส้นใยขนาดนาโน ขนาด รูปร่าง และ ความเป็นผลึกของเส้นใยตลอดจนความหนาของชั้นที่เกิดขึ้นบนแผ่นไทเทนียมขึ้นกับอุณหภูมิ และช่วงเวลาในการทำไฮโดรเทอร์มอล รวมถึงอุณหภูมิในการเผา จากการศึกษาพบว่าไทเทเนียที่อุณหภูมิในการทำไฮโดรเทอร์มอลที่ 180 องศาเซลเซียสเป็นเวลา 3 ชั่วโมง และ ทำการเผาที่ 600 องศาเซลเซียสให้เปอร์เซ็นการย่อยสลายดีที่สุด โดยไทเทเนียที่สภาวะนี้แสดงให้เห็นว่าสามารถทำการแยกแก๊สไฮโดรเจนออกจากน้ำได้โดยการใช้ขวดแก้วรูปตัวเอชภายใต้การฉายรังสีเหนือม่วง

ภาควิชา	วิศวกรรมเคมี	ลายมือชื่อนิสิต	นิสา เดชรัตน์
สาขาวิชา	วิศวกรรมเคมี	ลายมือชื่อ อ.ที่ปรึกษาวิทยานิพนธ์หลัก	
ปีการศึกษา	2553	ลายมือชื่อ อ.ที่ปรึกษาวิทยานิพนธ์ร่วม	นาวิน วิริยะเอี่ยมพิกุล

5270357121: MAJOR CHEMICAL ENGINEERING
KEYWORDS: TITANIA THIN FILM / HYDROTHERMAL PROCESS / WATER SPLITTING

NISA DECHRAT: GROWTH OF TITANIA ON TITANIUM PLATE VIA HYDROTHERMAL METHOD FOR THE APPLICATION IN WATER SPLITTING. ADVISOR: ASST. PROF. VARONG PAVARAJARN, Ph.D., CO-ADVISOR: NAWIN VIRIYA-EMPIKUL, D.Eng., 81 pp.

This research studies the condition to prepare titania thin film on titanium plate via the hydrothermal method. The photocatalytic properties were also studied by methylene blue degradation under UV radiation in a micro reactor. Then the TiO_2 thin film with the highest photocatalytic activity was used as the photoanode for the photoelectrochemical water splitting reaction. It was found that titania could be grown from titanium plate via the hydrothermal process. Majority of the product formed was nanofibers. Size, morphology and crystallinity of the fibers as well as the thickness of the growth layer depended upon temperature, duration of the hydrothermal treatment and calcination temperature. TiO_2 thin film obtained from the hydrothermal treatment at 180°C for 3h and calcined at 600°C exhibited the highest degradation percentage. It was also proved that the TiO_2 thin film synthesized under this condition could be used in the separated evolution of H_2 from water using an H-type glass container under UV light irradiation.

ศูนย์วิทยทรัพยากร
จุฬาลงกรณ์มหาวิทยาลัย

Department : Chemical Engineering	Student's Signature นิสา เดชรัตน์
Field of Study : Chemical Engineering	Advisor's Signature
Academic Year : 2010	Co-advisor's Signature Nawin V.

ACKNOWLEDGEMENTS

I would like to express my gratitude first to Assistant Professor Dr. Varong Pavarajarn, Ph.D., my thesis supervisor for his guidance, friendship, and support throughout the research and writing of this thesis. His patience and attention to details have helped me to remain on the path during the long and arduous course of my studies. Without him, there would be no thesis.

I am particularly grateful to Nawin Viriya-empikul, D.Eng. for her academic support and useful suggestion to my thesis.

My appreciation extends to the members of my thesis committee, Apinan Soottitantawat, D.Eng., Akawat Sirisuk, Ph.D.and Kajornsak Faungnawakij, D.Eng. Their comments and discussions have enriched and broadened the scope of the research.

I would like to thank a grant from Thailand Graduate Institute of Science and Technology (TGIST), Number TGIST 01-53-052 and the Centennial Fund of Chulalongkorn University for financial support.

I would like to thank National Nanotechnology Center, Thailand (NANOTEC). and all members for supporting the analytical equipments and their technical support.

I would also like to thank all my friends and all members of the Center of Excellent in Particle Technology, Department of Chemical Engineering, Chulalongkorn University for their assistance and friendly encouragement.

Finally, I would like to dedicate this thesis to my parents and my families, who generous supported and encouraged me through the year spent on this study.

CONTENTS

	Page
ABSTRACT (THAI)	iv
ABSTRACT (ENGLISH)	v
ACKNOWLEDGEMENTS	vi
CONTENTS	vii
LIST OF TABLES	x
LIST OF FIGURES	xi
CHAPTER	
I INTRODUCTION	1
II THEORY AND LITERATURE REVIEWS	3
2.1 Electronic Structure of Semiconductor	3
2.2 Physical and Chemical Properties of Titania	5
2.3 Hydrothermal Processing of TiO_2	8
2.4 Solar Electrochemical Water-Splitting or Photoelectrochemical Water-Splitting	11
2.4.1 Photoelectrochemistry	11
2.4.2 Photoelectrochemical Water-Splitting Reactions	11
2.4.2.1 Semiconductor−Liquid Junction (SCLJ) Approach	14
2.4.2.2 Photovoltaic/Semiconductor−Liquid Junction (PV/SCLJ) Approach	17
2.5 Photoelectrochemical Water-Splitting on Titania	18
III EXPERIMENTAL	21
3.1 Preparation of TiO_2 on Titanium Plate via Hydrothermal Method	21

Page

3.2 Characterizations of TiO_2..... 22
3.2.1 Scanning Electron Microscopy (SEM)..... 22
3.2.2 Transmission Electron Microscopy (TEM)..... 22
3.2.3 The Brunauer–Emmett–Teller (BET)..... 22
3.2.4 X-ray diffraction (XRD)..... 22
3.3 The Photocatalytic Water Splitting Reaction..... 22
3.3.1 Preliminary Photocatalytic Activity Testing..... 22
3.3.2 Water Splitting by Photocatalytic Reaction..... 24

IV RESULTS AND DISCUSSION..... 26
4.1 Synthesis of TiO_2 on Titanium via Hydrothermal Method.... 26
4.1.1 Primarily Investigation..... 26
4.1.2 Effect of hydrothermal temperature..... 27
4.1.3 Effect of hydrothermal time..... 37
4.1.4 Effect of calcination temperature..... 45

4.2 The Photocatalytic on the synthesized product..... 51
4.2.1 Photocatalytic degradation of methylene blue..... 51
4.2.1.1 The effect of hydrothermal temperature..... 40
4.2.1.2 The effect of hydrothermal time..... 54
4.2.1.3 The effect of calcination temperature..... 58
4.2.2 Water Splitting by Photocatalytic Reaction..... 61

V CONCLUSIONS AND RECOMMENDATIONS..... 66
5.1 Conclusions..... 66
5.2 Recommendations..... 67

Page

REFERENCES……..... 68
APPENDICES……..... 73
APPENDIX A CALIBRATION CURVE FOR DETERMINATION OF METHYLENE BLUE CONCENTRATION..... 74
APPENDIX B CALIBRATION CURVE FOR DETERMINATION OF HYDROGEN GENERATION..... 78
APPENDIX C STANDARD ELECTRODE (REDUCTION) POTENTIALS AT T = 298 K..... 79
VITA..... 81

ศูนย์วิทยทรัพยากร
จุฬาลงกรณ์มหาวิทยาลัย

LIST OF TABLES

Table **Page**

2.1 Typical physical and mechanical properties of titania..... 6

2.2 Crystallographic characteristic of anatase, brookite and rutile..... 7

4.1 Surface area of TiO_2/Ti thin film..... 32

4.2 Content of anatase phase in the product synthesized at different hydrothermal temperature..... 33

4.3 Surface area of TiO_2/Ti thin film..... 41

4.4 Anatase content (%) of products synthesized by usingdifferent hydrothermal time..... 44

A.1 Photolysis degradation of methylene blue (a) comparing with the photocatalytic degradation on TiO_2/Ti plate synthesized at 3 (b), 9 (c), 12 (d), 24 (e) and 48 h (f)..... 75

A.2 Photolysis degradation of methylene blue (a) comparing with the photocatalytic degradation on TiO_2/Ti plate synthesized at 120 (b), 150 (c) and 180°C (d)..... 76

A.3 Photolysis degradation of methylene blue (a) comparing with the photocatalytic degradation on TiO_2/Ti plate synthesized at 400 (b), 600 (c) and 800°C (d)..... 77

C.1 Standard electrode (reduction) potentials at T = 298 K..... 79

ศูนย์วิทยทรัพยากร
จุฬาลงกรณ์มหาวิทยาลัย

LIST OF FIGURES

Figure **Page**

2.1 Band structure of a semiconductor showing a full valence band and an empty conduction band. The Fermi level lies within the forbidden band gap..... 3

2.2 Crystal structure of TiO_2; (a) Rutile, (b) Anatase, (c) Brookite..... 7

2.3 Hydrothermal technology in the 21st century..... 9

2.4 Standard two electrode setup for PEC water splitting, shown in the photoanode configuration with a separated counter electrode..... 12

2.5 Schematic representation of a SCLJ approach with two semiconductors used as photoanode and photocathode, respectively..... 16

2.6 Scheme of a photoelectrolysis cell based on two semiconductor−liquid junctions. A n-type semiconductor is used for water oxidation into O_2 (photoanode) and a p-type semiconductor for H^+ reduction into H_2 (photocathode)..... 17

2.7 Schematic representation of a PV/SCLJ approach with a semiconductor photoanode and a Pt cathode [1]..... 18

3.1 Internal and external structure of autoclave ……..... 21

3.2 Equipment set-up for the photocatalytic degradation test: 1. syringe pump, 2. microchannel, 3. UV-lamp, 4. sampling vial..... 23

3.3 Relative spectra energy distribution of LP HP lamp..... 24

3.4 Schematic diagram of Water splitting by photocatalytic reactor. (1) TiO_2 anode: (2) platinum plate cathode, (3) nafion membrane, (4) gas collecting tubes, (5) power supply..... 25

4.1 EDX spectra obtained form the nanofibers washed with only distilled water (a), the nanofibers washed with 0.1 M HCl for 1h (b)…… 27

4.2 SEM images of products from 72 h hydrothermal treatment at 120°C (a,b),150°C (c,d) and 180°C (e,f). Images on the left were taken from the top most layer, while images on the right were taken after the top layer was peeled off....……..... 29

Figure **Page**

4.3 TEM images of products from hydrothermal treatment at 150°C for 72 h (a-b) and 180°C for 72 h (c-d)…….. 30

4.4 SEM images of products from hydrothermal treatment at 180°C for 72 h…… 30

4.5 XRD patterns of products synthesized by hydrothermal treatment in NaOH at different hydrothermal temperature for 72 h, and subsequently calcined at 600°C..……..……..... 33

4.6 XRD patterns of products synthesized by hydrothermal treatment in NaOH at 180°C for 24 h, and subsequently calcined at 600°C. The obtained product (a) was polished for 1 time (b) and 2 times (c) before being analyzed by XRD. The results are compared with the pattern obtained from a bare titanium plate calcined at 600°C (d) 34

4.7 SEM images of products from hydrothermal treatment at 180°C for 60 h (a,b) and products from 12 h additional hydrothermal treatment of the titanium plate (c,d) and that of the top layer scraped off from the product hydrothermally treated for 60 h was (e) 36

4.8 SEM images of products from hydrothermal treatment at 180°C for 3 h (a), 6 h (b), 9 h (c), 12 h (d), 48 h (e), 60 h (f), 66 h (g) and 72 h (h) 38

4.9 SEM images of each layer consisting of the products from hydrothermal treatment at 180°C for 3 h, i.e., top (a) and bottom (b) layers, for 48 h, i.e., top (c) and bottom (d) layers, for 66 h, i.e., top (e), middle (f) and bottom (g) layers..... 40

4.10 XRD patterns of products synthesized by hydrothermal treatment in NaOH at 180°C for different period of time, and subsequently calcined at 400°C..... 43

4.11 XRD patterns of products synthesized by hydrothermal treatment in NaOH at 180°C for different period of time, and subsequently calcined at 600°C. 44

Figure **Page**

4.12 XRD patterns of products synthesized by hydrothermal treatment in NaOH at 180°C for 24h, and subsequently calcined at 400°C. The obtained product (a) was polished for 1 time (b) and 2 times (c) before being analyzed by XRD…….. 45

4.13 Schematic diagram of layered composition (*X–Y* section) of nanotubed $H_2Ti_2O_4(OH)_2$……. 46

4.14 SEM images of products from hydrothermal treatment at 180 °C for 48 h before (a) and after calcination at 400°C (b), 600 (c) and 800 °C (d)….... 47

4.15 TEM images of products from hydrothermal treatment at 180 °C for 48 h before (a,b) and after calcination at 400 (c,d), 600 (e,f) and 800 °C (g,h)……. 47

4.16 XRD patterns of products synthesized by hydrothermal treatment in NaOH at 180 °C for 48 h, and subsequently calcined at 400, 600 and 800 °C……..... 49

4.17 XRD patterns of products synthesized by hydrothermal treatment in NaOH at 180°C for 3h, and subsequently calcined at 400, 600 and 800°C……. 50

4.18 Photolysis degradation of methylene blue (a) comparing with the photocatalytic degradation on TiO_2/Ti plate synthesized at 120 (b), 150 (c) and 180°C (d)……...…….. 51

4.19 Percentage of methylene blue degradation at residence time = 5 min. At the different the hydrothermal temperature……. 54

4.20 Photolysis degradation of methylene blue (a) comparing with the photocatalytic degradation on TiO_2/Ti plate synthesized at 3 (b), 9 (c), 12 (d), 24 (e) and 48 h (f)……... 55

4.21 Percentage of methylene blue degradation on TiO_2/Ti plate synthesized for different period of the hydrothermal time……. 58

4.22 Photolysis degradation of methylene blue (a) comparing with the photocatalytic degradation on TiO_2/Ti plate synthesized at 400 (b), 600 (c) and 800°C (d)…… 59

Figure **Page**

4.23 Percentage of methylene blue degradation on TiO_2/Ti plate synthesized for different period of the calcination temperature……. 61
4.24 Influence of applied voltage between the anode and cathode on H_2 generation from the system without TiO_2 thin film and irradiation……... 63
4.25 Influence of applied voltage provided supply between the anode and cathode H_2 generation from the PEC system using TiO_2 thin film as the anode, in which no irradiation is provided……. 64
4.26 Influence of applied voltage provided supply between the anod and cathode H_2 generation from the PEC system using TiO_2 thin film as the anode, in which irradiation is provided…….. 65
A.1 The calibration curve of methylene blue…… 74
B.1 The calibration curve of hydrogen generation…… 78

ศูนย์วิทยทรัพยากร
จุฬาลงกรณ์มหาวิทยาลัย

CHAPTER I

INTRODUCTION

Hydrogen economy in the future depends on availability of a low cost and environmental-friendly source of hydrogen. Presently, hydrogen production is mostly done by using fossil fuels, such as natural gas and coal. However, both of these fuels have a limited supply. In addition, they release greenhouse gases during the production of hydrogen. Therefore, for both environmental and economic reasons, alternative energy sources must be pursued for the purposes of producing hydrogen. Alternative energy is a term used for any energy source that is an alternative for fossil fuels. Although the cost of hydrogen from fossil fuel has historically been cheaper than alternative energy sources, the variable fuel cost of operating fossil-fueled facilities is increasing, while the cost of the alternative energy technology is decreasing as economies of scale are achieved. The alternative energy sources of hydrogen generally obtain the hydrogen molecules from water. The energy source is used to drive the hydrogen production process by using either electricity and electrolysis or heat and a thermochemical process to break apart water into its hydrogen and oxygen components. Examples of the alternative energy sources of hydrogen include nuclear energy, solar energy, wind energy and biomass [1]. In this works solar energy is used as the every source for hydrogen production via the photoelectrochemical process.

At the moment, energy sources produced from fossil has decreased. Therefore, it is urgent to find sources for alternative energy. Alternative energy is referring to energy used in substitution to the energy derived from fuel, without the undesired consequences. Examples of the alternative energy include natural gas, biodiesel, ethanol fuel, solar energy, wind, hydrogen gas etc. In this research, we are interested in hydrogen gas because it does not generate the “greenhouse” CO_2 during the combustion [2]. The main focus of the research emphasizes on the formation of TiO_2 photocatalyst for the application in photo-induced water-splitting reaction to produce hydrogen. Originally, the reactor for water splitting uses plate of TiO_2 photocatalyst with Pt sputtered on the back. In this work, TiO_2 was grown on titanium plate by

hydrothermal method. Titanium was used not only as the supporting plate during the water splitting reaction, but also as the source for the growth of titania.

Titanium dioxide (TiO_2) is a semiconductor having numerous applications, such as photocatalyst [3], solar cells [4], electrochromic devices [5], and sensors [6]. Increased attention has been paid on one-dimensional aligned nano-TiO_2 array. The synthesizing methods for one-dimensional TiO_2 nanostructures include high temperature oxidation [7], anode oxidation [8], glass phase topotaxy growth (GPT) method [9], templated sol-gel methods [10], electron beam deposition [11] and metal organic chemical vapor deposition (MOCVD) [12]. Nevertheless, most methods are costly and complicated. Hydrothermal method is another technique capable of producing one-dimensional TiO_2 that is simple and convenient. This technique has been used to synthesize well nanocrystals with uniform special morphology [13]. In this work, we investigated the growth mechanism of TiO_2 arrays during the hydrothermal synthesis in NaOH solution.

ศูนย์วิทยทรัพยากร
จุฬาลงกรณ์มหาวิทยาลัย

CHAPTER II

THEORY AND LITERATURE REVIEWS

Theory and literatures relating to hydrogen, electronic Structure of Semiconductor, physical and chemical properties of titania, hydrothermal processing of TiO_2 and photoelectrochemical water-splitting will be explained in this section.

2.1 Electronic Structure of Semiconductor

In solid-state physics, semiconductors (and insulators) are defined as solids in which the upper most band of occupied electron energy states, known as the valence band, is completely full at absolute zero temperature (0 K). In the other words, the Fermi energy of the electrons lies within the forbidden band gap as show in Figure 2.1. The Fermi energy or Fermi level can be thought of as the energy up to which available electron states are occupied at absolute zero temperature.

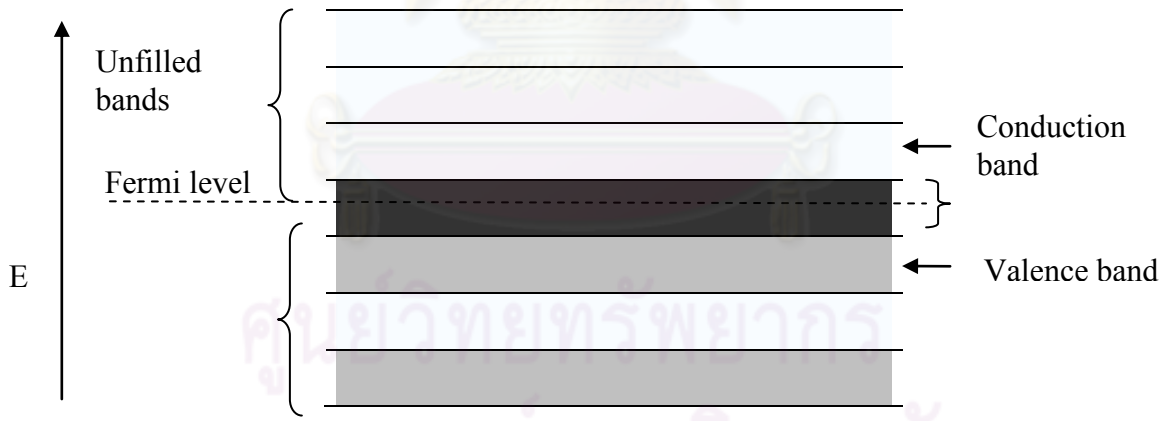

Figure 2.1. Band structure of a semiconductor showing a full valence band and an empty conduction band. The Fermi level lies within the forbidden band gap.

At room temperature, there is the smearing of the energy distribution of electrons, such that a small, but not insignificant number of electrons have enough energy to cross the energy band gap into the conduction band. These electrons break

loose from the covalent bonding among neighboring atoms in the solid, and they are free to move around, hence conducting charges. The covalent bonds from which these excited electrons had previously occupied now have missing electrons, or holes, which are free to move around as well. It should be noted that the hole itself does not actually move, but a neighboring electron can move to fill the hole, leaving a hole where it originally come from. By this way, the holes appear to move.

It is an important distinction between conductors and semiconductors such that, in semiconductors, movement of charge (current) is facilitated by both electrons and holes. For the conductors where the Fermi level lies within the conduction band, the band is only half filled with electrons. Therefore, only small amount of energy is needed for the electrons to find other unoccupied states in the conductor. On the contrary, the Fermi level in semiconductors lies in the valence band. The excitation of electrons from the valence band to the conduction band in semiconductors depends on the band gap.

The current-carrying electrons in the conduction band are known as "free electrons" although they are often simply called "electrons" if context allows this usage to be clear. The holes in the valence band behave very much like positively-charged counterparts of electrons, and they are usually treated as if they are real charged particles.

The band gap energy of the semiconductor can be classified into direct and indirect band gap energy.

Direct band gap means that the conduction band lies directly above the valence band. A semiconductor with direct band gap can be used to emit light. The prime example of a direct band gap semiconductor is gallium arsenide, a material commonly used in laser diodes.

Indirect band gap semiconductors are inefficient in emitting light. This is because any electrons present in the conduction band quickly settle into the minimum energy of that band. Electrons in this minimum require source of momentum to

overcome the offset and fall into the valence band. Momentum of photons is very small comparing to this energy offset. Since the electron cannot rejoin the valence band by irradiative recombination, conduction band electrons typically last quite some time before recombining through less efficient means. Silicon is an indirect bandgap semiconductor, and hence is not generally useful for light-emitting diodes or laser diodes. Indirect bandgap semiconductors can absorb light, however this only occurs for photons with significantly more energy than the band gap. This is why pure silicon appears dark grey and opaque, rather than clear.

2.2 Physical and Chemical Properties of Titania

Titanium (IV) oxide or titania (TiO_2) has great potential in various fields of science and technology such as catalyst, catalyst support, electronics, cosmetic pigment and filter coating. In recent years, main attention has been devoted to its photocatalytic activity and photoinduced superhydrophilicity. Since titania has relatively wide band gap (3.2 eV), charge carriers, i.e. electrons and holes, are produced when titania is excited. Consequently, highly reactive radicals are generated and oxidation-reduction reaction of species adsorbed on the surface of titania can occur.

Titania occurs in three crystalline forms, i.e. anatase, rutile and brookite. Rutile is a thermodynamically-stable phase of titania that can be found in igneous rock. It is one of two most important ores of titanium. Anatase is a metastable phase, which tends to be more stable at low temperature. For brookite, it is formed under hydrothermal conditions and usually found only in mineral. Among all crystalline phases of TiO_2, anatase is the most photoactive phase and has been employed as photocatalyst in wide range of applications for long time. Typical physical and mechanical properties of sintered titania are shown in Table 2.1. The crystallographic characteristic of titania are shown in Table 2.2 and in Figure 2.2.

Table 2.1. Typical physical and mechanical properties of titania.

Density	4 g cm^{-3}
Porosity	0%
Modulus of Rupture	140 MPa
Compressive Strength	680 MPa
Poisson‟s Ratio	0.27
Fracture Toughness	3.2 $MPa.m^{-1/2}$
Shear Modulus	90 GPa
Modulus of Elasticity	230 GPa
Microhardness (HV0.5)	880
Resistivity (25°C)	10^{12} ohm.cm
Resistivity (700°C)	$2.5x10^{4}$ ohm.cm
Dielectric Constant (1MHz)	85
Dissipation factor (1MHz)	$5x10^{-4}$
Dielectric strength	4 $kV.mm^{-1}$
Thermal expansion (RT-1000°C)	9 x 10^{-6}
Thermal Conductivity (25°C)	11.7 $W.m.K^{-1}$

ศูนย์วิทยทรัพยากร
จุฬาลงกรณ์มหาวิทยาลัย

Table 2.2 Crystallographic characteristic of anatase, brookite and rutile.

Properties	***Anatase***	***Brookite***	***Rutile***
Crystal Structure	Tetragonal	Orthorhombic	Tetragonal
Optical	Uniaxial	Biaxial	Uniaxial
Density, g/cm^3	3.9	4.0	4.23
Lattice parameter, nm			
a	0.3758	0.9166	0.4584
b		0.5436	
c	0.9514	0.5135	2.953

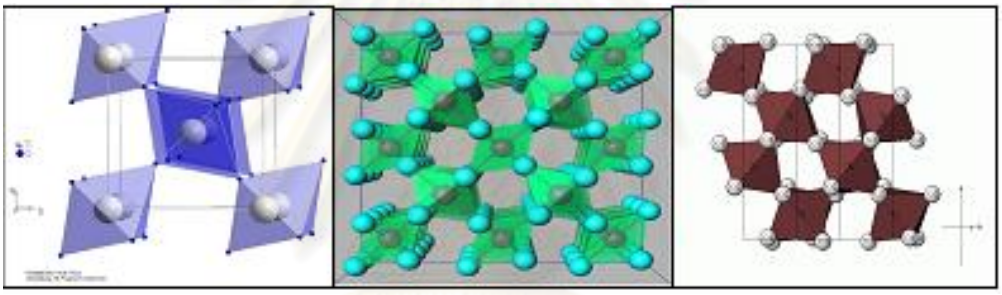

(a) (b) (c)

Figure 2.2. Crystal structure of TiO_2; (a) Rutile, (b) Anatase, (c) Brookite.

Three allotropic forms of titania have been prepared artificially, but only rutile has been obtained in the form of transparent large single crystal. The transformation from anatase to rutile is accompanied by evolution of ca. 12.6 kJ/mol (3.01 kcal/mol). The rate of phase transformation is greatly affected by temperature and by presence of other substances which may either catalyze or inhibit the transformation. The lowest temperature at which the conversion from anatase to rutile takes place at a measurable rate is approximately 500-550°C. The change is not reversible and it has been shown that ΔG for the transformation from anatase to rutile is always negative.

Many important applications of titania depend on its structure and optical properties. titania films have gained considerable importance as a photocatalyst, solar

cell application [14] and gas sensor [15]. titania in the form of thin film is more convenient than powder in photocatalysis since it is very easy to remove it from solution. Moreover, in thin-film form, it can be applied in various forms including coatings on various substrates such as ceramic, quartz and soda lime glass.

2.3 Hydrothermal Processing of TiO_2

The hydrothermal technique is becoming one of the most important tools for advanced materials processing, particularly owing to its advantages in the processing of nanostructural materials for a wide variety of technological applications such as electronics, optoelectronics, catalysis, ceramics, magnetic data storage, biomedical, biophotonics, etc. The hydrothermal technique not only helps in processing monodispersed and highly homogeneous nanoparticles, but also acts as one of the most attractive techniques for processing nano-hybrid and nanocomposite materials. The term „hydrothermal" is purely of geological origin. It was first used by the British geologist, Sir Roderick Murchison (1792-1871) to describe the action of water at elevated temperature and pressure, in bringing about changes in the earth"s crust leading to the formation of various rocks and minerals. It is well known that the largest single crystal formed in nature (beryl crystal of >1000 g) and some of the large quantity of single crystals created by man in one experimental run (quartz crystals of several 1000s of g) are both of hydrothermal origin.

In the 21st century, the hydrothermal technology is not just limited to the crystal growth, or leaching of metals, but it is going covering several interdisciplinary branches of science. Therefore, it has to be viewed from a different perspective. Further, the growing interest in enhancing the hydrothermal reaction kinetics using microwave, ultrasonic, mechanical, and electrochemical reactions will be distinct. Also, the duration of experiments is being reduced at least by 3-4 orders of magnitude, which will in turn, make the technique more economic. With an ever-increasing demand for composite nanostructures, the hydrothermal technique offers a unique method for coating of various compounds on metals, polymers and ceramics as well as for the fabrication of powders or bulk ceramic bodies. It has now emerged

as a frontline technology for the processing of advanced materials for nanotechnology. The hydrothermal technology in the 21st century has altogether offered a new perspective which is illustrated in Figure 2.3. It links all important technologies like geotechnology, biotechnology, nanotechnology and advanced materials technology. Thus it is clear that the hydrothermal processing of advanced materials is a highly interdisciplinary subject and the technique is popularly used by physicists, chemists, ceramists, hydrometallurgists, materials scientists, engineers, biologists, geologists, technologists, and so on.

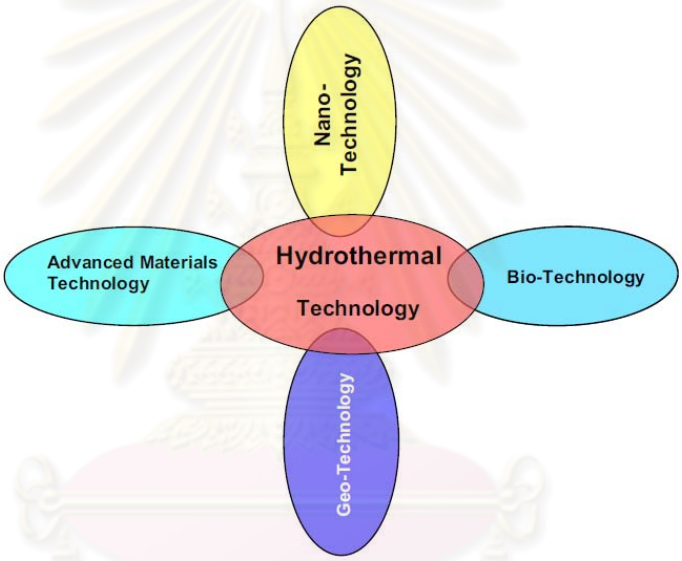

Figure 2.3. Hydrothermal technology in the 21st century.

The hydrothermal method has many advantages, e.g., highly homogeneous crystalline product can be obtained directly at a relatively low reaction temperature (<150 ^{o}C); it favors a decrease in agglomeration between particles, narrow particles size distribution, phase homogeneity, and controlled particle morphology; it also offers a uniform composition, purity of the product, monodispersed particles, control over the shape and size of the particles [16].

Many papers about the synthesis of TiO_2 on titanium have been presented in recent years. Zhengrong et al. synthesized TiO_2 nanoparticles that were deposited on a titanium (Ti) foil through dip coating in TiO_2 suspension. The Ti foil containing the predeposited TiO_2 nanoparticles was then reacted with 10 M NaOH in a sealed Teflon reactor. Morphology of TiO_2 on the titanium foil is nanotubes [17]. Gua et al. developed about hydrothermal synthesis titanate on titanium metal flakes. In our work, After hydrothermal treatment, the titanium metal flakes were polished with abrasive SiC paper. On treating the titanium flakes with 5-15 M NaOH solution in a sealed Teflon reactor at 90-150°C for 3-48h.When different concentrations of NaOH solution were used in the hydrothermal process, the formation of numerous nanoribbons were observed on treating titanium flakes with 5 M NaOH. In contrast, nanoparticles were observed in higher concentration (15 M NaOH) treated samples. But the nanotubes were observed on treating titanium flakes with 10 M NaOH. The overall formation of titanate nanotubes can be summarized, as a sequence of layered trititanate formation, splitting and scrolling process [18]. The addition study was a general formation mechanism for oriented titanate nanotube thin film on titanium flake. The overall formation of titanate nanotubes can be summarized as a sequence of four steps: (a) titanium dissolution and alkali titanate hydrogel formation; (b) alkali titanate hydrogel dissolution, increased TiO_3^{2-}, $TiO2(OH)_2^{2-}$, or $TinO_{2n+m}^{2m-}$, concentration and layered $Na_2Ti_3O_7$ formation; (c) layered $Na_2Ti_3O_7$ growth; (d) nanotube formation via $Na_2Ti_3O_7$ splitting and the multilayer scrolling process. The $Na_2Ti_3O_7$ lamellar structures split between the (010) planes into nanosheets [19]. Inoue et al. tried to transform sodium titanate into titanium dioxide. Using an aqueous solution with a lower hydrochloric acid concentration (0.01 mol/L) and a higher reaction temperature (90°C) than those previously employed, our obtained a hydrogen titanate nanotube thin film fixed onto a titanium metal metal plate by H^+ ion-exchange treatment of sodium titanate nanotube thin film. Calcinaion of hydrogen titanate nanotube thin film yielded porous thin film consisting of anatase nanotubes, anatase nanowire, and anatase nanoparticles grown directly from the titanium metal plate. H^+ ion-exchange treatment of sodium titanate nanotube thin film at 140°C resulted in porous thin film consisting of rhomboid-shaped anatase nanoparticles [20].

In this work, the system of hydrogen production was similar to the PV/SCLJ, power supply used instead solar cell. Semiconductor of PV/SCLJ is TiO_2.

2.4 Solar Electrochemical Water-Splitting or Photoelectrochemical Water-Splitting

2.4.1 Photoelectrochemistry

Photoelectrochemistry is a complex, and extremely rich scientific field drawing together fundamental concepts from chemistry, physics, optics, electronics and thermodynamics. In contrast with standard chemical processes involving interactions between chemical and ionic species, electrochemical processes can also involve interfacial interactions between ionic conductors, such as electrolyte solutions, and solid-state electronic conductors, such as semiconductors. Photoelectrochemical (PEC) processes comprise electrochemical systems exposed to light, where optical photons interact with the electrochemical reactions. In semiconductor photoelectrochemistry, photons typically create electron hole pairs within
the semiconductor that can cause redox chemistry to take place at semiconductor/electrolyte interfaces. Although a complicated set of fundamental electrochemical and solid-state optoelectronic principles govern the behavior of such systems, some useful simplifications can be helpful in providing a broad overview of the PEC water-splitting process.

2.4.2 Photoelectrochemical Water-Splitting Reactions

Most texts on PEC water splitting will start with the simple two-electrode setup shown in Figure 2.4 In this canonical model, a light-sensitive semiconductor photoelectrode is immersed in an aqueous solution, with electrical wiring connected to a metallic counter-electrode. With exposure to sunlight, photogenerated electron-hole pairs in the semiconductor interact electrochemically with ionic species in the solution at the solid/liquid interfaces. The photoexcited holes drive the oxygen-evolution reaction (OER) at the anode surface, while the photoexcited electrons drive the hydrogen-evolution reaction (HER) at the cathode surface. Figure 2.4 depicts a photoanode system where holes are injected into the solution at the semiconductor surface for evolving oxygen, while the photoexcited electrons are shuttled to the counter-electrode where hydrogen is evolved. Conversely, in photocathode systems,

electrons are injected into the solution and hydrogen is evolved at the semiconductor surface, while oxygen is evolved at the counterelectrode. Similar to solid-state pn-junction solar cells, PEC photoelectrodes typically act as minority carrier devices. The semiconductor/liquid junction allows the flow of minority carriers, while blocking majority-carrier flow. For this reason, n-type semiconductors allowing minority-carrier hole injection are better suited as photoanodes, while p-type semiconductors are used as photocathodes.

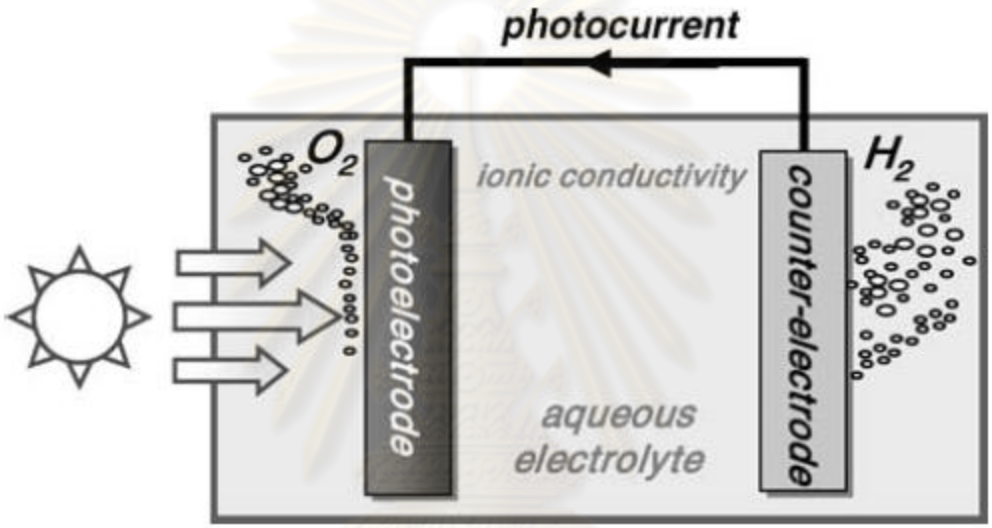

Figure 2.4 Standard two electrode setup for PEC water splitting, shown in the photoanode configuration with a separated counter electrode.

In the PEC water-splitting process, oxygen evolution at the anode and hydrogen evolution at the cathode can be modeled as two electrochemical "half-reactions." Both must be sustained simultaneously, coupled by their exchange of electrons in the solid state, and ions in solution. A simplified equation set describing the half-reactions in addition to the net conversion process can be written as follows:

$2\gamma \rightarrow 2e^- + 2h^+$ Photon-induced eletron-hole pair generation (2.1a)

$H_2O + 2h^+ \rightarrow 2H^+ + ½\ O_2(g)$OER: anodic water-oxidation half-reaction(2.1b)

$2H^+ + 2e^- \rightarrow H_2\,(g)$ HER: cathodic H^+ reduction half-reaction (2.1c)

$H_2O + 2\gamma \rightarrow H_2\,(g) + ½\,O_2\,(g)$ Net PEC water splitting reaction (2.1d)

where γ is photon energy, e^- is an electron, h^+ is a hole

Implicit in equation set 2.1, solid-state electrons/holes are exchanged between the anode and cathode through a conductive pathway (such as a wire), while H^+ ion migration from anode to cathode takes place through the aqueous media. It is clear from the equation set that PEC water splitting is a delicate balancing act, where photon-energized electron hole pairs under the right conditions can simultaneously drive the electrochemical half-reactions. In steady-state, the reactions in Equations 2.1b and 2.1c, must be sustained at the same reaction rate. Since H^+ ions are generated at the anode surface and consumed at the cathode surface, unless these events are proceeding concurrently at identical rates, charge build-up will impede or even stop the entire process. A similar situation exists with the charge carriers in the solid state. The anodic half-reaction consumes two holes (i.e., supplies two electrons) while the cathode half-reaction consumes two electrons. These electrons must be shuttled from anode to the cathode via electrical current (e.g., through the interconnecting wire shown in Figure 2.1), and steady state cannot be maintained if anode and cathode reaction rates are not the same. There are several additional key points that should be emphasized regarding the thermodynamic parameters included in equation set 2.1

The focus of equation set 2.1 is on electrochemical behavior and the losses in solution. Losses in the solid-state electrodes, including electron hole-pair recombination losses and electronic conductivity losses, among others, also degrade system performance. To drive the water-splitting process, including all solution and electrode losses, the absorbed photons must induce sufficient electrochemical potential to the electron hole pairs. The photoelectrolysis balancing act can be set into motion only if the photopotential requirement is met. Once in operation, the hydrogen evolution will be proportional to electron consumption, as shown in Equation 2.1c.

During steady-state operations, the solid-state shuttling of charges between anode and cathode represents a photon-induced current, or photocurrent, that is integrally tied to the
hydrogen-producing performance of the PEC system. Explicitly from Equation 2.1c, two
electrons are consumed in the evolution of one H_2 molecule. The rate of hydrogen production is therefore half the rate of electron flow, in other words, half the photocurrent. This is technically written as:

$$R_{H_2} = \frac{I_{ph}}{2e} = \frac{(J_{ph} \times Area)}{2e} \tag{2.2}$$

$$J_{ph} = \left(\frac{R_{H_2}}{Area}\right) \times 2e \tag{2.3}$$

where R_{H_2} is the hydrogen production rate (s^{-1}), I_{ph} is the photocurrent (A), e is the electronic charge (C), $Area$ is the illuminated photoelectrode area, J_{ph} is photocurrent density (Am^{-2}).

In Equation 2.3, the photocurrent density J_{ph} is normalized to the illuminated area of the photoelectrode, and is therefore inversely proportional to the incident photon flux. Upon closer look, J_{ph} is proportional to the ratio between the hydrogen production rate and the solar energy input [21].

2.4.2.1 Semiconductor−Liquid Junction (SCLJ) Approach

For arrangements based on semiconductor−liquid junctions, the water splitting potential is generated directly at the semiconductor−liquid interface. The ability of a semiconductor photoelectrode to drive either the oxidation of water into O_2, or the reduction of water into H_2, or the whole water splitting reaction is determined by its band gap and the position of the valence and conduction band edges relative to the water redox reactions. Besides the position of the band edges, there are other requirements that have to be considered for a material to be used for water splitting purpose in a SCLJ approach. The semiconductor has to be active over a broad spectral

range, and, upon light absorption, the material should efficiently separate the generated charges. Obviously, this is also valid for the photovoltaic approach. Moreover, the immersed semiconductor has to be stable in the electrolyte and corrosion free.

For example, TiO_2 is very stable in a wide range of pH, but it is active only in the UV region due to its large bandgap. WO_3 is also active only in the short wavelength range of the solar spectrum, but it is less stable in acidic medium. Fe_2O_3 has a smaller band gap and absorbs in the visible, but it is also not very stable in acidic solutions. Compounds such as CdTe or InP also have smaller band gaps that are better matched to the spectral distribution of sunlight reaching the earth, but these materials either corrode or become inert when used as photoelectrodes in aqueous solution. These few examples and the ones mentioned in the following show that every semiconductor has its drawbacks. In search of suitable semiconductors to be used for water oxidation, water reduction, as well as water splitting in semiconductor-liquid junctions, a large number of scientific efforts have been devoted worldwide for several decades.

Fujishima and Honda reported for the first time in 1972 on sunlight-assisted electrolysis of water using crystalline TiO_2 photoelectrodes. The photoelectrochemical cell consisted of TiO_2 (rutile) as a photoanode and platinum as a cathode. Illumination of the TiO_2 electrode led to O_2 evolution on the photoanode and H_2 evolution on the cathode. The quantum efficiency increased with an increase in alkalinity in the TiO_2 photoanode compartment and in acidity in the Pt cathode compartment [22, 23].

More promising is a photoelectrolysis cell based on two illuminated semiconductor−liquid junctions. Figure 2.5 shows a schematic representation of this approach. A n-type semiconductor is used for the evolution of O_2 and a p-type semiconductor for the evolution of H_2 (Figure 2.6). By separating the oxidation and reduction processes into half-cell reactions, one can deal with one reaction at a time. Besides, two semiconductors with smaller band gaps can be utilized since each needs only to provide part of the water splitting potential. The smaller band gap means more absorption in the visible region of the solar spectrum where the sun has a greater

photon flux. As a result, the maximum theoretical efficiency is considerably higher. The system is contingent on the efficient recombination of electrons formed in the n-type semiconductor (photoanode) with holes formed in the p-type semiconductor (photocathode) via back contact connections in both materials. This is theoretically possible only if the valence band of the photocathode lies positive (higher electrochemical potential) with respect to the conduction band of the photoanode. This means, that proper selection of both semiconductor electrodes characteristics ensures that the energy necessary for water photoelectrolysis is gathered entirely from the illumination, eliminating the necessity of applying energy from an external source.

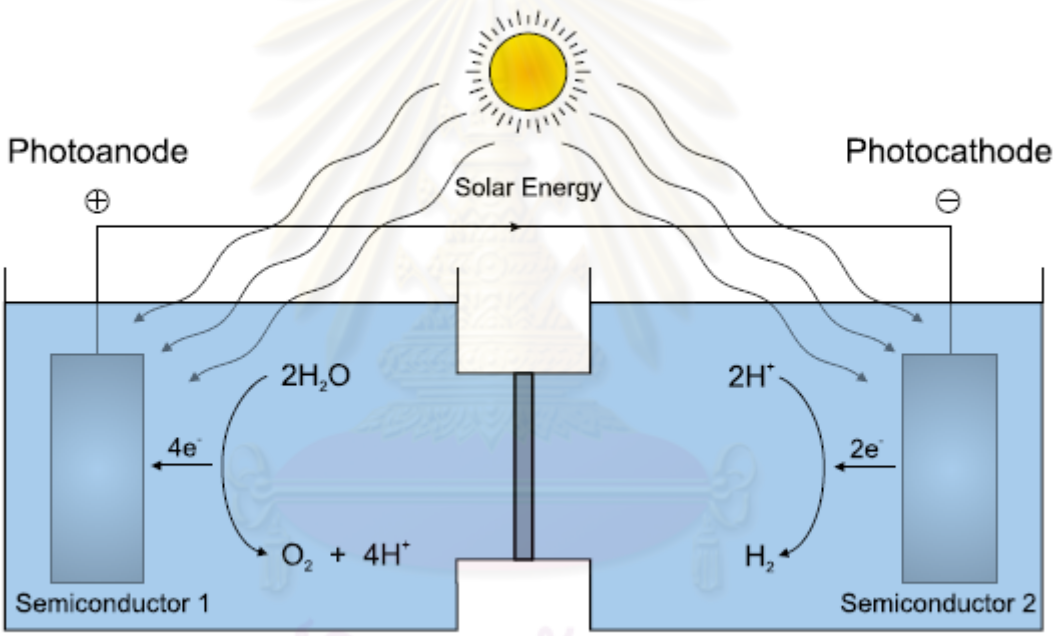

Figure 2.5 Schematic representation of a SCLJ approach with two semiconductors used as photoanode and photocathode, respectively.

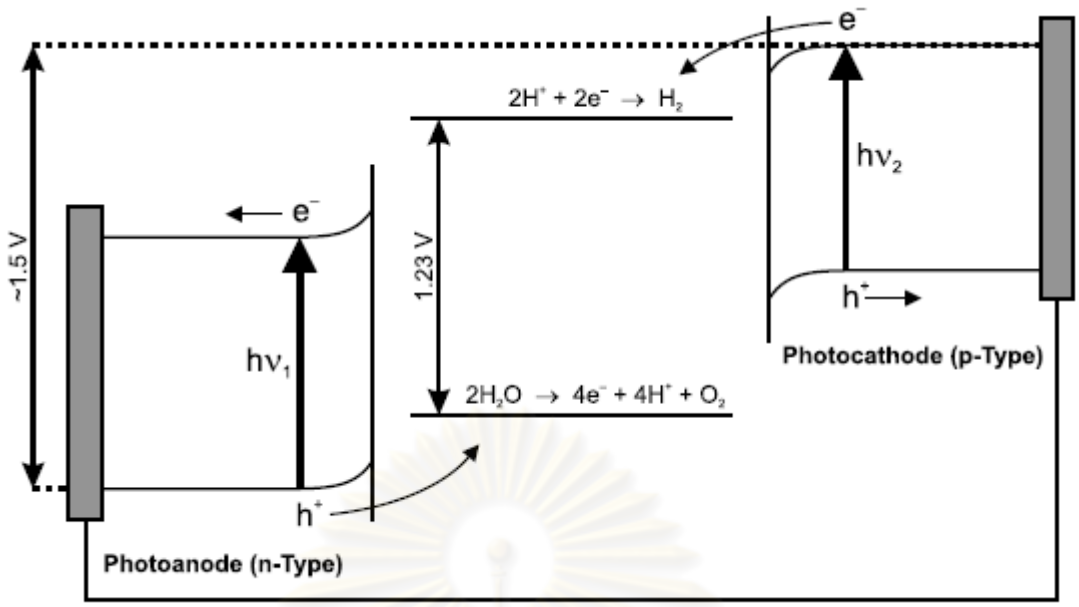

Figure 2.6 Scheme of a photoelectrolysis cell based on two semiconductor−liquid junctions. A n-type semiconductor is used for water oxidation into O_2 (photoanode) and a p-type semiconductor for H^+ reduction into H_2 (photocathode).

A multi-junction cell arrangement like in photovoltaic devices was adopted for a SCLJ approach with two semiconductors by using a composite of polycrystalline Si with a doped TiO_2 thin film layer on top. The doped TiO_2 absorbs the short-wavelength part of solar light (blue light, λ <500 nm). The long wavelength part is absorbed by the polycrystalline Si layer in the back. Upon light absorption, an electron is excited in two steps from a low lying valence band of TiO_2 to a high lying level of the conduction band of Si, which leads to hydrogen evolution on the Pt counter electrode and oxygen evolution on the doped TiO_2 surface. The stability problem of silicon electrodes could be overcome by surface alkylation and metal nano-dot coating.

2.4.2.2 Photovoltaic/Semiconductor−Liquid Junction (PV/SCLJ) Approach

In a PV/SCLJ approach for overall water splitting a photovoltaic (PV) cell is used together with a semiconductor that is in direct contact with electrolyte. The PV

cell can be combined either with a reduction (photocathode) or with an oxidation (photoanode) photocatalyst. The water splitting reaction involves a two-electron reducing process for the H_2 production (Eq2.1c) and a four-electron oxidizing process for the O_2 producing part. It is the water oxidation reaction that poses the greatest difficulty in achieving photocatalytic water splitting, mainly because four oxidative equivalents must be accumulated. Therefore, efficient oxygen production at a semiconducting photoanode is the most challenging aspect of PEC water splitting. The additional bias for the hydrogen evolution on a metallic cathode is provided by a solar cell, leading to a PV/SCLJ approach for overall water splitting (Figure 2.7).

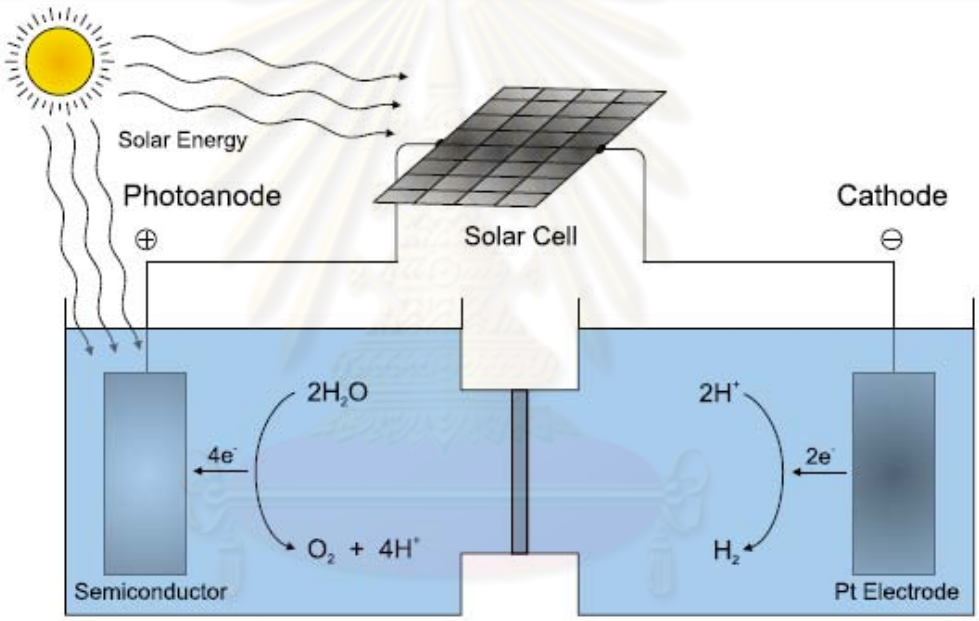

Figure 2.7 Schematic representation of a PV/SCLJ approach with a semiconductor photoanode and a Pt cathode [1].

2.5 Photoelectrochemical Water-Splitting on Titania

The photoelectrochemical water-splitting on titania originally got started in the late 1960s at The University of Tokyo in research on photoelectrochemical solar cells. One of the first types of electrode materials we looked at was semiconducting TiO_2, partly because it has a sufficiently positive valence band edge to oxidize water to

oxygen. It is also an extremely stable material in the presence of aqueous electrolyte solutions, much more so than other types of semiconductors that have been tried.

The possibility of solar photoelectrolysis was demonstrated for the first time with a system in which an n-type TiO_2 semiconductor electrode, which was connected though an electrical load to a platinum counter electrode, was exposed to near-UV light. When the surface of the TiO_2 electrode was irradiated with light consisting of wavelengths shorter than ~415 nm, photocurrent flowed from the platinum counter electrode to the TiO_2 electrode through the external circuit. The direction of the current reveals that the oxidation reaction (oxygen evolution) occurs at the TiO_2 electrode and the reduction reaction (hydrogen evolution) at the Pt electrode. This fact shows that water can be decomposed, using UV–VIS light, into oxygen and hydrogen, without the application of an external voltage, according to the following scheme:[24]

$$TiO_2 + 2hv \rightarrow 2e^- + 2H^+ \quad \text{(excitation of } TiO_2 \text{ by light)} \qquad (2.4.1)$$

$$H_2O + 2h^+ \rightarrow \tfrac{1}{2} O_2 + 2H^+ \quad \text{(at the } TiO_2 \text{ electrode)} \qquad (2.4.2)$$

$$2H^+ + 2e^- \rightarrow H_2 \quad \text{(at the Pt electrode)} \qquad (2.4.3)$$

$$H_2O + 2hv \rightarrow \tfrac{1}{2} O_2 + H_2 \quad \text{(The overall reaction)} \qquad (2.4.4)$$

Work about synthesize TiO_2 via hydrothermal for water splitting have many. M. Kitano et al synthesis visible light-responsive TiO_2 (Vis-TiO_2) thin flims which exhibit a unique declined O/Ti composition from the surface to the deep inside bulk have been successfully developed under a substrate temperature of 873 K by applying a radio-frequency magnetron sputtering deposition (RF-MS) method. These Pt-loaded Vis-TiO_2 thin films were found to decompose water involving methanol (H_2 production reaction from H_2O) or 0.05 M silver nitrate solution (O_2 production reaction from H_2O) under visible light ($\lambda \geq 420$ nm) irradiation. In particular, the photo-oxidation of water to produce O_2 proceeds under visible light of wavelengths longer than 550 nm. The conduction and valence bands of Vis-TiO_2 thin film photocatalysts were, thus, seen to have enough potential for the

decomposition of water into H_2 and O_2 under visible light irradiation. Vis-TiO_2 thin flim separate evolution of H_2 and O_2 from H_2O could be successfully achieved using an H-type glass container even under visible light [25]. And study more about synthesis nanowire TiO_2 thin flim prepared on Ti metal substrates by hydrothermal method of calcined Ti foils in 10 M NaOH. These nanowire flims were shown act as an efficient photoanodes for the photoelectrochemical water splitting reaction in an H-type glass container [26]. M. Matsuoka studied The effect of the hydrothermal treatment with aqueous NaOH solution on the photoelectrochemical and photocatalytic properties of visible light-responsive TiO_2 thin films prepared on Ti foil substrate (Vis-TiO_2/Ti) by a radio-frequency magnetron sputtering (RF-MS) deposition method has been investigated. The hydrothermally treated Vis-TiO_2/Ti electrodes exhibited a significant increase in their photocurrent under UV and visible light irradiation as compared to untreated Vis-TiO_2/Ti electrode. SEM investigations revealed that the surface morphology of Vis-TiO_2/Ti are drastically changed from the assembly of the TiO_2 crystallites to the stacking of nanowires with diameters of 30–50 nm with increasing hydrothermal treatment time (3–24 h), accompanying the increase in their surface area. The separate evolution of H_2 and O_2 from water under solar light irradiation was successfully achieved using the Vis-TiO_2/Ti/Pt which is hydrothermally treated for 5 h, while the H_2 evolution ratio was 15 μmol $h^{-}1$ in the early initial stage, corresponding to a solar energy conversion efficiency of 0.23% [27]. and study more about Vis-TiO_2 were affected by various calcination treatments such as calcination in air or NH_3. Calcination treatment in NH_3 ($1.0x10^4$ Pa, 673 K) was particularly effective in increasing the visible light absorption of Vis-TiO_2 as well as in enhancing its photoelectrochemical performance and photocatalytic activity [28].

CHAPTER III

EXPERIMENTAL

3.1 Preparation of TiO_2 on Titanium Plate via Hydrothermal Method.

Titanium plate (1 cm x 1.5 cm x 0.127 cm, 99.99%, Sigma-Aldrich) was washed with acetone. The sample was put into 50 ml solution of 10 M NaOH in a 50 ml Teflon-lined stainless steel autoclave (Figure 3.1.1) and heated to temperature in the range of 120, 150 and 180°C for 1- 72 h. After being held at the desired temperature for predetermined period of time, the sample was took out of the autoclave, completely washed with distillated water and dried in an oven at 80°C. At this point, the obtained product was consisted of sodium titanate. To transform sodium titanate into hydrogen titanate, 100 ml of 0.1 M HCl solution was used to soak the sample for 1 h. Then, the product was washed with water to remove excess HCl and calcined at 400, 600 and 800°C for 2 h to transform hydrogen titanate into titanium dioxide.

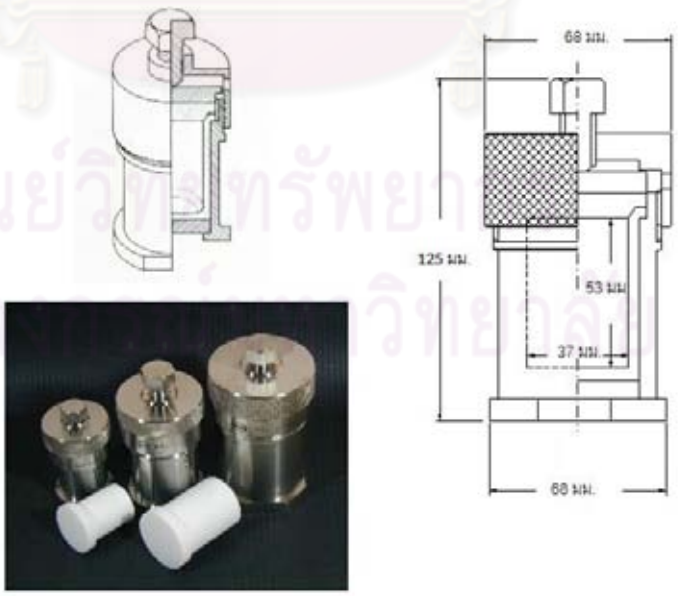

Figure 3.1 Internal and external structure of autoclave

3.2 Characterizations of TiO_2

3.2.1 Scanning Electron Microscopy (SEM)

Scanning electron microscope (SEM, Hitachi S-3400N TypeII) was used to observe morphology of the TiO_2 thin film.

3.2.2 Transmission Electron Microscopy (TEM)

Transmission electron microscope (TEM, Hitachi H-9000UHR III) was used for the observation of nanostructure, high resolution TEM image, and diffraction image.

3.2.3 The Brunauer–Emmett–Teller (BET)

A nitrogen adsorption system (BEL Japan Bellsorp-max) was employed to determine adsorption–desorption isotherms at liquid nitrogen temperature. The Brunauer–Emmett–Teller (BET) approach was employed to determine the surface area of the TiO_2 thin film.

3.2.4 X-Ray Diffraction (XRD)

The crystalline phase of the TiO_2 thin film was measured by powder X-ray diffraction (XRD) technique using a Bruker D8 Advance equipped with a Cu Kα radiation source (λ = 0.15406 nm) and operated at 40 kV and 40 mA.

3.3 The Photocatalytic Water Splitting Reaction

3.3.1 Preliminary Photocatalytic Activity Testing

The photocatalytic activity of the synthesized TiO_2 was preliminarily examined by Methylene Blue (MB) degradation in homemade micro reactor figure 3.2. LAMBDA 650 UV-vis spectrometer was applied for measuring the MB

concentration change during the monitoring period. The initial concentration of methylene blue solution was fixed at 5 ppm. The solution was continuously pumped into microchannal of the microreactor via a syringe pump. Flow rate of the solution was fixed at 5.4 mL/h. At first, the solution was supplied to the reactor in the dark to monitor adsorption behavior of the synthesized TiO_2. After the sample was saturated with methylene blue, the photocatalytic reaction was initiated by exposing microreactor to light from UV light (SEN UVL20PL-6 20W low pressure mercury lamp). Relative spectra energy distribution of UV light shown in figure 3.3.

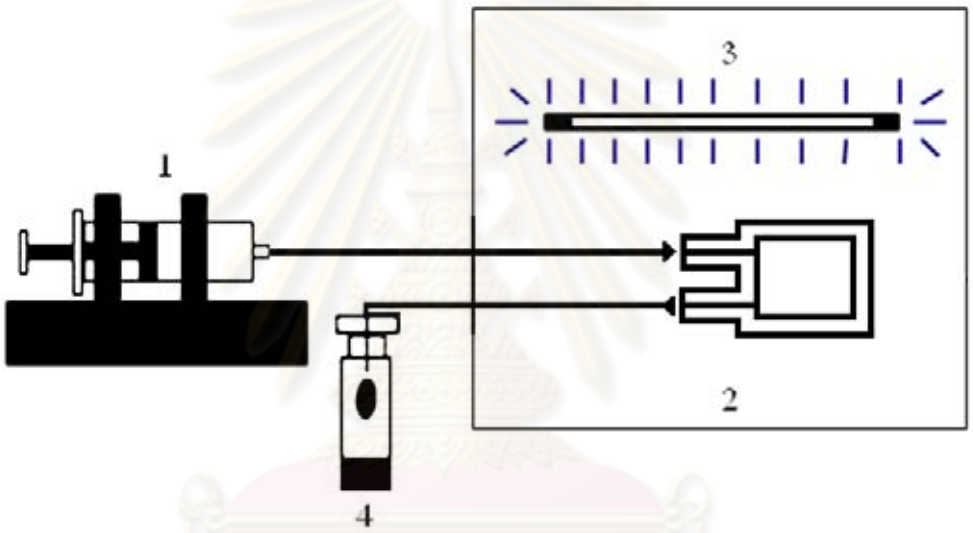

Figure 3.2 Equipment set-up for the photocatalytic degradation test: 1. syringe pump, 2. microchannel, 3. UV-lamp, 4. sampling vial.

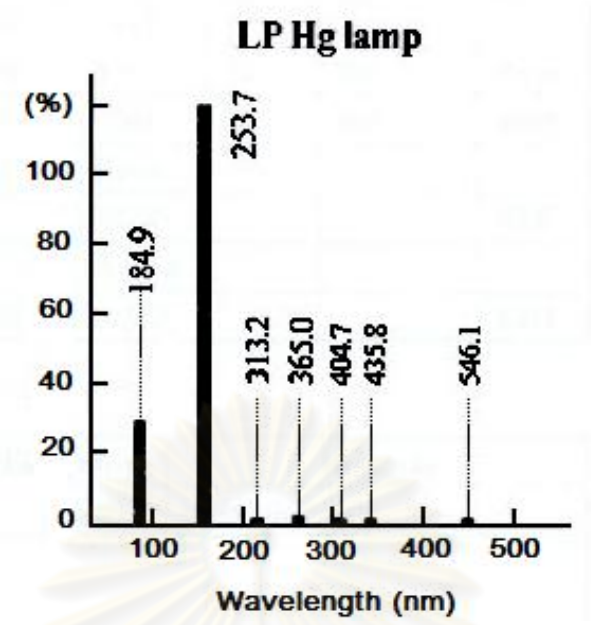

Figure 3.3 Relative spectra energy distribution of LP HP lamp

3.3.2 Water Splitting by Photocatalytic Reaction

As show in figure 3.3, our homemade photocatalytic water splitting reactor was in two–electrode configuration with two separate compartments connected by an 1-inch diameter the nafion membrane. The anode was TiO_2 nanotubes arrays with geometric area about 1.5 cm^2. The cathode was a platinum plate (1.5 x 1 cm^2, 0.127 thick). In the TiO_2-side and in the Pt-side containers, 1.0 M NaOH and 0.5 M H_2SO_4 aqueous solution were used as electrolyte, respectively. The UV light was focused on the anode by a quartz lens. An adjustable voltage provided by a power supply between the anode and cathode. The values of external voltage and the photocurrent were directly read using multimeter.

Hydrogen products from the Water splitting by photocatalytic reaction reaction using the gas chromate-graphy (SHIMADZU, GC-14B) on an active charcoal packed column was em-ployed for analysis of hydrogen gas.

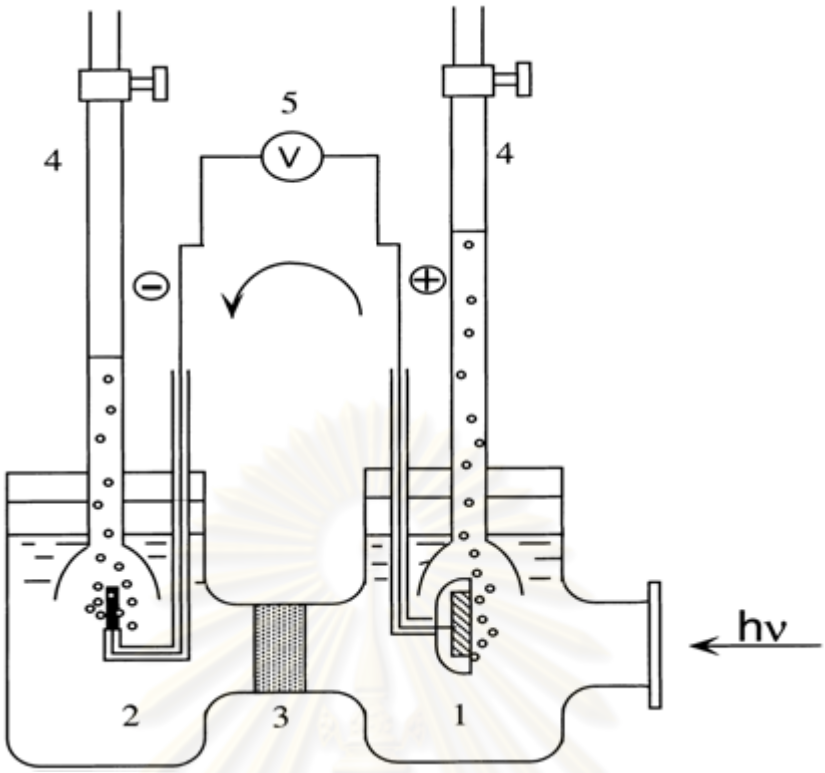

Figure 3.4 Schematic diagram of Water splitting by photocatalytic reactor. (1) TiO_2 anode: (2) platinum plate cathode, (3) nafion membrane, (4) gas collecting tubes, (5) power supply.

ศูนย์วิทยทรัพยากร
จุฬาลงกรณ์มหาวิทยาลัย

CHAPTER IV

RESULTS AND DISCUSSION

TiO_2 can be grown on titanium plate via hydrothermal method in NaOH solution. In this study, effects of hydrothermal temperature, hydrothermal time and calcination temperature on morphology, crystallinity and orientation of TiO_2 grown on the titanium plate are investigated. Then, TiO_2 thin film was tested for its photocatalytic activity by using methylene blue degradation in a micro reactor. The TiO_2 thin film with the highest photocatalytic activity was further applied as a photoanode for the photoelectrochemical water splitting reaction.

4.1. Synthesis of TiO_2 on Titanium via Hydrothermal Method

4.1.1 Primarily Investigation

It has been known that the product from the hydrothermal treatment of titanium in NaOH is sodium titanate [20]. To transform sodium titanate into hydrogen tatanate by acid treatment, it is use H^+ ion-exchange treatment with a 0.1 M HCl was used Energy dispersive x-ray spectroscopy (EDX) studies showed that Ti, Na and O (H cannot be detected by EDX) are present in TiO_2 thin film before H^+ ion-exchange treatment (Figure 4.1a). In the sample treated with 0.1 M HCl for 1 h, only Ti and O were present (Figure 4.1b). It is confirmed that Na^+ ions do not remain in the samples after the treatment. We therefore performed the H^+ ion-exchange treatment with a 100 ml of 0.1 M HCl for 2 h to ensure completeness of the H^+ ion-exchange reaction for all samples.

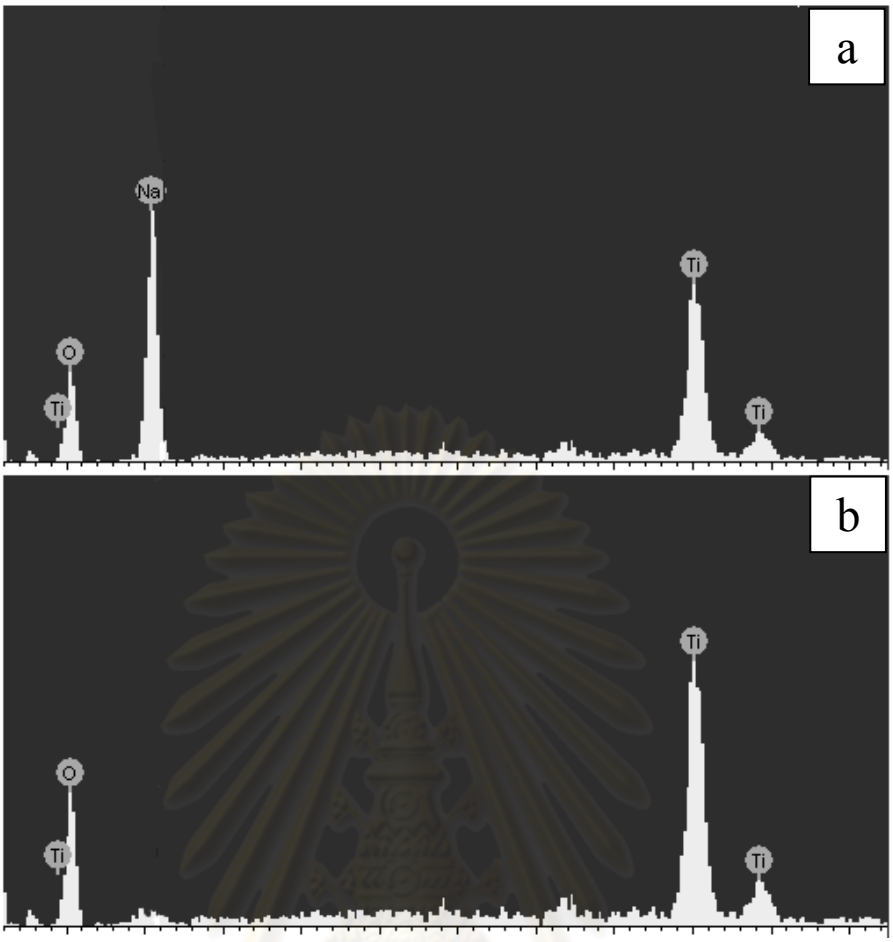

Figure 4.1 EDX spectra obtained form the nanofibers washed with only distilled water (a), the nanofibers washed with 0.1 M HCl for 1h (b).

4.1.2 Effect of hydrothermal temperature

To study the effect of hydrothermal temperature, morphology of TiO_2 layer formed on titanium plate and its surface area were studied by varying the temperature of the oven from 120, 150 and 180°C, respectively. The hydrothermal treatment was conducted for 72 h. For this parameter, the concentration and volume of NaOH solution were fixed at 10 M and 50 ml, respectively. The results are illustrated in Figure 4.2.

Figure 4.2 shows SEM micrographs of the samples synthesized by hydrothermal for 72h for various temperatures. For the hydrothermal treatment at 120

^{o}C, a sponge-like layer consisting of rod-shape particles is formed on the surface of titanium plate (Figure 4.2a). When the hydrothermal temperature is increased to 150 ^{o}C (Figure 4.2c), the rods appear longer than that observed in Figure 4.2a, while the morphology of TiO_2 on titanium plate is nanofibers. Though the SEM image of the product shows nanofibers, the TEM image of the product reverls that it is in fact nanotubes (Figure 4.3a,b). The nanotubes were formed by layered sodium titanate splitting and the multilayer scrolling process [19]. According to SEM micrographs from other research, the formation of numerous nanoribbons was observed on titanium flakes treated with 5 M NaOH. These nanoribbons was reported as the incomplete scroll of nanotubes [18]. When the hydrothermal temperature increased to 180°C, large nanofibers are observed (Figure 4.2e). The TEM images of the sample synthesized at 180°C confirm that the nanofibers are solid fiber (Figure 4.4c,d). From the results, the probable formation mechanism for the large fiber can be summarized as a sequence of four steps: (1) titanium dissolution and sodium titanate formation, (2) layered sodium titanate growth and splitting, (3) some of mutilayer sodium titanate dissolved into the NaOH solution, (4) large fiber formation via sodium titanate deposited from saturated solution of sodium titanate. The large fiber formation via sodium titanate deposition was proved by large fiber had unequal density. The center of large fiber has density more than the extreme of large fiber Figure 4.4.

ศูนย์วิทยทรัพยากร
จุฬาลงกรณ์มหาวิทยาลัย

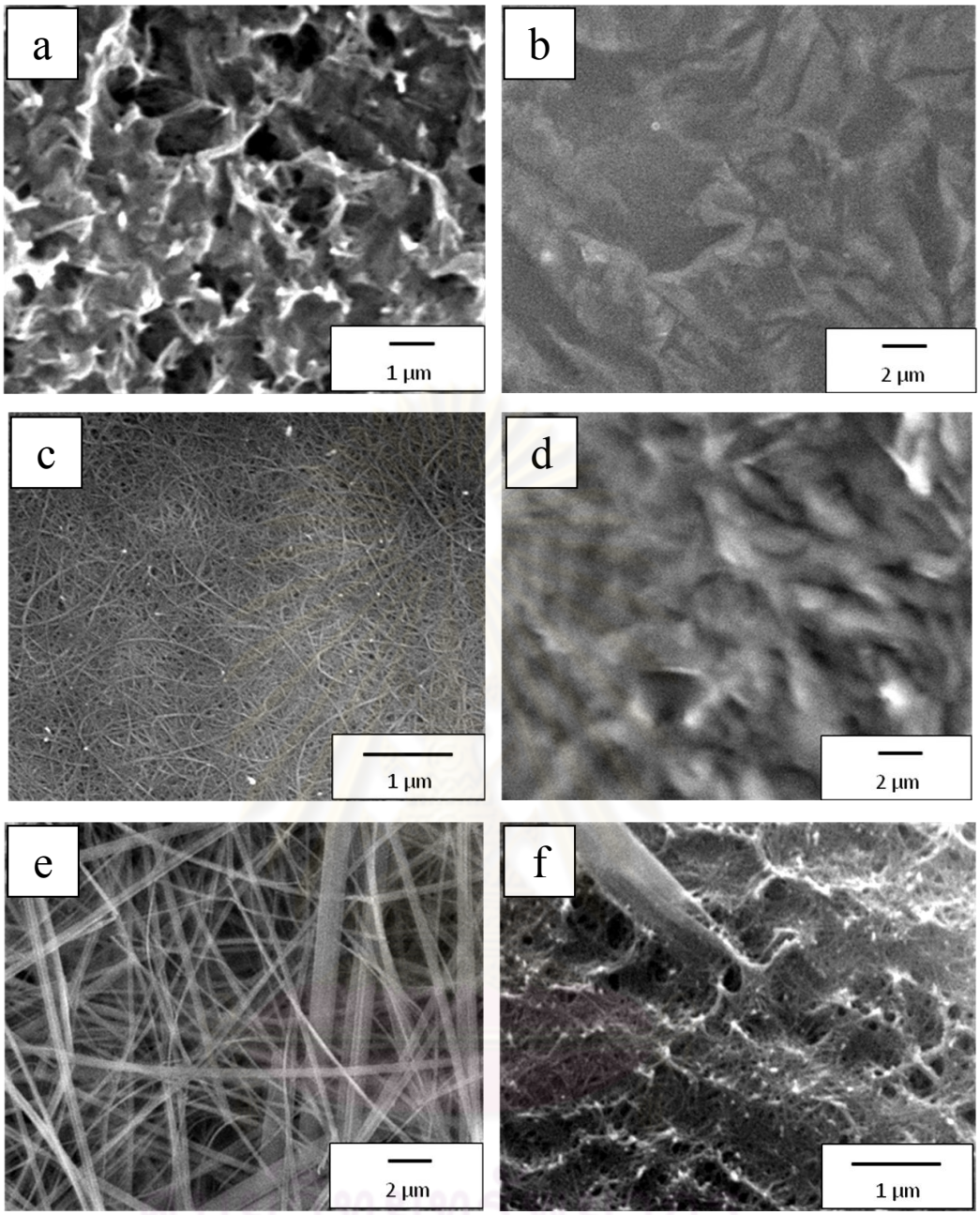

Figure 4.2 SEM images of products from 72 h hydrothermal treatment at 120°C (a,b), 150°C (c,d) and 180°C (e,f). Images on the left were taken from the top most layer, while images on the right were taken after the top layer was peeled off.

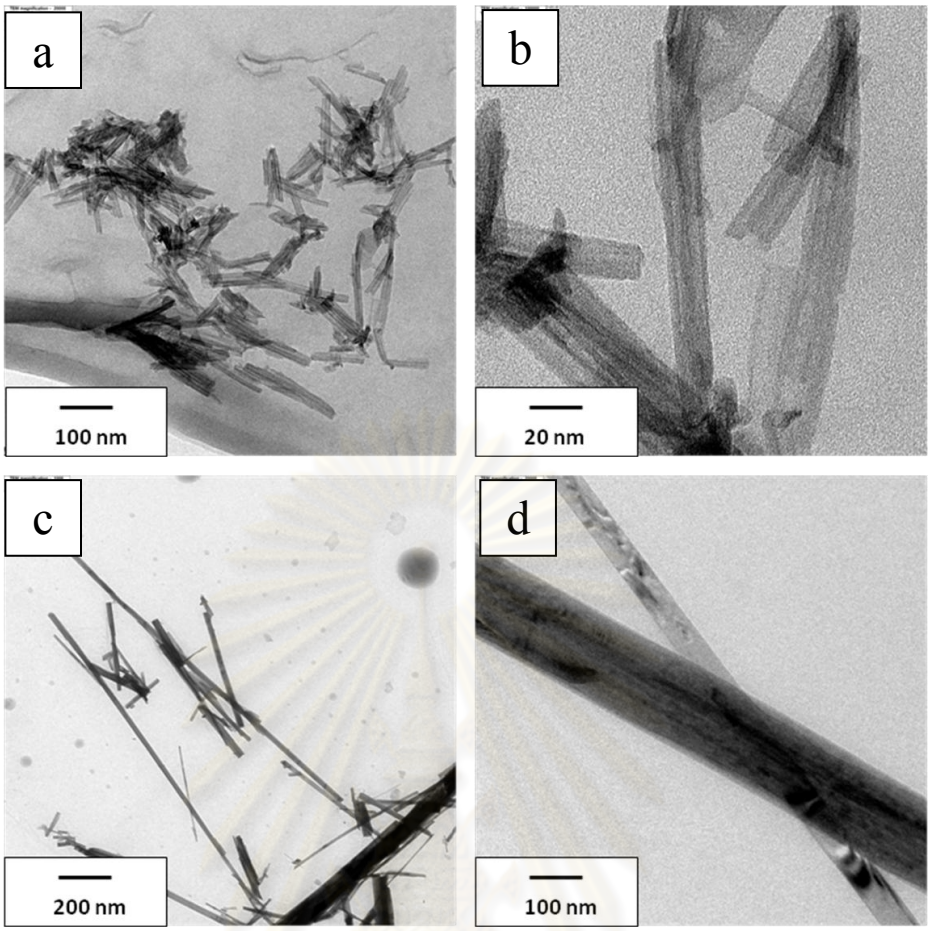

Figure 4.3 TEM images of products from hydrothermal treatment at 150°C for 72 h (a-b) and 180°C for 72 h (c-d).

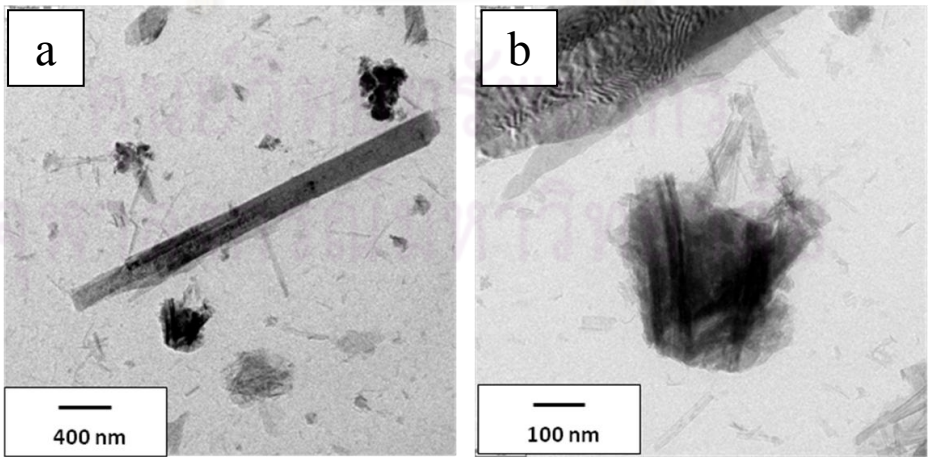

Figure 4.4 TEM images of products from hydrothermal treatment at 180°C for 72 h.

The hydrothermal temperature affects the formation of layers of samples. For the hydrothermal treatment at 120°C, the underneath layer of the sample is relatively smooth (Figure 4.2b). When the hydrothermal temperature is increased to 150°C, the underneath layer of the sample is a rough surface (Figure 4.2d). At the hydrothermal temperature of 180°C, a sponge-like layer consisting of rod-shape particles is formed as a layer, next to the surface of titanium plate (Figure 4.2f). The surface area of the TiO_2/Ti thin film was investigated by nitrogen adsorption measurement. As summarized in Table 4.1, the surface area of the TiO_2/Ti thin film increases as the hydrothermal temperature increased. At high hydrothermal temperature, the reaction is better than at low hydrothermal temperature. When the hydrothermal temperature is increased, the dissolution of the layer of titanium plate is increased. The dissolved titanium reacts with NaOH and is transformed into the layer of sodium titanate. As the thickness of the layer of sodium titanate increases, the surface area increases. The hydrothermal temperature at 180°C results in a product with surface area higher than that obtained from the hydrothermal temperature at 150°C, although the product synthesized at 180°C is large nanofibers while that synthesized at 150°C is small nanofibers. Because the layer of large nanofibers is thicker than the layer of small nanofibers. Normally, the surface area is increased when the pore diameter decreased. However, the results show that the surface area of the product in this work increases, while the pore sized is also increased. This indicates that the thickness of TiO_2 layer has move influence toward the surface area, since the thickness of TiO_2 layer synthesized at high hydrothermal temperature was thicker than the thickness of TiO_2 synthesized at low temperature. The BET adsorption-desorption isotherms from majority of the products showe Type IV which corresponds of mesoporous material. A mesoporous material is a material containing pores with diameters between 2 and 50 nm.

Table 4.1 Surface area of TiO_2/Ti thin film

Hydrothermal temperature (^oC)	Surface area TiO_2/Ti (m^2)	Pore volume (cm^3)	Average pore diameter (nm)
120	0.46	0.0006	4.9799
150	0.71	0.0006	3.5669
72	0.94	0.005	19.52

Sample size: 1×1.5 cm^2

The effect of hydrothermal temperature on phase of the product was studied by varying the period of temperature in oven from 120, 150 and 170 ^oC, respectively. For this parameter, the concentration and volume of NaOH solution were fixed at 10 M and 50 ml, respectively. The obtained product was calcined at 600 ^oC for 2 h. The results are illustrated in Figure 4.5.

Figure 4.5 compares XRD patterns of samples prepared using different hydrothermal temperature. It should be noted that the XRD analysis was done on the as-prepared sample without removing TiO_2 from the titanium plate. In this work, higher intensity of anatase phase is the result from thicker layer of TiO_2 formed on top of the titanium plate, while the decreased in intensity of signal from titanium is the result from titanium is being covered by thicker layer of TiO_2. It is found that the increased hydrothermal temperature induces the increase in intensity of the characteristic peaks of anatase phase. It could be interpreted that the layer of anatase is formed on top of the titanium plate. The layer of anatase becomes thicker as the hydrothermal temperature progresses. When TiO_2 is removed from titanium plate by polishing, it is found that the intensity of the characteristic peaks of anatase phase is decreased while the intensity of the characteristic peaks of rutile phase remains unchanged (Figure 4.6). For the bare titanium plate calcined at 600 ^oC, it shows the characteristic peaks of rutile phase and titanium plate. Therefore, the characteristic peaks of rutile detected from the synthesized products and suggested to be the result from the oxidation of titanium plate itself during the calcination at 600 ^oC.

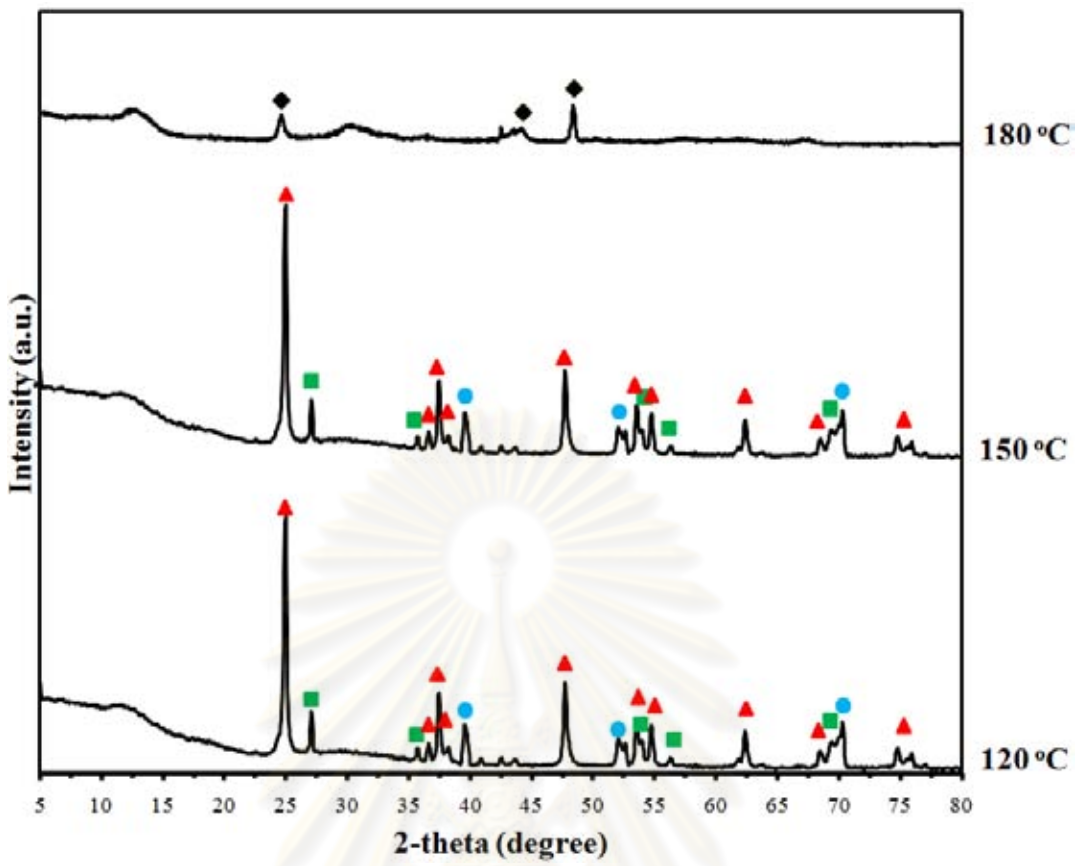

Figure 4.5 XRD patterns of products synthesized by hydrothermal treatment in NaOH at different hydrothermal temperature for 72h, and subsequently calcined at 600°C; ● titanium, ▲ anatase, ■ rutile , ◆ unidentified.

Table 4.2 Content of anatase phase in the product synthesized at different hydrothermal temperature.

Hydrothermal temperature (°C)	Anatase content (%)	Rutile content (%)
120	57	43
150	78	22
180	-	-

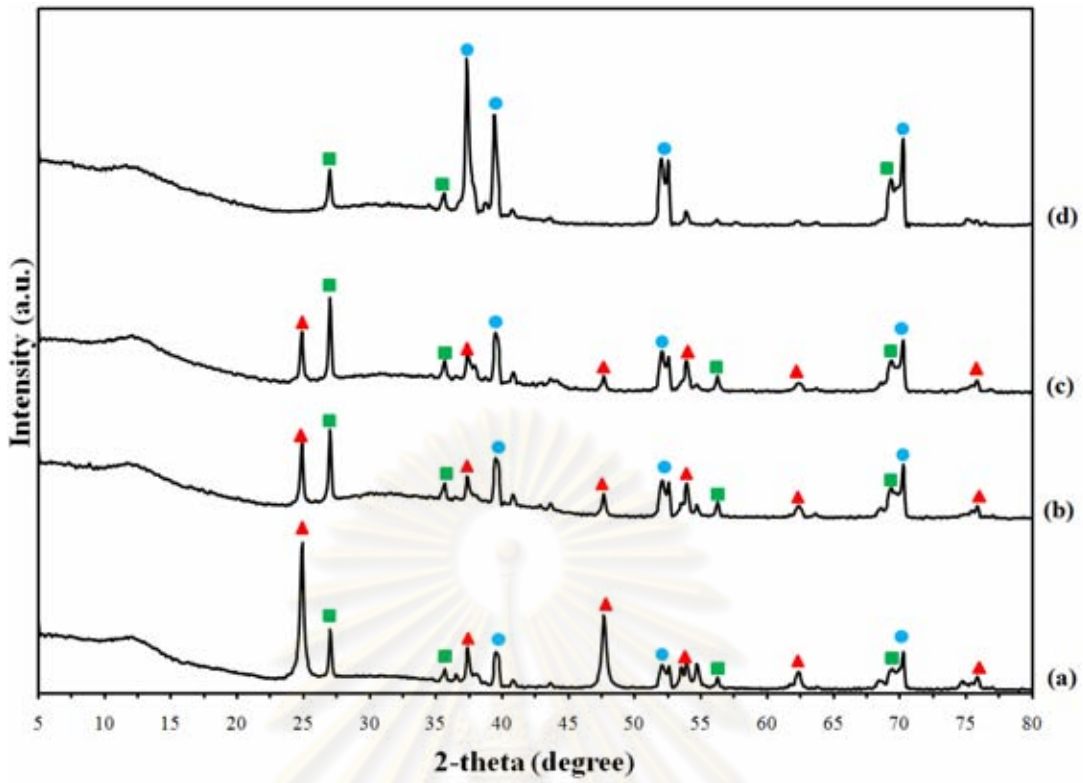

Figure 4.6 XRD patterns of products synthesized by hydrothermal treatment in NaOH at 180 °C for 24 h, and subsequently calcined at 600 °C. The obtained product (a) was polished for 1 time (b) and 2 times (c) before being analyzed by XRD. The results are compared with the pattern obtained from a bare titanium plate calcined at 600 ^{o}C (d)
; ● titanium, ▲ anatase, ■ rutile.

The hydrothermal treatment at 180°C for 72 h was studied further for its mechanism by stripping the top layer of the product from the titanium plate after 60 h of the hydrothermal. The top layer of titanate and the titanate on the plate were further hydrothermally treated at 180°C for another 12 h to complete the hydrothermal time of 72 h. after the hydrothermal treatment at 180°C for 60 h, a layer of pale white product is formed on the titanium plate. However, this layer is not uniform. Collection of white fluffy spots are formed Sparsingly on the layer. These white fluffy spots are formed to be sub-micrometered fibers (Figure 4.7a). The rest of the product are nanofibers formed on the surface of titanium plate (Figure 4.7b). As mentioned earlier, the top layer, i.e. the white fluffy products, was removed from the plate and

subjected to hydrothermal treatment for another 12 h, while the rest of the plate was treated separately for the same period of time. The product obtained from additional 12 h treatment of the titanium plate is also formed to be similar to that of the plate treated for 60 h, i.e., a layer of plate white product is formed together with white fluffy spots. Their morphologies are shown in Figure 4.7c and 4.7d, respectively. The large nanofibers originally formed from the hydrothermal treatment at 180°C for 60 h (Figure 4.7a) are longer than the nanofibers obtained after additional 12 h of the hydrothermal treatment (Figure 4.7d). Due to the hydrothermal time of synthesis was long time. So the short large nanofibers formed form nanofibers, then long large nanofibers formed form short large nanofibers. on the other hand, the product from the additional treatment of the top layer, which was scraped off from the titanium plate treated for 60 h, is found to remain as fibers (Figure 4.7e). The top layer from hydrothermal treatment at 180°C for 60 h of additional synthesis at hydrothermal time at 12 h (figure 4.7e) had not thicked because not had nanofibers for fromed large nanofibers.

ศูนย์วิทยทรัพยากร
จุฬาลงกรณ์มหาวิทยาลัย

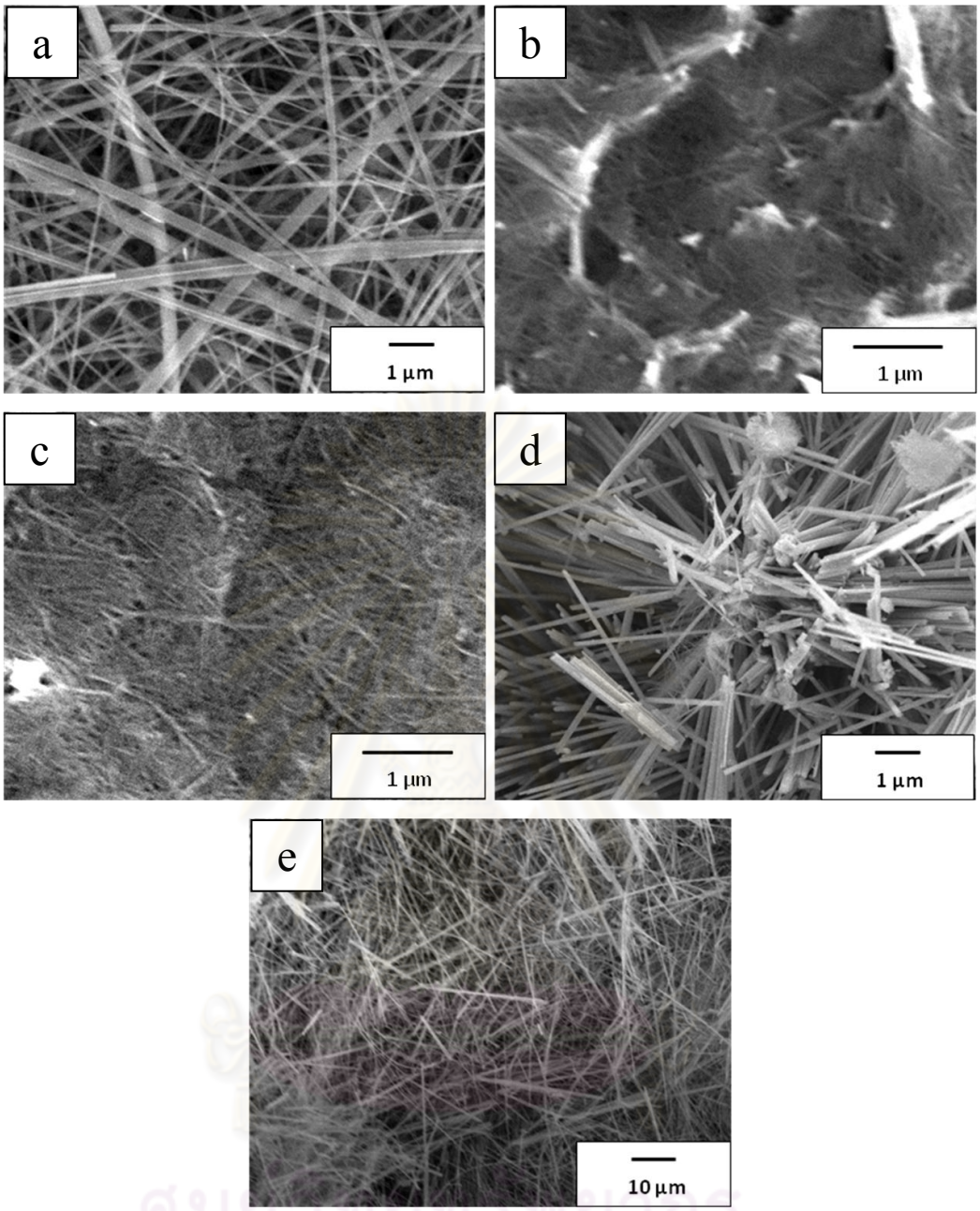

Figure 4.7 SEM images of products from hydrothermal treatment at 180 °C for 60 h (a,b) and products from 12 h additional hydrothermal treatment of the titanium plate (c,d) and that of the top layer scraped off from the product hydrothermally treated for 60 h was (e).

4.1.3 Effect of hydrothermal time

The effect of hydrothermal time was studied by varying the period of time in oven from 3, 6, 9, 12, 48, 60, 66 and 72 h, respectively. For this parameter, the concentration and volume of NaOH solution were fixed at 10 M and 50 ml, respectively The results are illustrated in Figure 4.8.

Figure 4.8 shows SEM micrographs of the samples synthesized by hydrothermal at 180°C for various periods of time. It should be noted that surface of titanium plate before the treatment was relatively smooth. After 3 h of hydrothermal treatment, a sponge-like layer consisting of rod-shape particles is formed on the surface of titanium plate (Figure 4.8a). When the hydrothermal time is increased to 6 h (Figure 4.8b), the rods appeared longer than that observed in Figure 4.8a. For 9 h of the hydrothermal treatment, diameters of the rods were decreased, while the length increases dramatically (Figure 4.8c), becoming nanofibers. The nanofibers were clearly observed on the surface of the titanium plate after the 12 h treatment (Figure 4.8d). The morphology of the products remains unchanged during the period of hydrothermal treatment of 12-60 h (Figure 4.8e-f). However, after 60 h of the treatment, large nanofibers are observed (Figure 4.8g-h). By the naked eyes, thick layer of the white product was formed on the titanium plate more uniformly as the hydrothermal time is prolonged from 66 to 72 h. The large nanofibers are observed on the titanium plate, which is a result from aggregation of nanofibers which grow independently during the hydrothermal synthesis (see Figure 4.3).

ศูนย์วิทยทรัพยากร
จุฬาลงกรณ์มหาวิทยาลัย

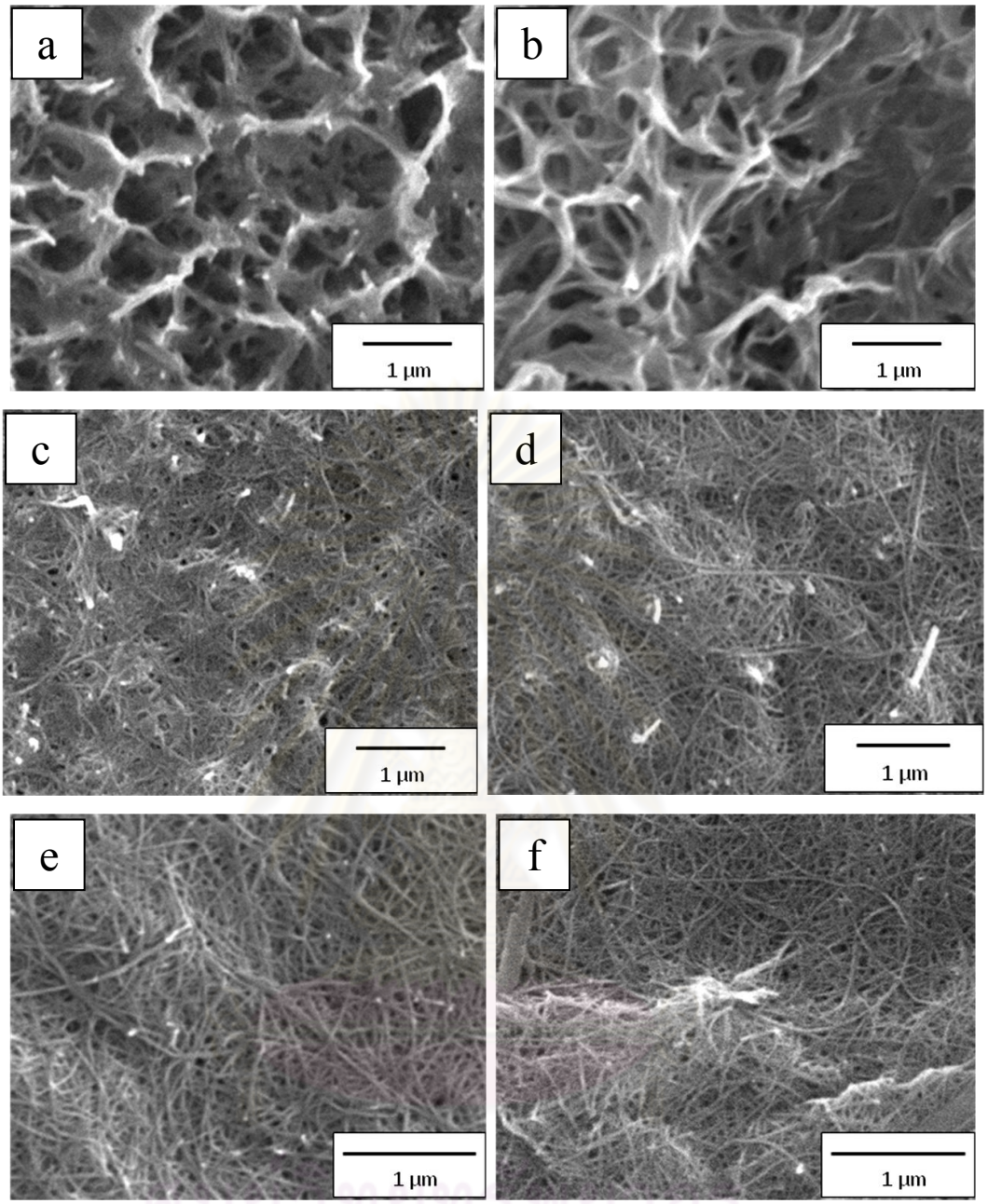

Figure 4.8 SEM images of products from hydrothermal treatment at 180 °C for 3 h (a), 6 h (b), 9 h (c), 12 h (d), 48 h (e), 60 h (f), 66 h (g) and 72 h (h).

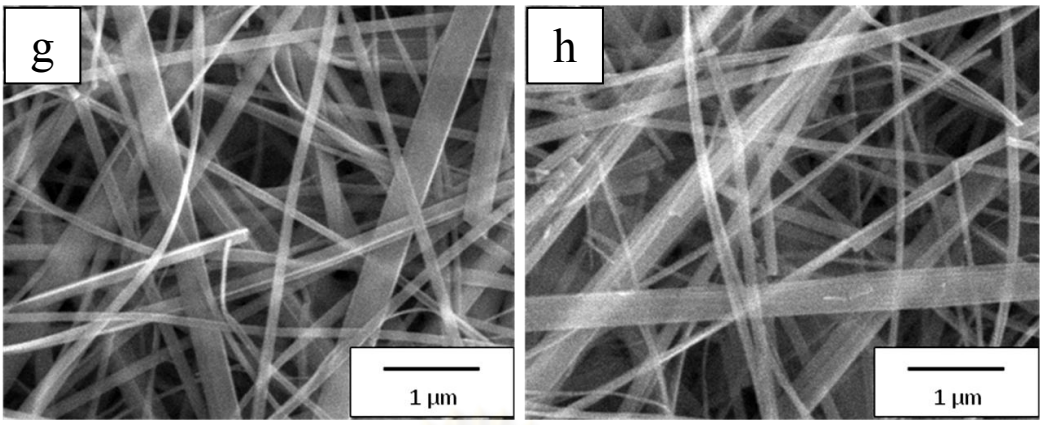

Figure 4.8 (continued)

For the product that is hydrothermal treated in NaOH at different time, the layer of the samples formed on the surface of titanium plate is different. When the hydrothermal time is increased, the thickness of the layers increases. At 3h-treatment, the sample is consisted of one layer. A spong-like layer consisting rod-shape particles is formed on the surface of titanium plate (Figure 4.9a). When, the hydrothermal is increased to 48 h. The layers of the sample are consisted of two layers, i.e., irregular aggregates of thin nanocrystals formed next to the surface of titanium plate (Figure 4.9d) and nanofibers formed as a top layer (Figure 4.9c). For 66 h, the sample is consisted of three layers. Irregular aggregates of thin nanocrystals are formed into a bottom layer, next to the surface of titanium plate (Figure 4.9g). In the middle layer, much larger crystals, in form of short nanofibers are found (Figure 4.9f). Their size was much larger than that of the crystals in the bottom layer. Finally, as the top layer, very long nanofibers are found (Figure 4.9e). As summarized in Table 4.3, the surface area of the TiO_2/Ti thin film increases as the hydrothermal time is increased. That might be the result from the increase in the thickness of the coated layer. This result agrees with the report by Gou et al. [19]. However, for the product synthesized by hydrothermal treatment for 48 h, the surface area is rather small, since the fibers formed grow into large fiber on the titanium plate. On the other hand, the hydrothermal time of 72 h results in product with high surface area because the layer of large fiber was much thicker than the layer of nanofibers. When the hydrothermal is time increased, the reaction of the TiO_2 thin film formed on the titanium plate was good.

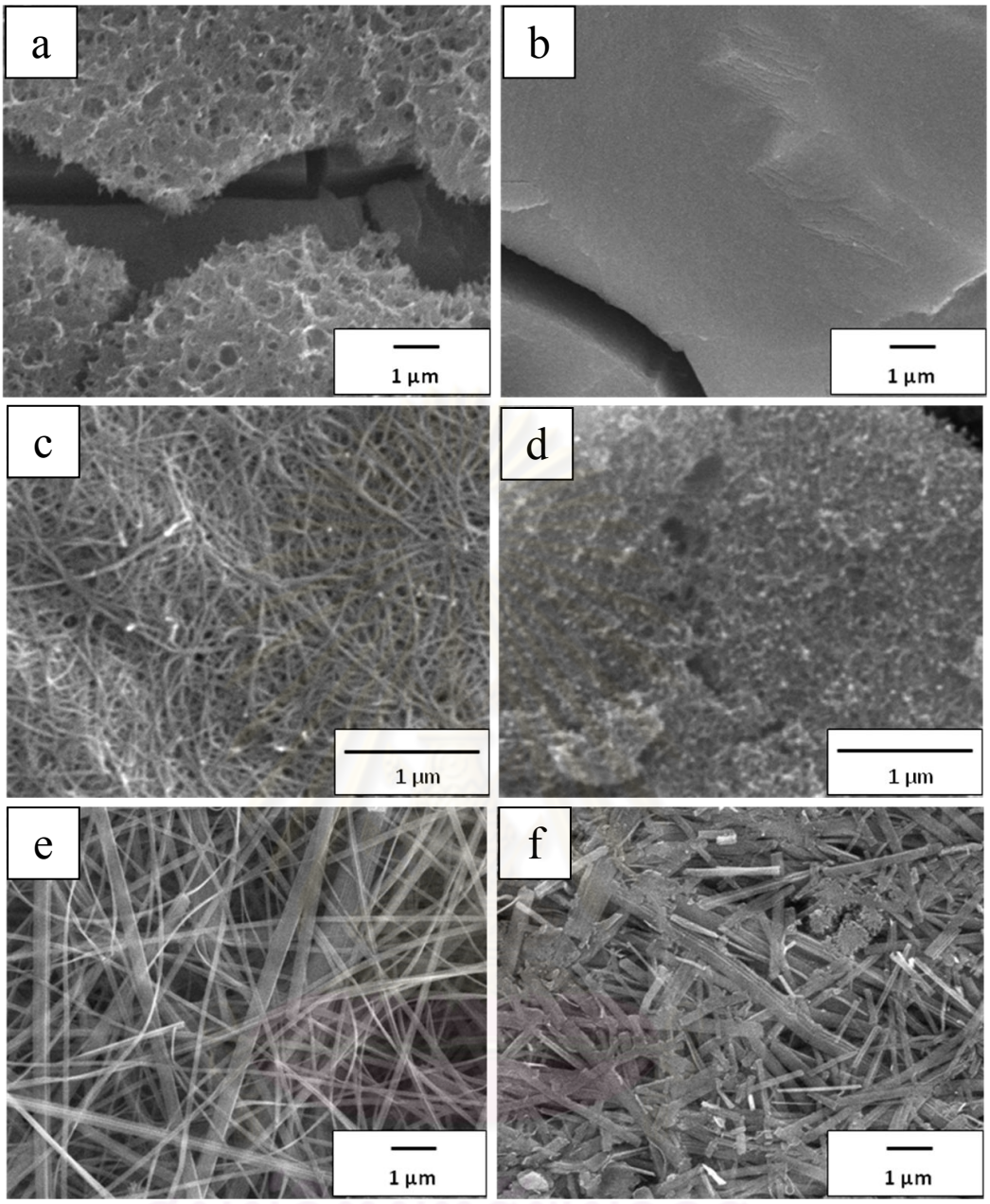

Figure 4.9 SEM images of each layer consisting of the products from hydrothermal treatment at 180 ^{o}C for 3 h, i.e., top (a) and bottom (b) layers, for 48 h, i.e., top (c) and bottom (d) layers, for 66 h, i.e., top (e), middle (f) and bottom (g) layers.

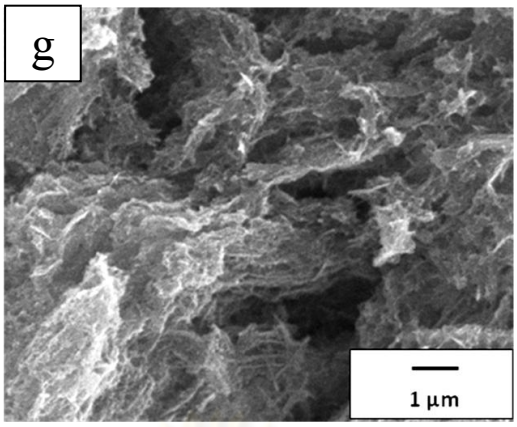

Figure 4.9 (continued)

Table 4.3 Surface area of TiO_2/Ti thin film

Hydrothermal time (h)	Surface area TiO_2/Ti (m^2)	Pore volume (cm^3)	Average pore diameter (nm)
3	0.2	0.0003	0.56
9	0.24	0.0002	5.3512
12	0.68	0.0001	7.6271
24	1.17	0.0002	6.5005
48	1.36	0.0006	13.498
72	0.94	0.005	19.52

Sample size: 1×1.5 cm^2

The effect of hydrothermal time for phase of product was studied by varying the period of temperature in oven from 3, 9, 12, 24, 48, 60, 66 and 72 h respectively. For this parameter, the concentration and volume of NaOH solution were fixed at 10 M and 50 ml, respectively. The samples were subsequently calcined at 400°C for 2 h. The results are illustrated in Figure 4.10.

Figure 4.10 compares XRD patterns of samples prepared using different hydrothermal time. It is found that the increased hydrothermal time induces the increase in intensity of the characteristic peaks of anatase phase, while that for titanium is decreased. It could be interpreted that the layer of anatase is formed on top of the titanium plate. The layer of anatase becomes thicker as the hydrothermal treatment progresses. The crystallinity of anatase phase is also improved by the prolonged hydrothermal time, as witnessed from the increased in intensity of the XRD signals. At the hydrothermal time of 60 h, peaks attributed to rutile phase are also observed. It should be noted that rutile has been known to be transformed from anatase phase. Therefore, it is suggested that anatase within the product synthesized by hydrothermal treatment for 60 h has lowered thermal stability, comparing with the products synthesized for shorter period of time, such that it could easily be transformed into rutile during calcination at 400°C. The most interesting feature comes from the product synthesized using very long period of hydrothermal treatment (i.e., 66 and 72 h). These products mostly remain as amorphous phase even after calcination. At the hydrothermal treatment at 180°C for 66 h - 72 h, the XRD pattern of the product does not match with either anatase or rutile. At this point, phase of the product from the hydrothermal treatment at 180°C for 66 h – 72 h was unidentified. Therefore, the reason why the product synthesized at 180°C for 72 h and calcined at 400°C does not show XRD peak was undetermined. It is found that the decreased in hydrothermal time induces the increase in intensity of the characteristic peaks of anatase phase, while that for rutile phase is decreased (Table 4.4). When the hydrothermal time is increased, anatase could easily be transformed into rutile during calcination at 600°C. As the hydrothermal time is increased, the thermal stability of the product decreases. This result is confirmed by XRD analysis of samples that were polished to remove the layer of TiO_2 synthesized by hydrothermal treatment at 180°C for 24 h on the titanium plate. When TiO_2 is polished from the titanium plate, decrease in intensity of the characteristic peaks of anatase phase and increase in intensity of the characteristic peaks of titanium phase (Figure 4.12) are observed.

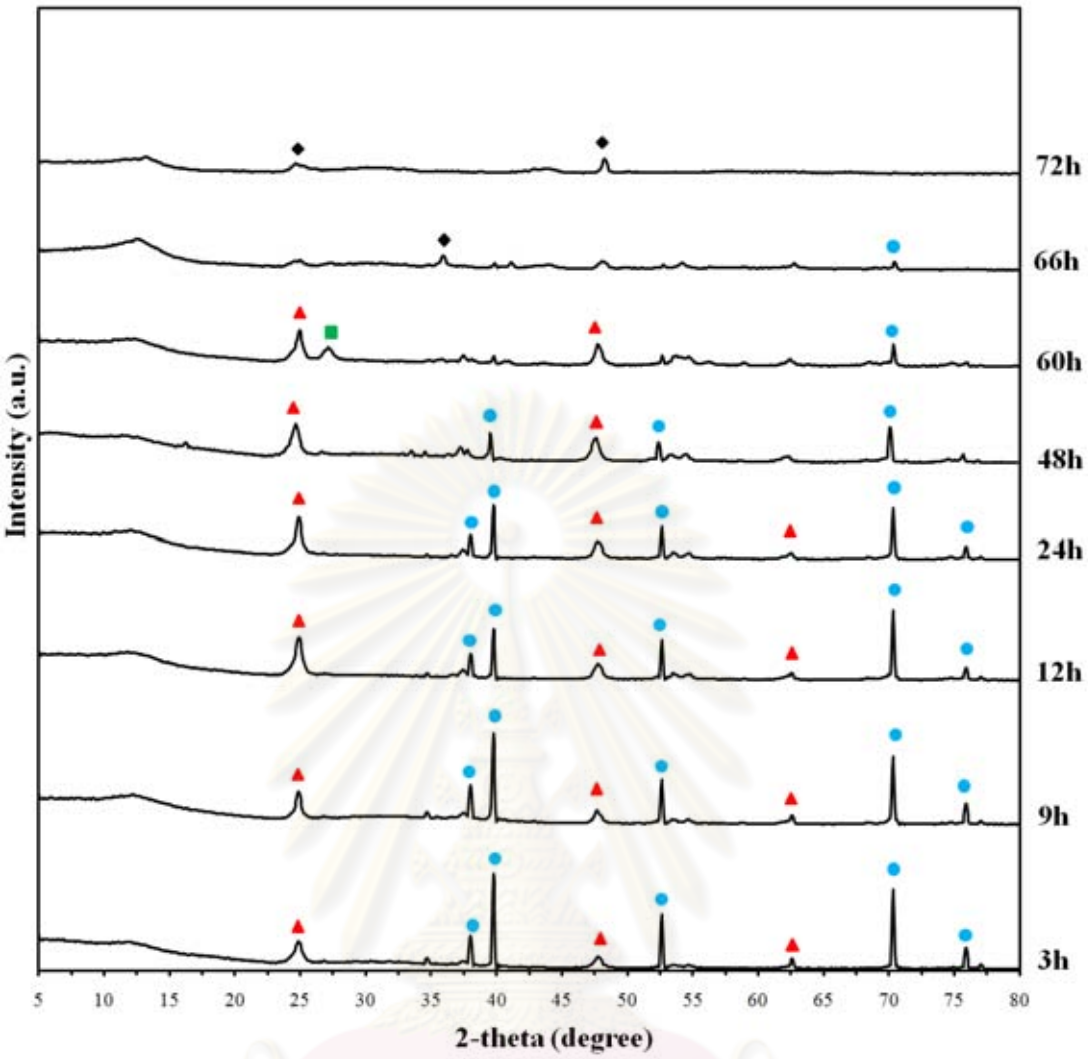

Figure 4.10 XRD patterns of products synthesized by hydrothermal treatment in NaOH at 180 °C for different period of time, and subsequently calcined at 400 °C; ● titanium, ▲ anatase, ■ rutile, ◆ unidentified.

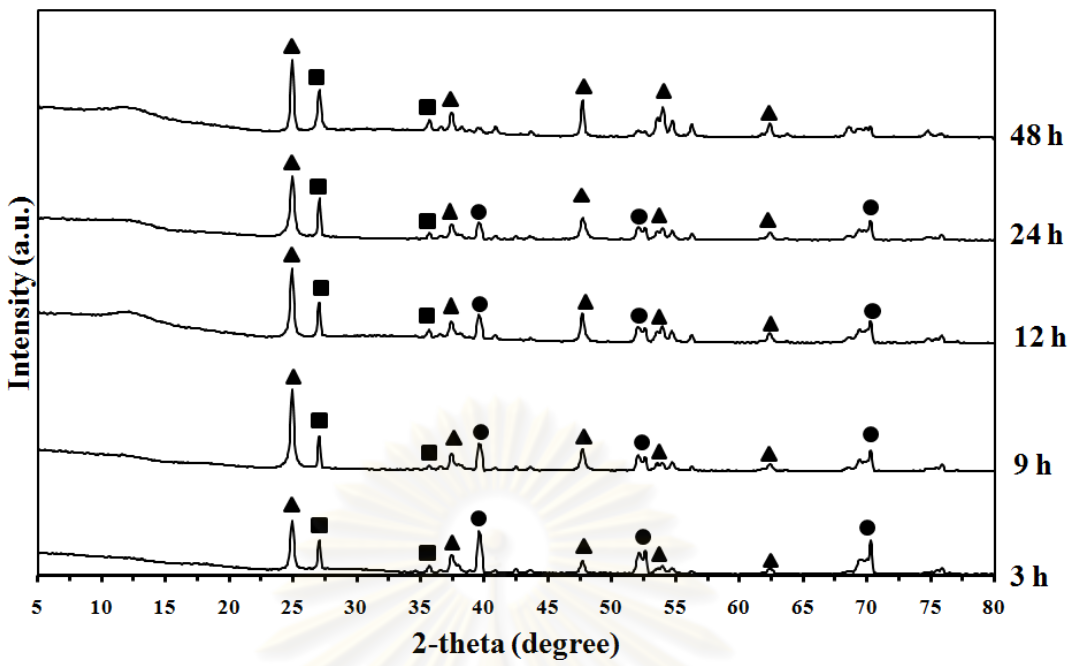

Figure 4.11 XRD patterns of products synthesized by hydrothermal treatment in NaOH at 180°C for different period of time, and subsequently calcined at 600°C; ● titanium, ▲ anatase, ■ rutile.

Table 4.4 Anatase content (%) of products synthesized by using different hydrothermal time

Hydrothermal time (h)	Anatase content (%)	Rutile content (%)
3	73.2	26.8
9	66.7	33.3
12	61.8	38.2
24	59.2	40.8
48	58.8	41.2

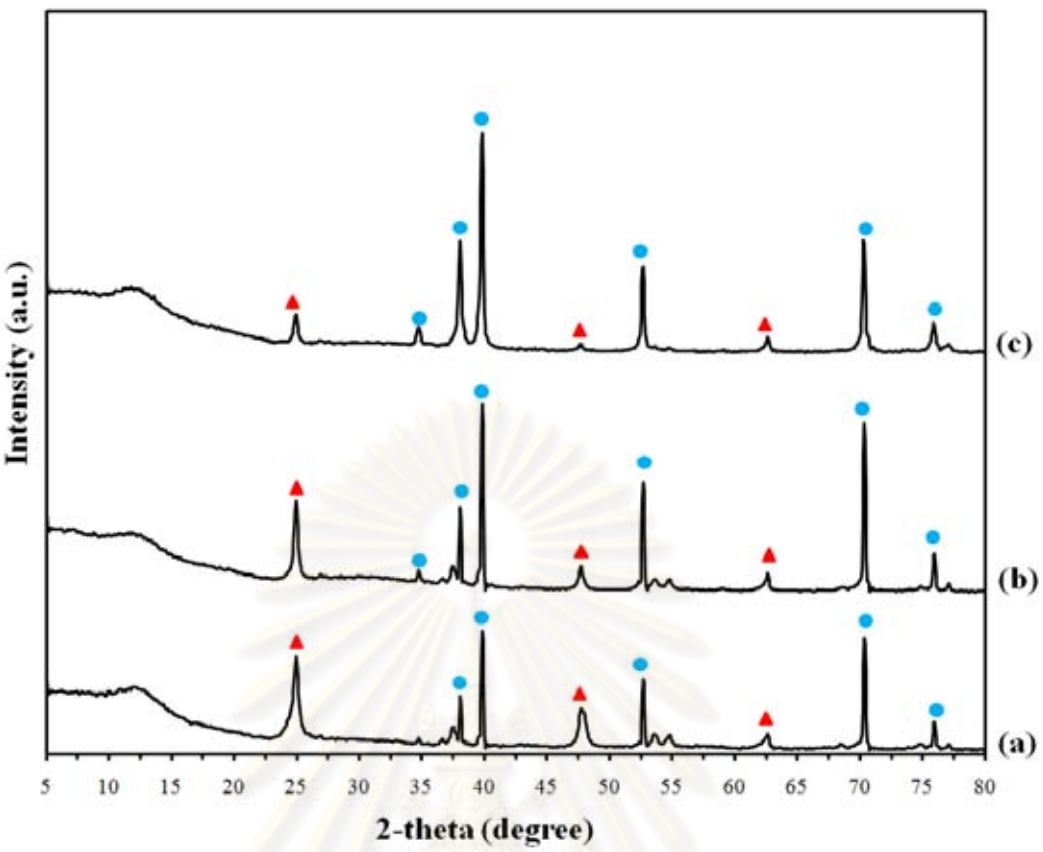

Figure 4.12 XRD patterns of products synthesized by hydrothermal treatment in NaOH at 180 °C for 24 h, and subsequently calcined at 400 °C. The obtained product (a) was polished for 1 time (b) and 2 times (c) before being analyzed by XRD; ● titanium, ▲ anatase, ■ rutile.

4.1.4 Effect of calcination temperature

The effect of temperature of calcination for morphology and structure of TiO_2 thin film on titanium plate was studied by varying the calcinations temperature of hydrothermal treatment at 180 ^{o}C for 48 h. For this parameter, the concentration and volume of NaOH solution were fixed at 10 M and 50 ml, respectively The results are illustrated in figure 4.14.

When the temperature of calcination, the morphology of the TiO_2 thin film on titanium plate is changed, by the SEM images, nanotubes calcined at 600°C started deformation (Figure 4.14c). But figure 4.16 TEM images, nanotubes of product

calcined started aggregates wherein nanoparticles. But nanofibers were structure preservation (Figure 4.15 d,f,h). At lower calcination temperature, the dehydration of intralayered OH groups caused a little change in the nanotube morphology while resulted in some defects presenting in the nanotube. When the calcination temperature was high, the dehydration of interlayered OH groups resulted in the gradual decrease in the interlayer distance of the nanotubes (Figure4.13) and the transformation into lotus-root-like structure (Figure 4.14c-d), at the same time, previously formed defects transformed into amorphous nanoparticles attached to the nanorod [29]. Then, the temperature of calcinations affected the morphology and structure of TiO_2 thin film on titanium plate.

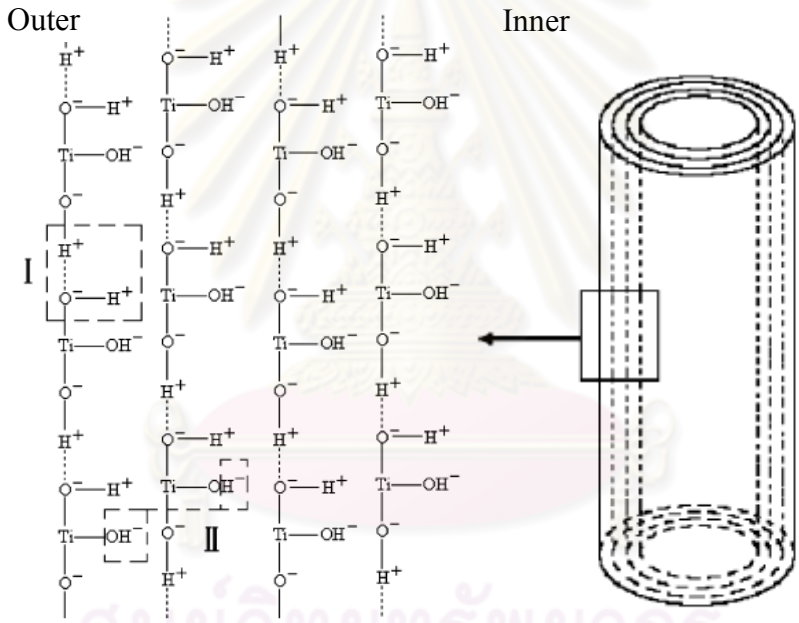

Figure 4.13 Schematic diagram of layered composition (*X–Y* section) of nanotubed $H_2Ti_2O_4(OH)_2$.

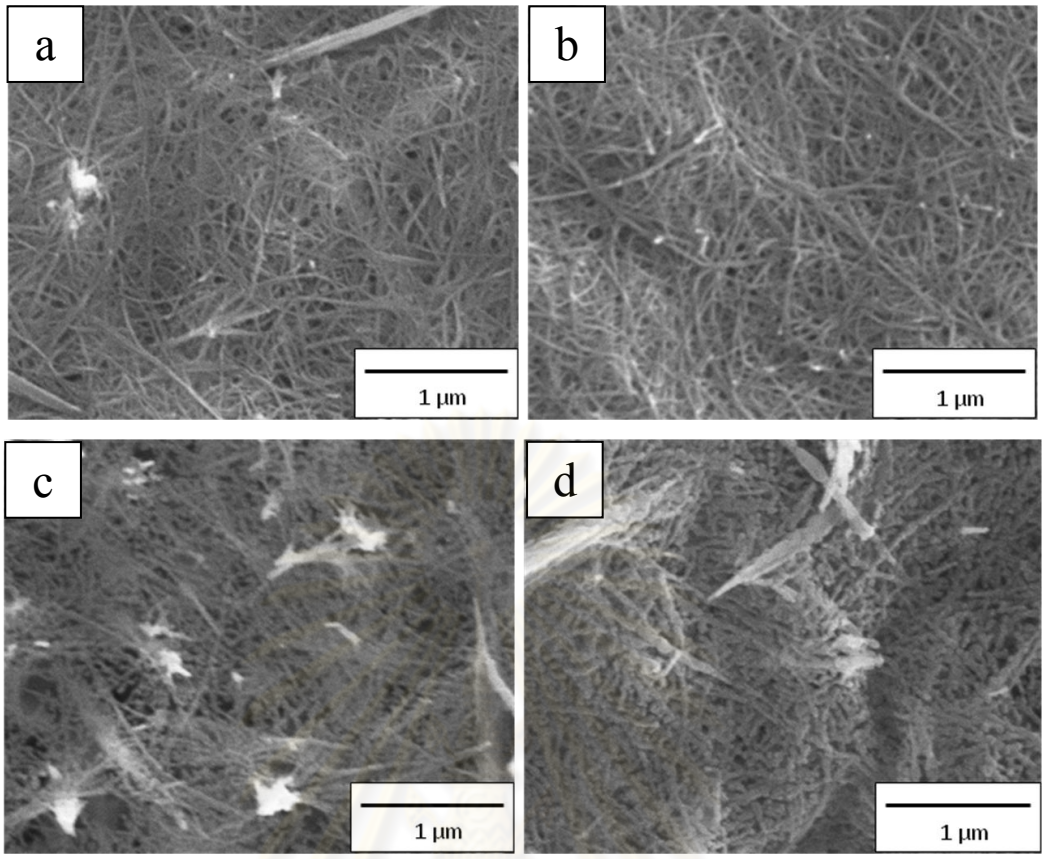

Figure 4.14 SEM images of products from hydrothermal treatment at 180 °C for 48 h before (a) and after calcination at 400°C (b), 600 (c) and 800 °C (d)

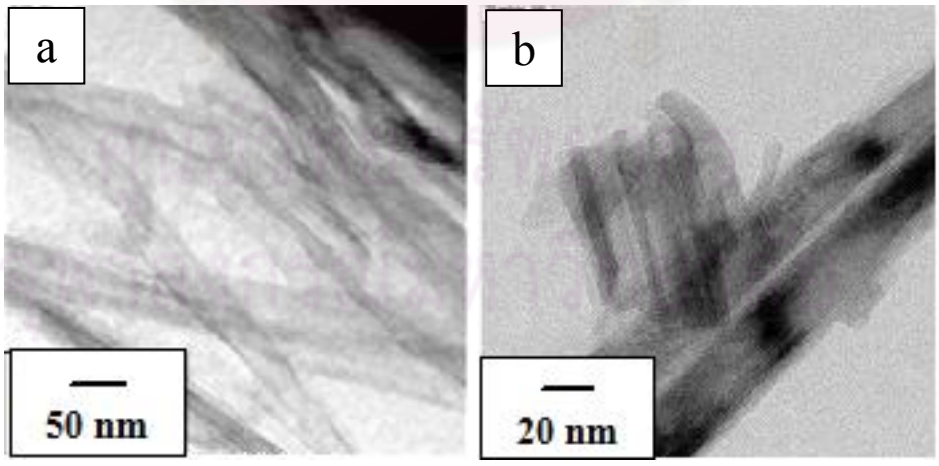

Figure 4.15 TEM images of products from hydrothermal treatment at 180 °C for 48 h before (a,b) and after calcination at 400 (c,d), 600 (e,f) and 800 °C (g,h)

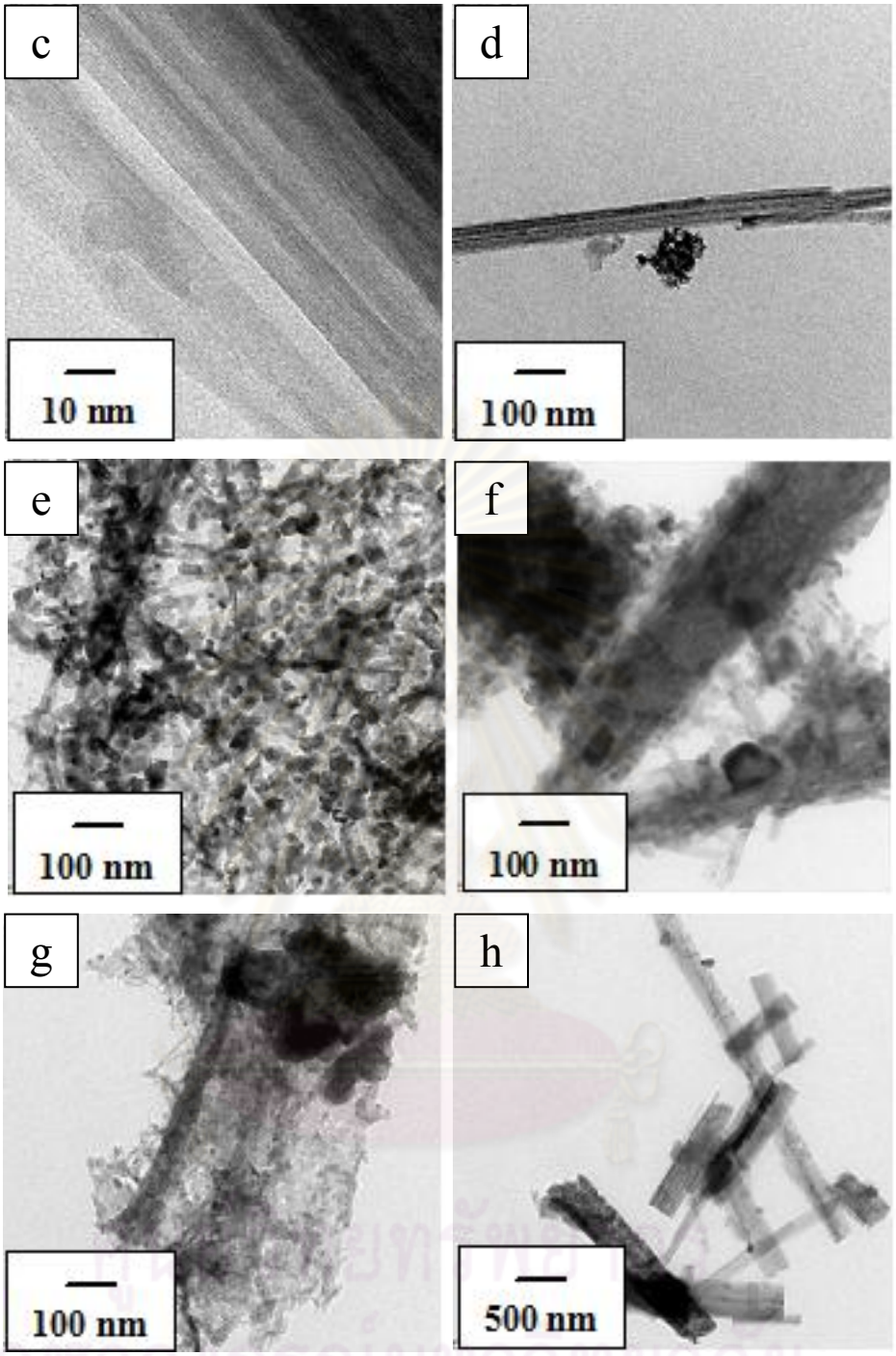

Figure 15. (continued)

The effect of calcination temperature on anatase phase was studied by varying the calcination temperature for the sample prepased by hydrothermal treatment at 180 ^{o}C for 48 h. For this parameter, the concentration and volume of NaOH solution were

fixed at 10 M and 50 ml, respectively. The results are illustrated in Figure 4.16 and 4.17.

Figure 4.17 shows comparison of the XRD patterns of samples synthesized at 180°C for 48 h calcined at different temperature. When the temperature of the calcinations is increased, it induces the increase in intensity of the characteristic peak of rutile. At 600°C, the intensity of anatase was maximum. The phase transformation from anatase to rutile phase can occur when calcination at 600°C. Then, as the calcination temperature increased, the thermal stability is decreased.

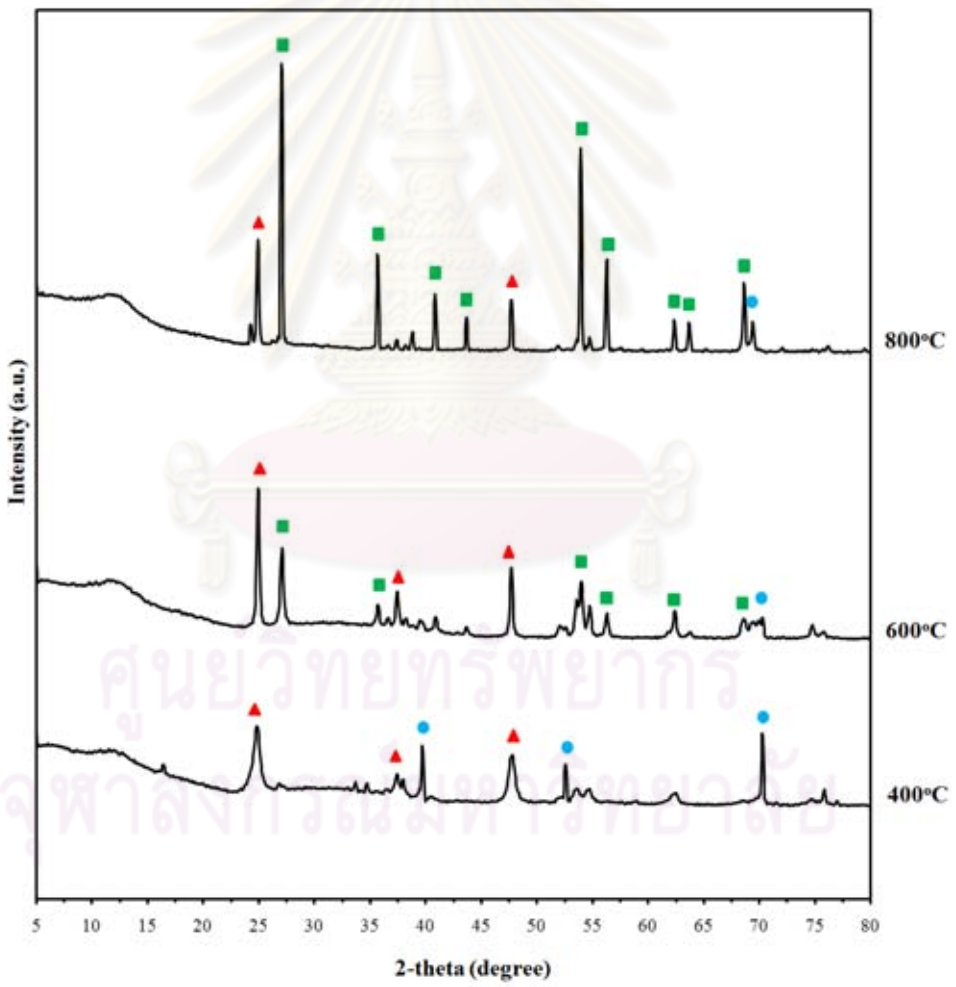

Figure 4.16 XRD patterns of products synthesized by hydrothermal treatment in NaOH at 180 °C for 48 h, and subsequently calcined at 400, 600 and 800 °C; ● titanium, ▲ anatase, ■ rutile.

Figure 4.18 shows comparison of the XRD patterns of samples synthesized at 180°C for 3 h calcined at different temperature. When the temperature of the calcinations is increased, it induces the increase in intensity of the characteristic peak of rutile. At 800°C, the intensity of anatase was maximum. It is found that the increased hydrothermal time induces the increase in intensity of the characteristic peaks of rutile phase, while that for titanium is decreased. Therefore, the characteristic peaks of rutile detected from the synthesized products and suggested be the result form the oxidation of titanium plate itself during the calcination.

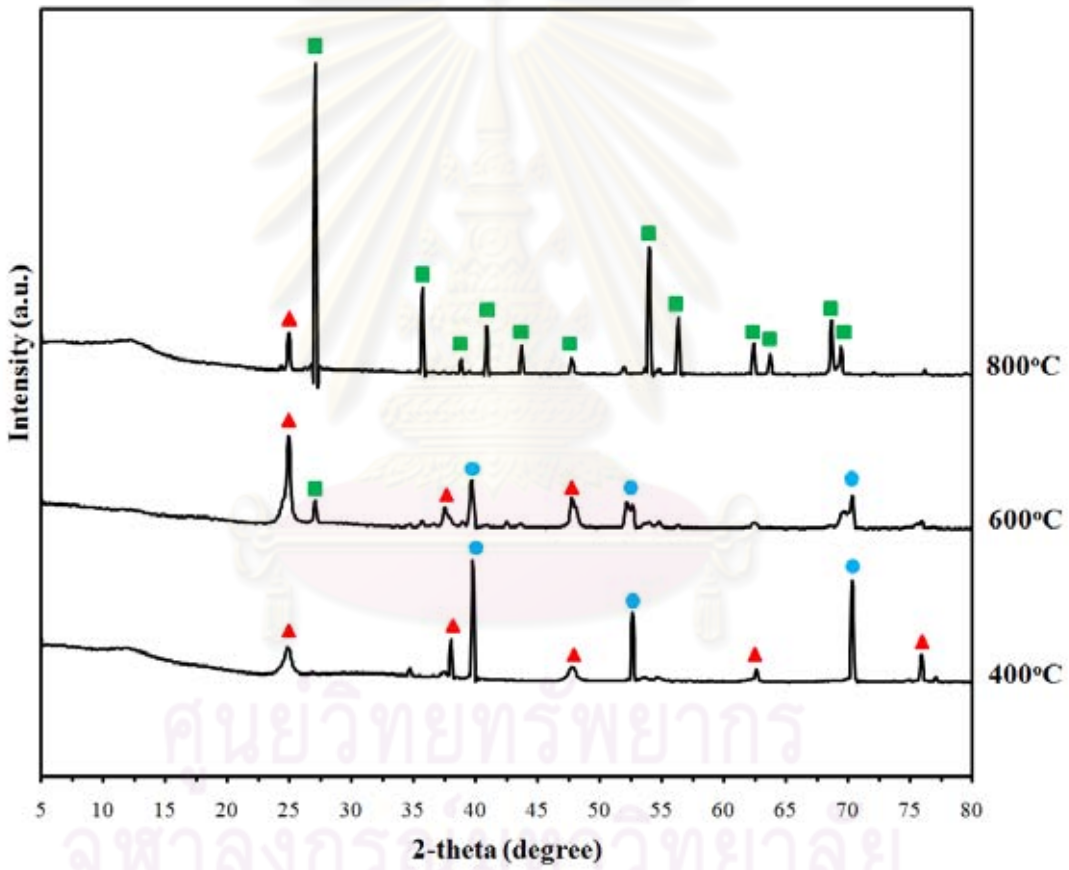

Figure 4.17 XRD patterns of products synthesized by hydrothermal treatment in NaOH at 180°C for 3h, and subsequently calcined at 400, 600 and 800°C. ; ● titanium, ▲ anatase, ■ rutile.

4.2 Photocatalytic on the synthesized product

4.2.1 Photocatalytic degradation of methylene blue

4.2.1.1 The effect of hydrothermal temperature

The effect of hydrothermal temperature on the photocatalytic degradation of methylene blue was studied. TiO_2 on titanium plate was prepared by varying the temperature of oven from 120, 150 and 180°C for 72 h, respectively. For the study of this parameter, the TiO_2 thin film tests with the methylene blue solution at 5 ppm. Flow rate of the methylene blue solution was fixed at 5.4 mL/h. The results are illustrated in Figure 4.18.

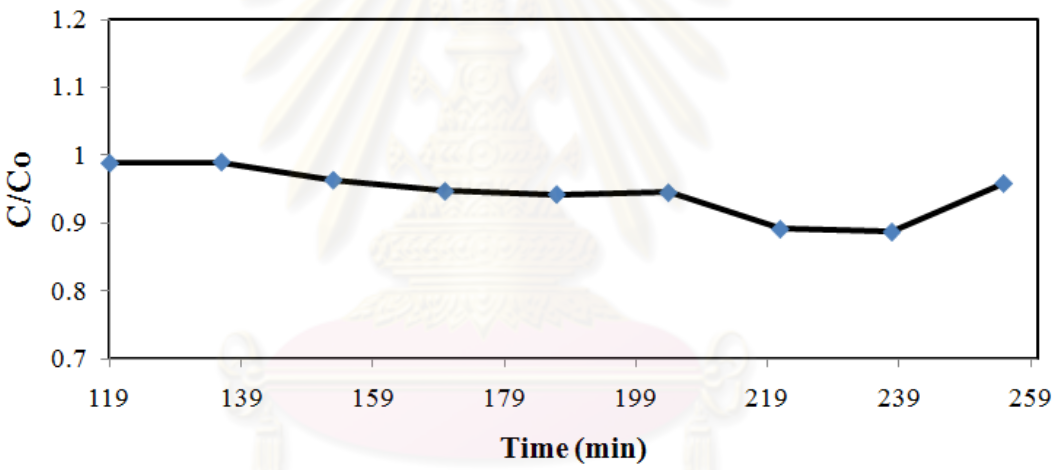

(a)

Figure 4.18 Photolysis degradation of methylene blue (a) comparing with the photocatalytic degradation on TiO_2/Ti plate synthesized at 120 (b), 150 (c) and 180°C (d).

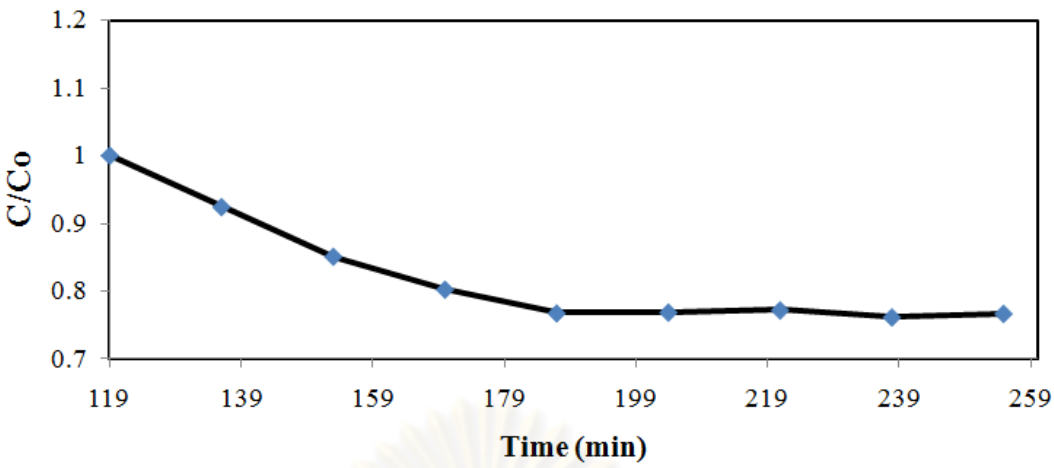

(b)

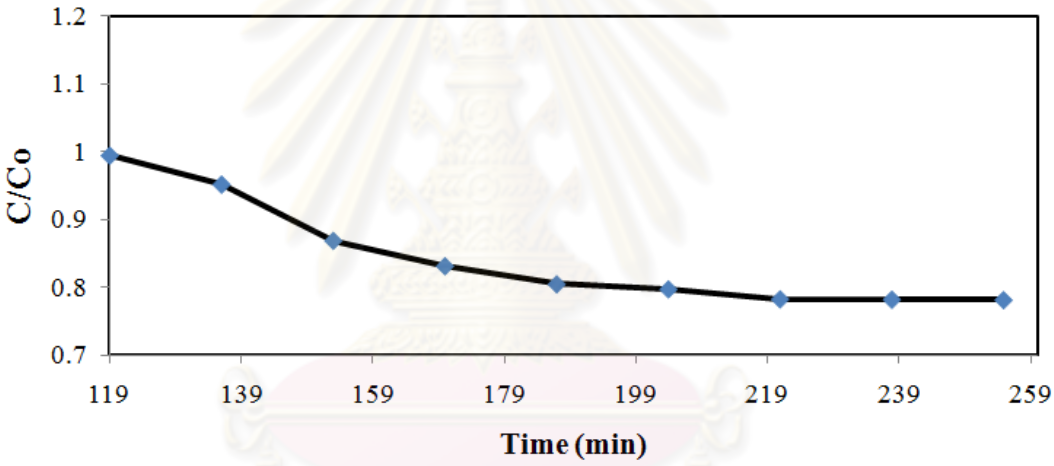

(c)

Figure 4.19 Continued

ศูนย์วิทยทรัพยากร
จุฬาลงกรณ์มหาวิทยาลัย

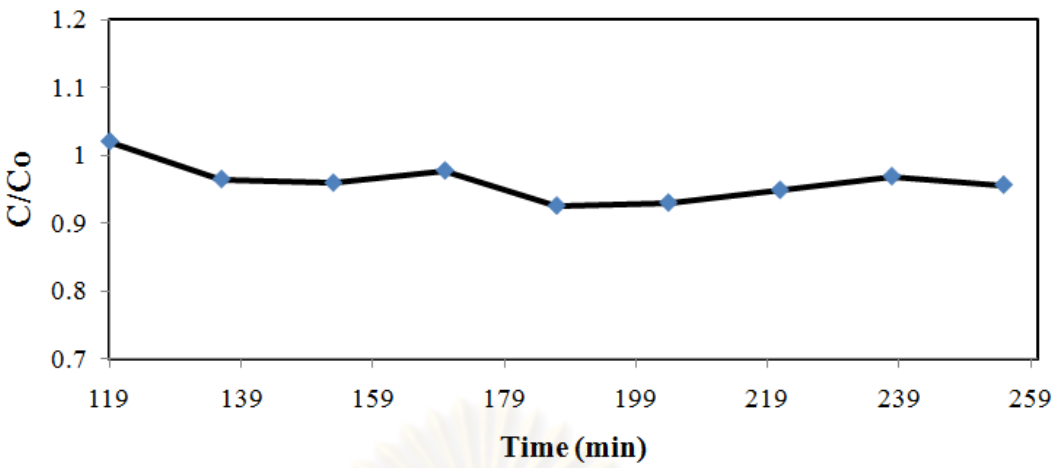

(d)

Figure 4.19 Continued

Figure 4.19 shows the percentage of methylene blue degradation on titania that was synthesized using of different hydrothermal time. The residence time in the reaction system, i.e. a micro reactor, was kept at 5 min. When the hydrothermal temperature is increased, the percentage of methylene blue degradation decreases. The product synthesized at 120°C has anatase content less than that in the product synthesized at 150°C (Table 4.2). However, the photocatalytic activity toward methylene blue degradation of the product synthesized at 120°C is higher. As the product synthesized at 120°C has surface roughness than the product synthesized at 150°C. An increase in the surface roughness leads to an increase in the surface are.

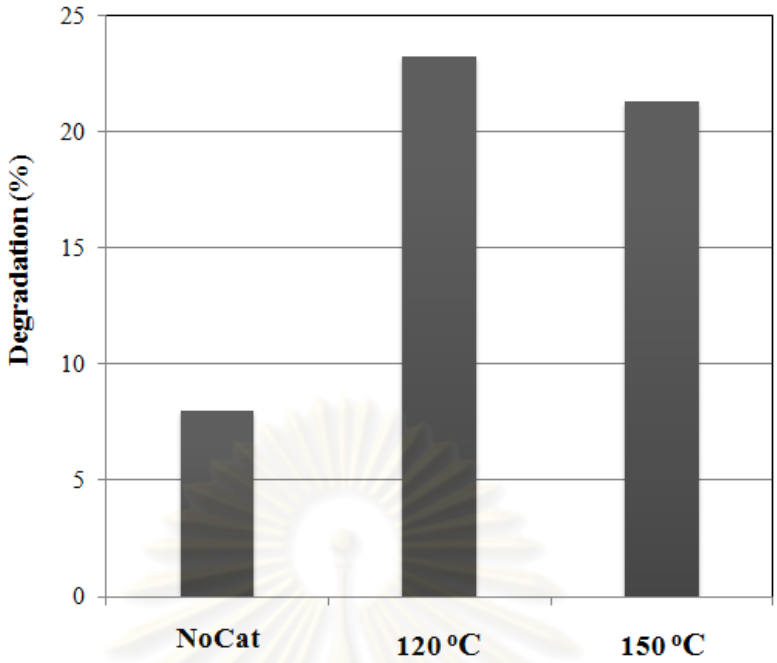

Figure 4.19 Percentage of methylene blue degradation at residence time = 5 min. At the different the hydrothermal temperature.

4.2.1.2 The effect of hydrothermal time

The effect of hydrothermal temperature on the photocatalytic degradation of methylene blue was studied. TiO_2 on titanium plate was prepared by varying the time of oven from 3, 9, 12, 24 and 48h at 180°C, respectively. For the study of this parameter, the TiO_2 thin film tests with the methylene blue solution at 5 ppm. Flow rate of the methylene blue solution was fixed at 5.4 mL/h. The results are illustrated in Figure 4.20.

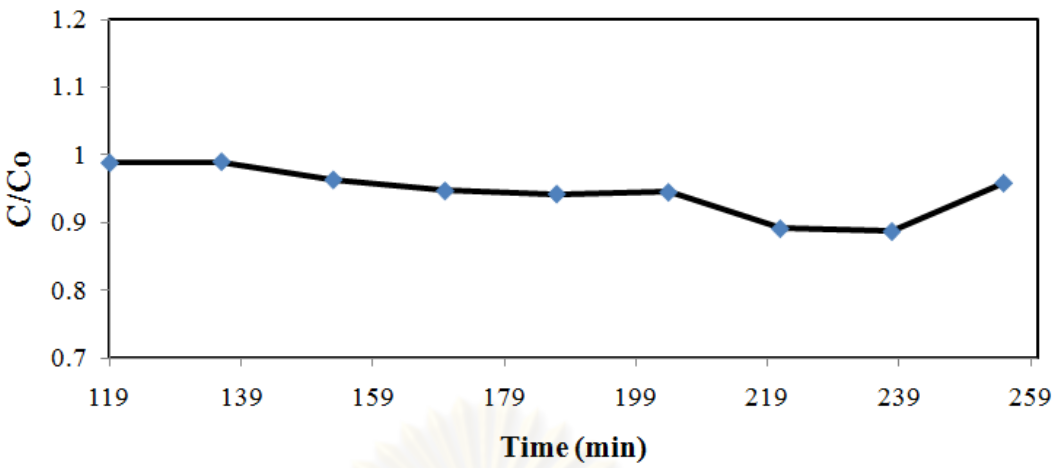

(a)

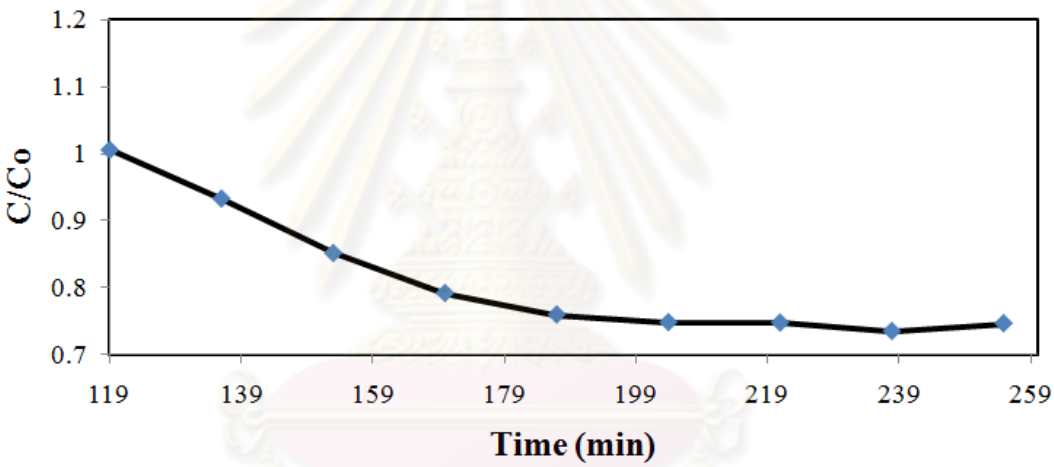

(b)

Figure 4.20 Photolysis degradation of methylene blue (a) comparing with the photocatalytic degradation on TiO_2/Ti plate synthesized at 3 (b), 9 (c), 12 (d), 24 (e) and 48 h (f).

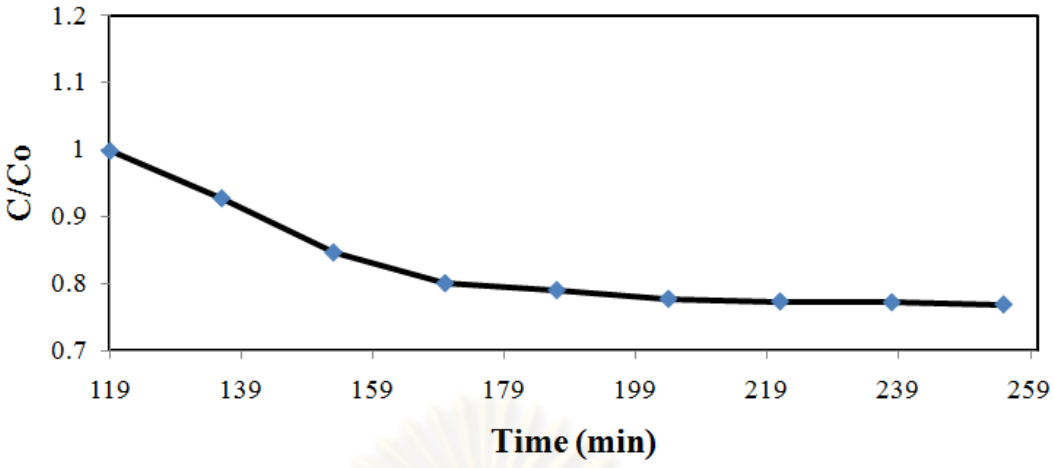

(c)

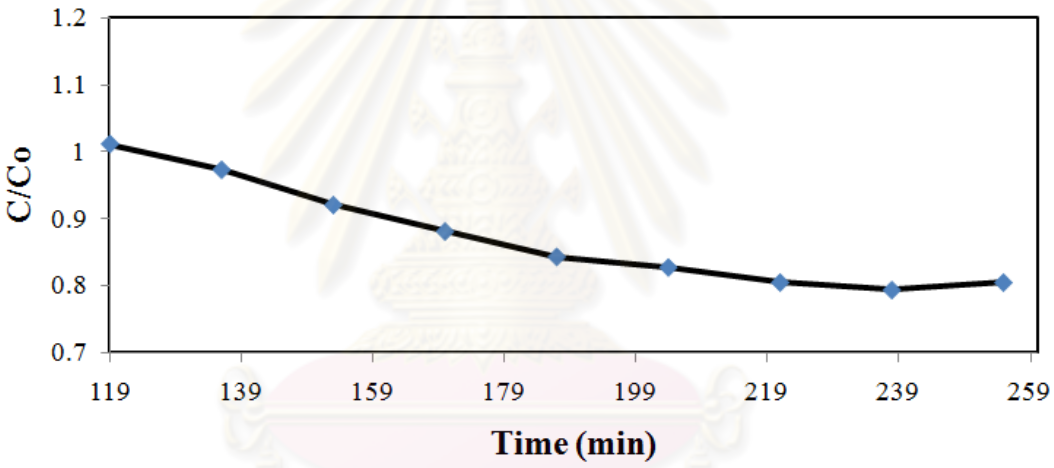

(d)

Figure 4.21 (continued)

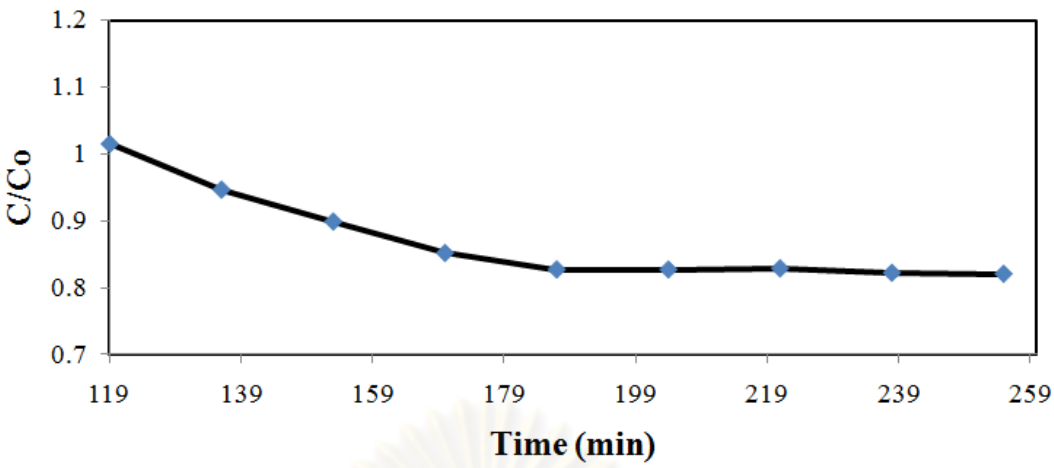

(e)

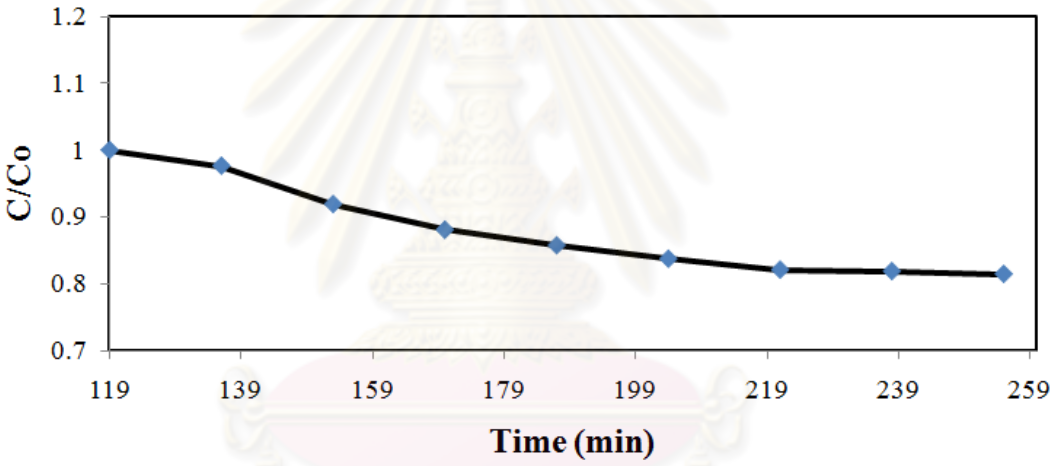

(f)

Figure 4.21 (continued)

Figure 4.21 shows the percentage of methylene blue degradation on titania that was synthesized using of different hydrothermal time. The residence time in the reaction system i.e. a micro reactor, was kept at 5 min. In this study, TiO_2 thin film calcined at 600°C was used because this calcination temperature result in both natase and rutile phases. It has been reported that the rutile/anatase mixed phase has higher photocatalytic activity than the pure anatase [30]. When the hydrothermal time is increased, the percentage of methylene blue degradation is decreased because the

content of anatase phase is decreased. The hydrothermal time of 3 h yields the highest degradation percentage, since it yields the highest content of anatase phase in the product (Table 4.4).

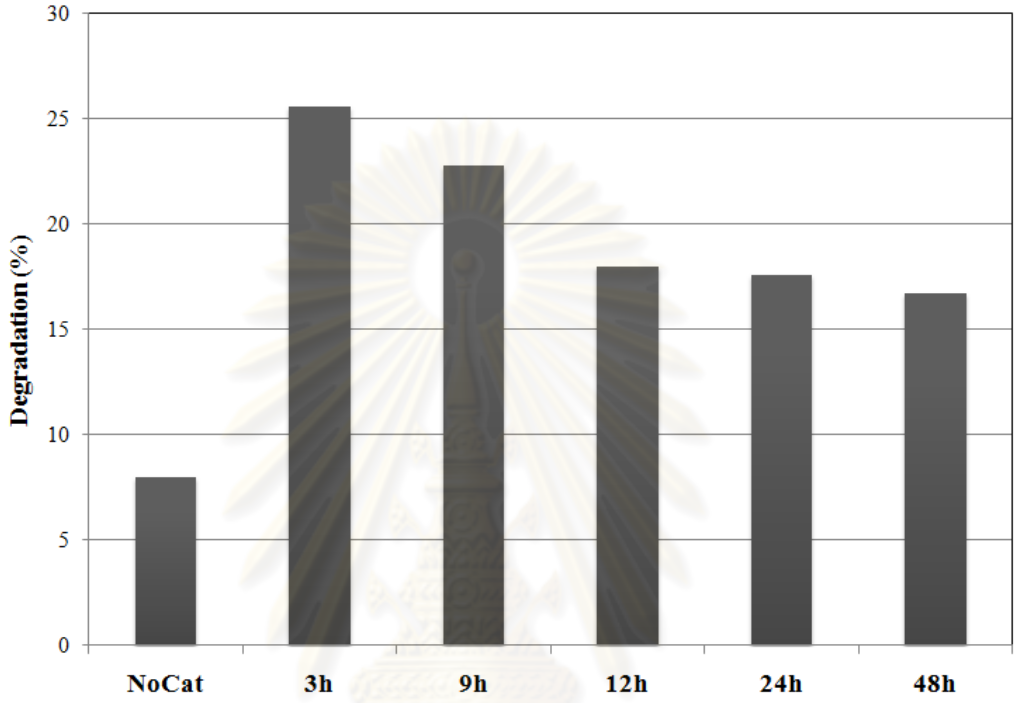

Figure 4.21 Percentage of methylene blue degradation on TiO_2/Ti plate synthesized for different period of the hydrothermal time.

4.2.1.3 The effect of calcination temperature

The effect of hydrothermal temperature on the photocatalytic degradation of methylene blue was studied. TiO_2 on titanium plate was prepared by varying the temperature of furnace from 400, 600 and 800°C for 2 h, respectively. For the study of this parameter, the TiO_2 thin film tests with the methylene blue solution at 5 ppm. Flow rate of the methylene blue solution was fixed at 5.4 mL/h. The results are illustrated in Figure 4.22.

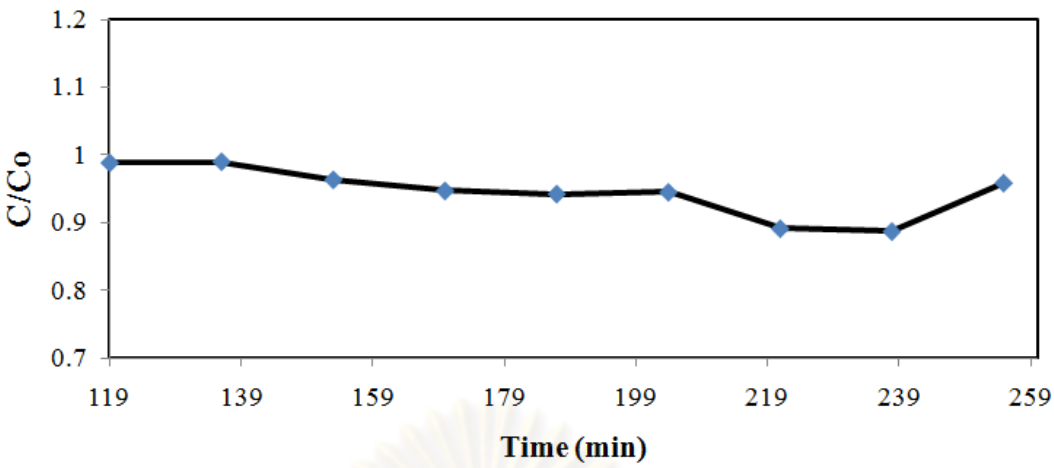

(a)

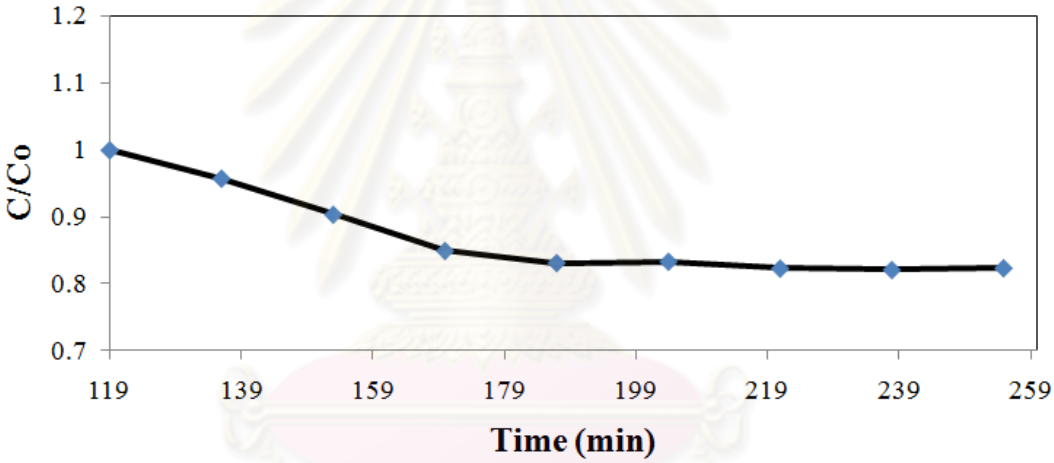

(b)

Figure 4.22 Photolysis degradation of methylene blue (a) comparing with the photocatalytic degradation on TiO_2/Ti plate synthesized at 400 (b), 600 (c) and 800°C (d).

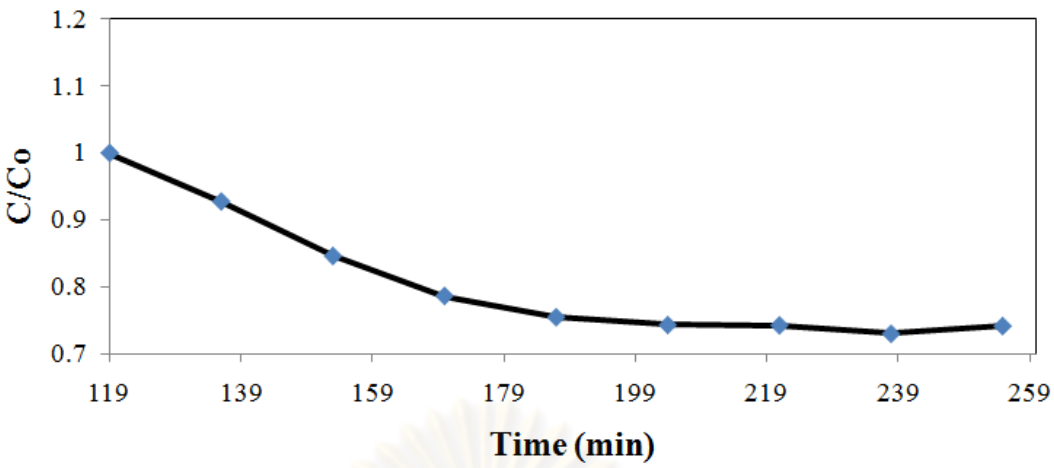

(c)

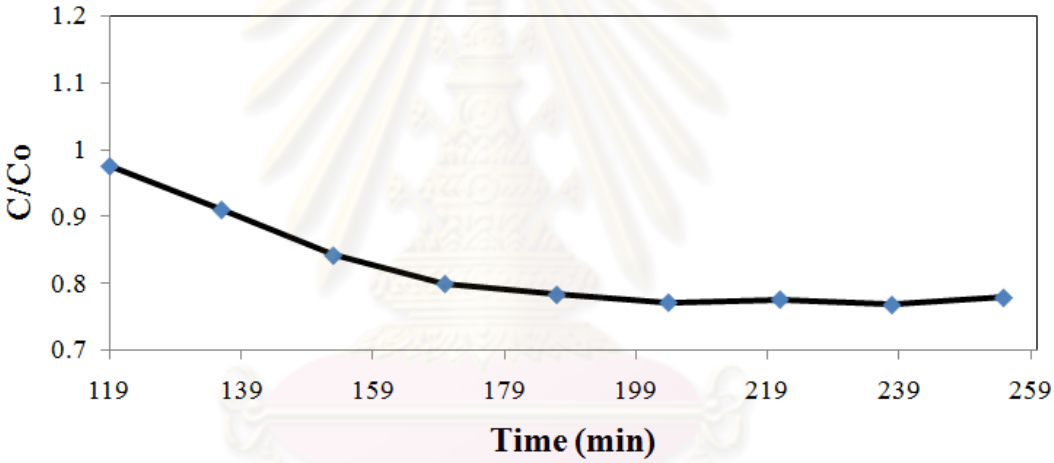

(d)

Figure 4.22 Continued

Figure 4.23 shows the percentage of methylene blue degradation on titania that was synthesize using of different calcination temperature. The residence time in the reaction system, i.e. a micro reactor, was kept at 5 min. The calcination temperature of 600°C gives the titania product with the highest photocatalytic activity toward methylene blue degradation, mainly because it was the highest content anatase phase (Figure 4.21). The photocatalytic activity of the product calcined at 800°C is higher than that calcined at 400°C.

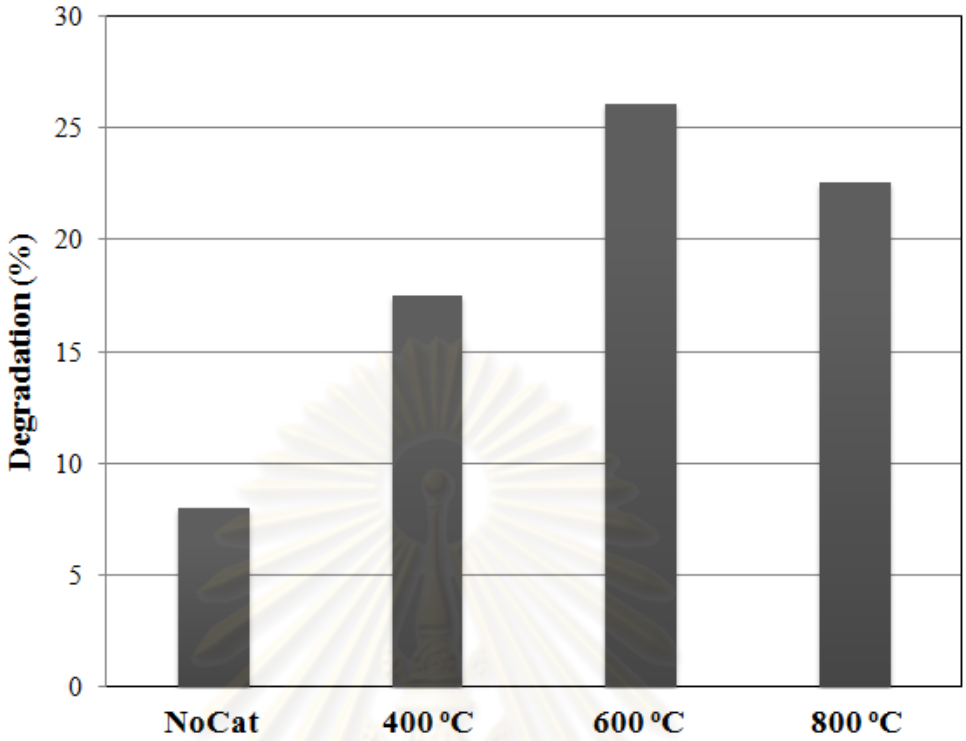

Figure 4.23 Percentage of methylene blue degradation on TiO_2/Ti plate synthesized for different period of the calcination temperature.

4.2.2 Water Splitting by Photocatalytic Reaction

In this study, TiO_2/Ti plate prepared by the hydrothermal treatment at 180°C for 3 h and subsequently calcined at 600°C for 2 h was use as the anode for the water splitting reaction because that product showed for the highest photocatalytic activity. The cathode was a platinum plate (2 x 2 cm^2). In the TiO_2-side and Pt-side containers, 1.0 M NaOH and 0.5 M H_2SO_4 aqueous solution were used as electrolyte, respectively. An adjustable voltage provided by a power supply between the anode and cathode was supplied in the range of 0.4-1V.

Initially, electrochemical reaction without a catalyst was studied by applying potential between the anode and the cathode in the range of 0.4-1 V. The energy of a chemical system drives the charges to move. The energy aspect is also related to

the chemical equilibrium. All of these relationships are tied together and can be described by Nernst equation. At first, the Electromotive Force (EMF), which the maximum potential difference between two electrodes of a galvanic or voltaic cell was calculated. This quantity is related to the tendency for an element, a compound or an ion to acquire (i.e. gain) or release (loss) electrons. EMF of this work was calculated by Nernst equation. At the standard condition of 298 K (25°C), the Nernst equation for the reaction $aA + bB \rightarrow cC + dD$ becomes;

$$\Delta E = \Delta E^{o} - \frac{0.0592V}{n} \log \frac{[C]^{c}[D]^{d}}{[A]^{a}[B]^{b}}$$

$$E^{o}_{cell} = E^{o}_{cathode} - E^{o}_{anode}$$

In this work, the reaction involved are:

Reduction $2\,H^{+}_{(aq)} + 2e^{-} \rightarrow H_{2(g)}$ $E^{o}_{cathode} = 0.00\,\text{V}$

Oxidation $4\,OH^{-}_{(aq)} \rightarrow O_{2(g)} + 2H_2O_{(l)} + 4e^{-}$ $E^{o}_{anode} = -0.40\,\text{V}$

Net reaction $4\,H^{+}_{(aq)} + 4\,OH^{-}_{(aq)} \rightarrow 2H_{2(g)} + O_{2(g)} + 2H_2O_{(l)}$

$$E^{o}_{cell} = 0.00\text{V} - (-0.40\text{V})$$
$$= 0.40\text{V}$$

Therefore,

$$\Delta E = 0.40 - \frac{0.0592V}{4} \log \frac{1}{(0.5)^{4}(1)^{4}}$$

with n = 4 in this case, because the reaction involves 4 electrons.

$$\Delta E = 0.38\text{V}$$

According to the experimental results shown in Figure 4.24 shows that 0.9V is the minimum voltage to get substantial amount of hydrogen produced in which, an average hydrogen generation rate of 0.51 μmol/h is obtained. The hydrogen generation rate at the beginning of the electrochemical reaction is a small. It increases as the reaction time and voltage is increased. At the onset of the reaction, the newly generated gas bubbles become attached at the surface of the platinum plate. The minimum voltage found from the experiment is higher than ΔE calculated from Nernst equation because the electric wire need in the experiment is very long. The long electric wire has high resistance.

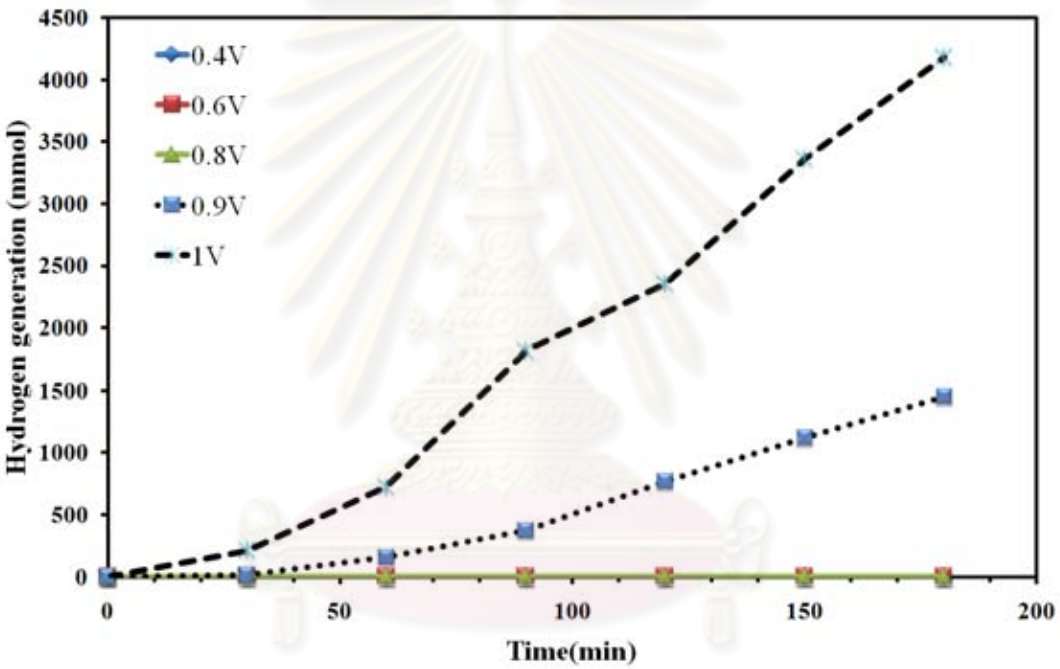

Figure 4.24 Influence of applied voltage between the anode and cathode on H_2 generation from the system without TiO_2 thin film and irradiation.

For the PEC system using TiO_2 thin film as the anode, the hydrogen generation rate at the beginning of the photochemical reaction is faster than the system that does not use TiO_2 thin film as the anode because TiO_2 is a semiconductor. With better electron flowing, the reaction becomes faster. By applying a small electrical bias at 0.8 V for 150 min (Figure 4.25), an average hydrogen generation rate of 17.7 μmol/h is obtained without any light irridiation.

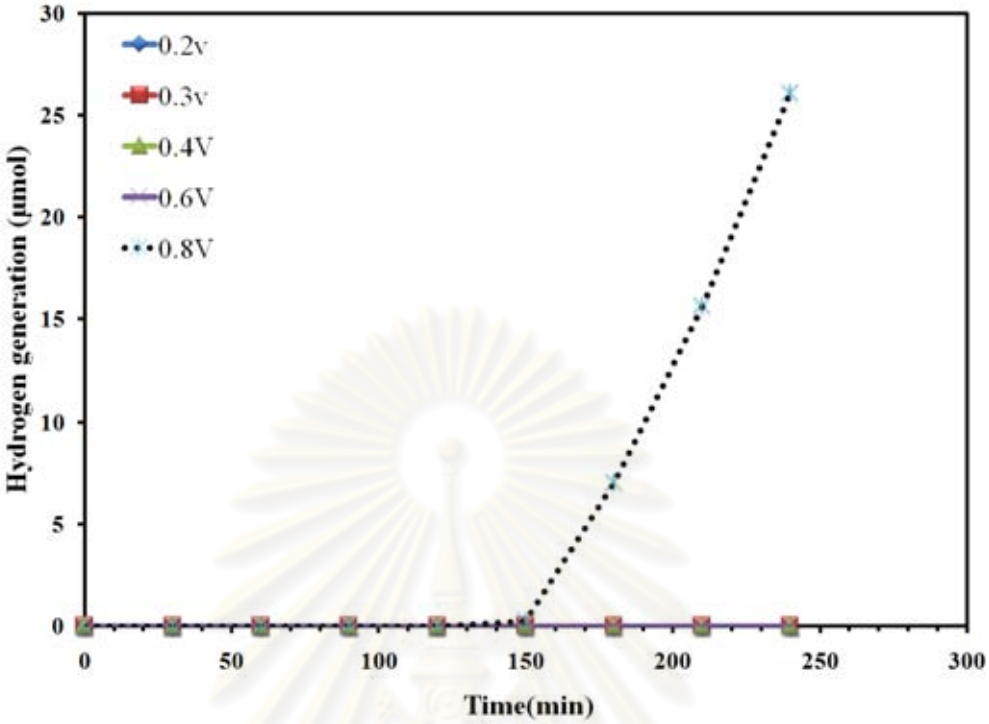

Figure 4.25 Influence of applied voltage provided supply between the anode and cathode H_2 generation from the PEC system using TiO_2 thin film as the anode, in which no irradiation is provided.

The photo-irradiation of the TiO_2 electrode under a small electric bias leads to the evolution of H_2 and O_2 at the surface of the Pt electrode and TiO_2 electrode, respectively.

$$TiO_2 \rightarrow e^- + h^+$$

$$H_2O + 2h^+ \rightarrow (1/2)O_2 + 2H^+$$

$$2H^+ + 2e^- \rightarrow H_2$$

That reaction is Bard"s concept [31]. The PEC system using TiO_2 thin film as the anode, in which irradiation is provided. The reaction becomes faster. By applying a small electrical bias at 0.8 V for 60 min (Figure 4.26), an average hydrogen

generation rate of 43.2 µmol/h, so the separate evolution of H_2 from water could be successfully achieved using an H-type glass container even under UV light.

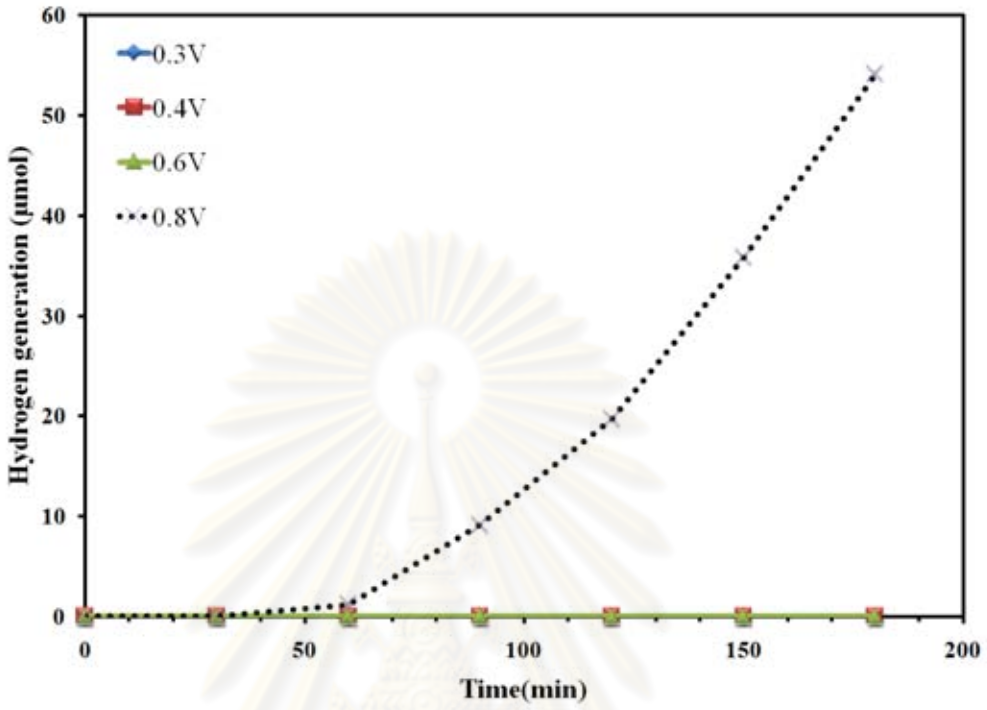

Figure 4.26 Influence of applied voltage provided supply between the anod and cathode H_2 generation from the PEC system using TiO_2 thin film as the anode, in which irradiation is provided.

CHAPTER V

CONCLUSIONS AND RECOMMENDATIONS

5.1 Conclusions

The conclusions of the present research are the following:

1. Titania could be grown from titanium plate via hydrothermal process.

2. Majority of the product formed is nanofiber.

3. Size, morphology and crystallinity of the fibers as well as the thickness of the growth layer depend upon temperature, duration of the hydrothermal treatment and calcination temperature.

4. TiO_2 thin film shown the separate evolution of H_2 from water could be successfully achieved using an H-type glass container even under UV light.

ศูนย์วิทยทรัพยากร
จุฬาลงกรณ์มหาวิทยาลัย

5.2 Recommendations for the Future Studies

Regarding the previous conclusions, the following recommendations for the future studies are proposed.

1. Study the effect of hydrothermal temperature, hydrothermal time and calcination temperature for water splitting.

2. Study the increase the efficiency of TiO_2 thin film for water splitting.

ศูนย์วิทยทรัพยากร
จุฬาลงกรณ์มหาวิทยาลัย

REFERENCES

[1] Currao, A. Photoelectrochemical Water Splitting. *Transformation and storage of solar energy,* vol. 61, p. 815, 2007.

[2] Yoong, L. S. Chong, F.K. and Dutta, B. K. Development of copper-doped TiO_2 photocatalyst for hydrogen production under visible light. *Energy,* vol. 34, pp. 1652-1661, 2009.

[3] Negishi, N. Iyoda, T. Hashimoto, K. and Fujishima, A. Preparation of transparent TiO_2 thin-film photocatalyst and its photocatalytic activity. *Chem. Lett. 9,* vol. 841–842, 1995.

[4] Bach, U. Lupo, D. Comte, P. Moser, J. E. Weissortel, F. Salbeck, J. Spreitzer, H. and Gratzel, M. Solid-state dye-sensitized mesoporous TiO_2 solar cells with high photon-to-electron conversion efficiencies. *Nature,* vol. 395, pp. 583-585, 1998.

[5] Cinnsealach, R. Boschloo, G. Nagaraja Rao, S. and Fitzmaurice, D. Electrochromic windows based on viologen-modified nanostructured TiO_2 films. *Solar Energy Materials and Solar Cells,* vol. 55, pp. 215-223, 1998.

[6] Chen, X. and Mao, S. S. Titanium Dioxide Nanomaterials: Synthesis, Properties, Modifications, and Applications. *Chem. Rev.,* vol. 107, pp. 2891–2959, 2007.

[7] Peng, X. and Chen, A. Dense and high-hydrophobic rutile TiO_2 nanorod arrays. *Appl. Phys. A Mater. ,* vol. 80, pp. 473-476, 2005.

[8] Centi, Passalacqua, G. R. Perathoner,S. Su,D. Weinberg,S. G. and Schlögl,R. Oxide thin films based on ordered arrays of 1D nanostructure. A possible approach toward bridging material gap in catalysis. *Phys. Chem. Chem. Phys.,* vol. 9, pp. 4930 - 4938, 2007.

[9] Liu, Y. Chen, W. Yang, Y. Ong, J. Tsuru, L. Hayakawa, K. S. and Osaka, A. Novel fabrication of nano-rod array structures on titanium and in vitro cell responses. *J. Mater. Sci: Mater. Med.,* vol. 19, pp. 2735-2741, 2008.

[10] Wei, Q. Hirota, K. Tajima, K. and Hashimoto, K. Design and Synthesis of TiO_2 Nanorod Assemblies and Their Application for Photovoltaic Devices. *Chem. Mater.,* vol. 18, pp. 5080–5087, 2006.

[11] Smith, W. and Zhao, Y. Enhanced Photocatalytic Activity by Aligned WO_3/TiO_2 Two-Layer Nanorod Arrays. *J. Phys. Chem. C,* vol. 112, pp. 19635–19641, 2008.

[12] Chen, C. A. Chen, K. Y. Huang, Y. S. Tsai, D. S. Tiong, K. K. and Chien, F. Z. X-ray diffraction and Raman scattering study of thermal-induced phase transformation in vertically aligned TiO_2 nanocrystals grown on sapphire(1 0 0) via metal organic vapor deposition. *J. Cryst. Growth.,* vol. 310, pp. 3663-3667, 2008.

[13] Chen-Chi Wang, J. Y. Y. Sol−Gel Synthesis and Hydrothermal Processing of Anatase and Rutile Titania Nanocrystals. *Chem. Mater.,* vol. 11, pp. 3113–3120, 1999.

[14] Mathews, N. R. Morales, E. R. Cortes-Jacome, M. A. and Toledo Antonio, J. A. TiO_2 thin films - Influence of annealing temperature on structural, optical and photocatalytic properties. *Solar Energy,* vol. 83, pp. 1499-1508, 2009.

[15] Sreemany, M. and Sen, S. Influence of calcination ambient and film thickness on the optical and structural properties of sol-gel TiO_2 thin films. *Mater. Res. Bull. ,* vol. 42, pp. 177-189, 2007.

[16] Byrappa, K. and Adschiri, T. Hydrothermal technology for nanotechnology. *Prog. Cryst. Growth Charact. Mater.,* vol. 53, pp. 117-166, 2007.

[17] Tian, Z. R., J. A. Voigt, J. L. Mckenzie, B. and Xu, H. Large Oriented Arrays and Continuous Films of TiO_2-Based Nanotubes. *J. Am. Chem. Soc.,* vol. 125, pp. 12384–12385, 2003.

[18] Guo, Y. Lee, N.-H. Oh, H.-J. Yoon, C.-R. Park, K.-S. Jung, S.-C. and Kim, S.-J. The growth of oriented titanate nanotube thin film on titanium metal flake. *Surf. Coat. Technol.,* vol. 202, pp. 5431-5435, 2008.

[19] Guo, Y. Lee, N.-H. Oh, H.-J. Yoon, C.-R. Park, K.-S. Lee, H.-G. Lee, K.-S. and Kim, S.-J. Structure-tunable synthesis of titanate nanotube thin films via a simple hydrothermal process. *Nanotechnol.,* vol. 18, p. 295608, 2007.

[20] Inoue, Y. Noda, I. Torikai, T. Watari, T. Hotokebuchi, T. and Yada, M. TiO_2 nanotube, nanowire, and rhomboid-shaped particle thin films fixed on a titanium metal plate. *J. Solid State Chem.,* vol. 183, pp. 57-64.

[21] Vayssieres, L. On Solar Hydrogen & Nanotechnology. WILEY, 2010.

[22] Fujishima, A. and Honda, K. Electrochemical Photolysis of Water at a Semiconductor Electrode. *Nature,* vol. 238, pp. 37-38, 1972.

[23] Osa, T. and Fujihira, M. Photocell using covalently-bound dyes on semiconductor surfaces. *Nature,* vol. 264, pp. 349-350, 1976.

[24] Fujishima, A. Rao, T. N. and Tryk, D. A. Titanium dioxide photocatalysis. *Journal of Photochemistry and Photobiology C: Photochemistry Reviews,* vol. 1, pp. 1-21, 2000.

[25] Kitano, M. Mitsui, R. Eddy, D. R. El-Bahy, Z. M. A. Matsuoka, M. Ueshima, M. and Anpo, M. Synthesis of Nanowire TiO_2 Thin Films by Hydrothermal Treatment and their Photoelectrochemical Properties. *Catal. Lett.,* vol. 119, pp. 217-221, 2007.

[26] Matsuoka, M. Kitano, M. Fukumoto, S. Iyatani, K. Takeuchi, M. and Anpo, M. The effect of the hydrothermal treatment with aqueous NaOH solution on the photocatalytic and photoelectrochemical properties of visible light-responsive TiO_2 thin films. *Catalysis Today,* vol. 132, pp. 159-164, 2008.

[27] Matsuoka, M. M Kitano,. Fukumoto, S. Iyatani, K. Takeuchi, M. and Anpo, M. The effect of the hydrothermal treatment with aqueous NaOH solution on the photocatalytic and photoelectrochemical properties of visible light-responsive TiO_2 thin films. *Catalysis Today,* vol. 132, pp. 159-164, 2008.

[28] Matsuoka, M. Ebrahimi, A. Nakagawa, M. Kim, T. H. Kitano, M. Takeuchi, M. and Anpo, M. Separate evolution of H_2 and O_2 from H_2O on visible light-responsive TiO_2 thin film photocatalysts prepared by an RF magnetron sputtering method: The effect of various calcination treatments on the photocatalytic reactivity. *Research on Chemical Intermediates,* vol. 35, pp. 997-1004, 2009.

[29] Xiao, N. Li, Z. Liu, J. and Gao, Y. Effects of calcination temperature on the morphology, structure and photocatalytic activity of titanate nanotube thin films. *Thin Solid Films,* vol. 519, pp. 541-548.

[30] Jung, K. Y. and Park, S. B. Anatase-phase titania: preparation by embedding silica and photocatalytic activity for the decomposition of trichloroethylene. *Journal of Photochemistry and Photobiology A: Chemistry,* vol. 127, pp. 117-122, 1999.

[31] Matsuoka, M. Kitano, M. Takeuchi, M. Tsujimaru, K. Anpo, M. and Thomas, J. M. Photocatalysis for new energy production: Recent advances in photocatalytic water splitting reactions for hydrogen production. *Catal. Today,* vol. 122, pp. 51-61, 2007.

ศูนย์วิทยทรัพยากร
จุฬาลงกรณ์มหาวิทยาลัย

APPENDICES

ศูนย์วิทยทรัพยากร
จุฬาลงกรณ์มหาวิทยาลัย

APPENDIX A

CALIBRATION CURVE FOR DETERMINATION OF METHYLENE BLUE CONCENTRATION

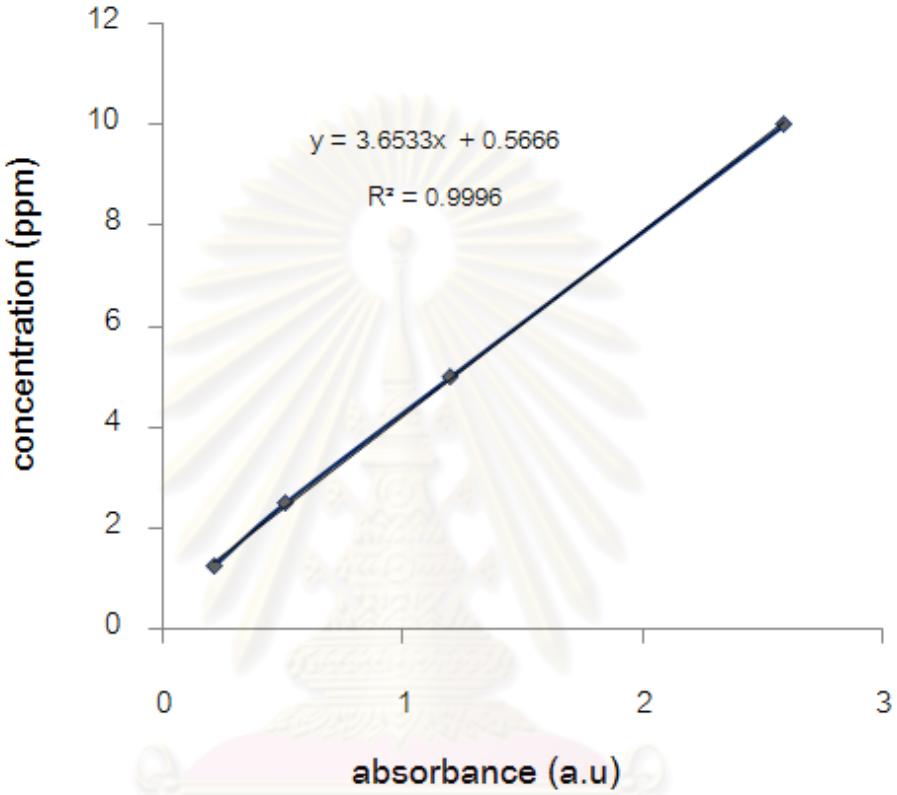

Figure A.1 The calibration curve of methylene blue.

ศูนย์วิทยทรัพยากร
จุฬาลงกรณ์มหาวิทยาลัย

Table A.1 Photolysis degradation of methylene blue (a) comparing with the photocatalytic degradation on TiO_2/Ti plate synthesized at 120 (b), 150 (c) and 180°C (d).

Absorpbance (A.U)						
Time (min)	Sample					
	NoCat	3h	9h	12h	24h	48h
0	0.882683	0.81179	0.91731	0.90573	0.802031	0.788153
17	0.850808	0.637485	0.66612	0.617973	0.665562	0.605446
34	0.840538	0.75375	0.770851	0.73411	0.68496	0.654258
51	0.862576	0.780658	0.842475	0.763091	0.727405	0.697007
68	0.888133	0.803453	0.882858	0.785202	0.765883	0.736038
85	0.886154	0.782737	0.903877	0.862182	0.791033	0.755319
102	0.89234	0.80667	0.908074	0.899053	0.79906	0.777416
119	0.883706	0.811714	0.927646	0.902061	0.792102	0.790058
136	0.872004	0.81698	0.916214	0.916075	0.814932	0.796984
153	0.873551	0.756183	0.849414	0.880402	0.758203	0.777842
170	0.849602	0.687868	0.77292	0.831848	0.718676	0.730952
187	0.834952	0.637796	0.729383	0.795389	0.679589	0.699512
204	0.830851	0.610985	0.719567	0.760317	0.659147	0.680554
221	0.833106	0.601344	0.707451	0.745679	0.659059	0.664115
238	0.785087	0.600901	0.703635	0.724986	0.660503	0.650833
255	0.781241	0.590298	0.702413	0.714585	0.654979	0.64907
262	0.84527	0.600062	0.699428	0.724845	0.653675	0.645543

Table A.2 Photolysis degradation of methylene blue (a) comparing with the photocatalytic degradation on TiO_2/Ti plate synthesized at 3 (b), 9 (c), 12 (d), 24 (e) and 48 h (f).

Absorpbance (A.U)				
Time (min)	Sample			
	NoCat	120°C	150°C	180°C
0	0.882683	0.797143	0.798474	0.795339
17	0.850808	0.605694	0.549736	0.304223
34	0.840538	0.685019	0.672988	0.267738
51	0.862576	0.721869	0.759095	0.25019
68	0.888133	0.768358	0.775155	0.262459
85	0.886154	0.778571	0.780405	0.32078
102	0.89234	0.794845	0.797328	0.335023
119	0.883706	0.798797	0.803449	0.345493
136	0.872004	0.797787	0.794645	0.403365
153	0.873551	0.735653	0.759623	0.35779
170	0.849602	0.675527	0.691473	0.353416
187	0.834952	0.635658	0.660782	0.368064
204	0.830851	0.606996	0.63893	0.3258
221	0.833106	0.608005	0.632736	0.329281
238	0.785087	0.61062	0.620589	0.344677
255	0.781241	0.602141	0.620058	0.361234
262	0.84527	0.606471	0.619582	0.350986

Table A.3 Photolysis degradation of methylene blue (a) comparing with the photocatalytic degradation on TiO_2/Ti plate synthesized at 400 (b), 600 (c) and 800°C (d).

Absorpbance (A.U)				
Time (min)	Sample			
	NoCat	400°C	600°C	800°C
0	0.882683	0.774817	0.91698	0.780063
17	0.850808	0.512249	0.637485	0.559739
34	0.840538	0.574367	0.75375	0.622067
51	0.862576	0.687946	0.780658	0.689214
68	0.888133	0.742342	0.803453	0.723512
85	0.886154	0.759251	0.782737	0.755875
102	0.89234	0.768848	0.80667	0.762008
119	0.883706	0.768848	0.811714	0.780063
136	0.872004	0.774817	0.81698	0.760509
153	0.873551	0.741074	0.756183	0.708224
170	0.849602	0.698047	0.687868	0.653422
187	0.834952	0.6547	0.637796	0.619394
204	0.830851	0.640348	0.610985	0.606391
221	0.833106	0.641851	0.601344	0.596959
238	0.785087	0.633678	0.600901	0.600708
255	0.781241	0.632049	0.590298	0.59421
262	0.84527	0.634126	0.600062	0.602726

APPENDIX B

CALIBRATION CURVE FOR DETERMINANTION OF HYDROGEN GENERATION

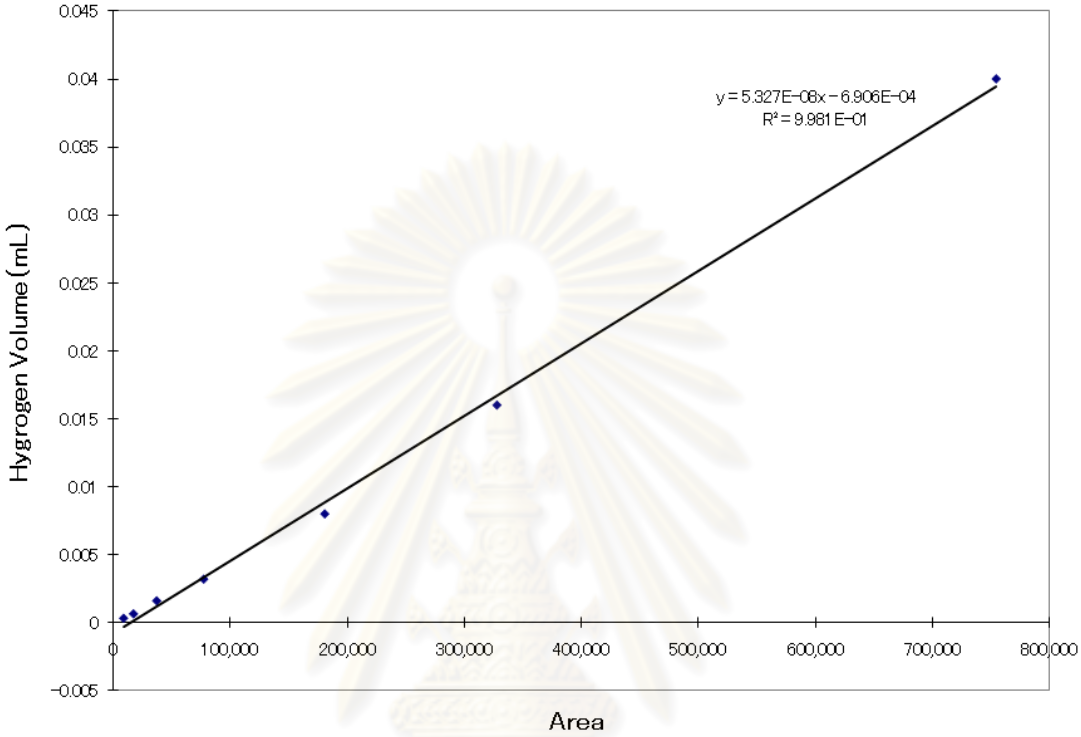

Figure B.1 The calibration curve of hydrogen generation.

APPENDIX C

Table C.1 Standard electrode (reduction) potentials at T = 298 K

Reduction half – reaction	E^o(V)
$F_{2(g)} + 2e^- \rightarrow 2F^-_{(aq)}$	+ 2.89
$O_{3(g)} + 2H^+_{(aq)} + 2e^- \rightarrow O_{2(g)} + 2H_2O_{(l)}$	+ 2.07
$S_2O_8^{2-}{}_{(aq)} + 2e^- \rightarrow 2SO_4^{2-}{}_{(aq)}$	+ 2.01
$H_2O_{2(aq)} + 2H^+_{(aq)} + 2e^- \rightarrow 2H_2O_{(l)}$	+ 1.71
$PbO_{2(aq)} + SO_4^{2-} + 4H^+_{(aq)} + 2e^- \rightarrow PbSO_{4(aq)} + 2H_2O_{(l)}$	+ 1.69
$MnO_4^-{}_{(aq)} + 8H^+_{(aq)} + 5e^- \rightarrow Mn^{2+}_{(aq)} + 2H_2O_{(l)}$	+ 1.51
$Au^{3+}_{(aq)} + 3e^- \rightarrow Au_{(s)}$	+1.50
$PbO_{2(s)} + 2H^+_{(aq)} + 2e^- \rightarrow Pb^{2+}_{(aq)} + 2H_2O_{(l)}$	+1.45
$Cl_{2(g)} + 2e^- \rightarrow 2Cl^-_{(aq)}$	+1.36
$Cr_2O_7^{2-}{}_{(aq)} + 14H^+_{(aq)} + 6e^- \rightarrow Cr^{3+}_{(aq)} + 7H_2O_{(l)}$	+1.33
$O_{3(g)} + H_2O_{(l)} + 2e^- \rightarrow O_{2(g)} + OH^-_{(aq)}$	+1.24
$O_{2(g)} + 4H^+_{(aq)} + 4e^- \rightarrow 2H_2O(l)$	+1.23
$2IO_3^-{}_{(aq)} + 12H^+_{(aq)} + 10e^- \rightarrow I_{2(s)} + 6H_2O_{(l)}$	+1.20
$Br_{2(l)} + 2e^- \rightarrow 2Br^-{}_{(aq)}$	+1.08
$NO_3^-{}_{(aq)} + 4H^+_{(aq)} + 3e^- \rightarrow NO_{(g)} + 2H_2O_{(l)}$	+ 0.96
$ClO^-{}_{(aq)} + H_2O_{(l)} + e^- \rightarrow Cl^-_{(aq)} + OH^-_{(aq)}$	+0.89
$Hg^{2+}_{(aq)} + 2e^- \rightarrow Hg_{(l)}$	+ 0.86
$Ag^+_{(aq)} + e^- \rightarrow Ag_{(s)}$	+ 0.80
$Hg_2^{2+}{}_{(aq)} + 2e^- \rightarrow Hg_{(l)}$	+ 0.79
$Fe^{3+}_{(aq)} + e^- \rightarrow Fe^{2+}_{(aq)}$	+ 0.77
$I_{2(s)} + 2e^- \rightarrow 2I^-_{(aq)}$	+ 0.54
$O_{2(g)} + 2H_2O_{(l)} + 4e^- \rightarrow 4OH^-_{(aq)}$	+ 0.40
$Cu^{2+}_{(aq)} + 2e^- \rightarrow Cu_{(s)}$	+ 0.34
$Sn^{4+}_{(aq)} + e^- \rightarrow Sn^{2+}_{(aq)}$	+ 0.15
$2H^+_{(aq)} + 2e^- \rightarrow H_{2(g)}$	0.00
$CrO_4^{2-}{}_{(aq)} + 4H_2O_{(l)} + 3e^- \rightarrow Cr(OH)_{3(s)} + 5OH^-_{(aq)}$	- 0.126
$Pb^{2+}_{(aq)} + 2e^- \rightarrow Pb_{(s)}$	- 0.13
$Sn^{2+}_{(aq)} + 2e^- \rightarrow Sn_{(s)}$	- 0.14

Table C.1 (Continued)

Reduction half – reaction	E^o(V)
$Ni^{2+}_{(aq)} + 2e^- \rightarrow Ni_{(s)}$	- 0.24
$Co^{2+}_{(aq)} + 2e^- \rightarrow Co_{(s)}$	- 0.28
$PbSO_{4(s)} + 2e^- \rightarrow Pb_{(s)} + SO_4^{2-}{}_{(aq)}$	- 0.36
$Cd^{2+}_{(aq)} + 2e^- \rightarrow Cd_{(s)}$	- 0.40
$Fe^{2+}_{(aq)} + 2e^- \rightarrow Fe_{(s)}$	- 0.44
$Cr^{3+}_{(aq)} + 3e^- \rightarrow Cr_{(s)}$	- 0.74
$Zn^{2+}_{(aq)} + 2e^- \rightarrow Zn_{(s)}$	- 0.76
$SO_4^{2-}{}_{(aq)} + H_2O_{(l)} + e^- \rightarrow SO_3^{2-}{}_{(aq)} + 2OH^-_{(aq)}$	- 0.93
$H_2O_{(l)} + 2e^- \rightarrow H_{2(g)} + OH^-_{(aq)}$	- 0.83
$Mn^{2+}_{(aq)} + 2e^- \rightarrow Mn_{(s)}$	- 1.18
$Al^{3+}_{(aq)} + 3e^- \rightarrow Al_{(s)}$	- 1.68
$Mg^{2+}_{(aq)} + 2e^- \rightarrow Mg_{(s)}$	- 2.36
$Na^+_{(aq)} + e^- \rightarrow Na_{(s)}$	- 2.71
$Ca^{2+}_{(aq)} + 2e^- \rightarrow Ca_{(s)}$	- 2.87
$Ba^{2+}_{(aq)} + 2e^- \rightarrow Ba_{(s)}$	-2.91
$K^+_{(aq)} + e^- \rightarrow K_{(s)}$	- 2.93
$Li^+_{(aq)} + e^- \rightarrow Li_{(s)}$	- 3.05

ศูนย์วิทยทรัพยากร
จุฬาลงกรณ์มหาวิทยาลัย

VITA

Miss Nisa Dechrat was born on September 26, 1986 in Surin, Thailand. She received the Bachelor‟s Degree in Chemical Engineering from King Mongkut‟s University of Technology Thonburi in March 2009, She entered the Master of Engineering in Chemical Engineering at Chulalongkorn University in June, 2009.

LIST OF PUBLICATIONS

1. Nisa Dech-rat, Thirapong Napapruekchart, Tawat Chaiyangyuen, Nawin Viriya-empikul, Kajornsak Faungnawakij and Varong Pavarajarn. "Growth of TiO_2 on Titanium Plate via Hydrothermal Method". The 17th Regional Symposium on Chemical Engineering (MSE 389), Bangkok, November 22-23, 2010.

2. Nisa Dech-rat, Nawin Viriya-empikul, Kajornsak Faungnawakij and Varong Pavarajarn. "Hydrothermal Synthesis of TiO_2 Nanostructured Arrays and Their Photocatalytic Activity for Methylene Blue Degradation in Microreactor". The 7th Asian Aerosol Conference, Xi‟an, China, August 17-20, 2011.

ศูนย์วิทยทรัพยากร
จุฬาลงกรณ์มหาวิทยาลัย